Lacunes chargées, étude dans des nano-agrégats de silicium

Arpan Deb

UNIVERSITÉ DE GRENOBLE

THÈSE

Pour obtenir le grade de

DOCTEUR DE L'UNIVERSITÉ DE GRENOBLE

Spécialité : **Doctorat Physique des Materiaux**

Arrêté ministériel : 15 Fevrier 2012

Présentée par

Arpan Krishna DEB

Thèse dirigée par **Thierry DEUTSCH** et
codirigée par **Damien CALISTE**

préparée au sein du CEA/INAC/SP2M/L SIM
dans **l'Ecole Doctorale de Physique des Materiuax**

Lacunes chargees, etude dans des nano-agregats de silicium

Thèse soutenue publiquement **le 6 Mars 2012**,
devant le jury composé de :

Dr. Christophe DELERUE
Rapporteur
Dr. Guy TREGLIA
Rapporteur
Dr. Noel JAKSE
Président
Dr. Guido ROMA
Membre
Dr. Damien CALISTE
Membre
Dr. Thierry DEUTSCH
Membre)

To my mother Mrs. Chhabi Deb.

I do not put my faith in any new institutions, but in the individuals all over the world who think clearly, feel nobly and act rightly. They are the channels of moral truth. ... **Rabindranath Tagore**

Contents

Chapitre 1

Ce chapitre traite des éléments d'introduction à cette thèse. J'y introduits la description des divers types de défauts présents dans un solide. Certains résultats et leur importance sont aussi mentionnés. Une rapide comparaison avec les méthodes existantes pour étudier les défauts est présente. Les défauts décrits sont les défauts ponctuels, les défauts plans, les dislocations, avec ou sans charge. Une rapide histoire de l'étude des défauts est aussi mentionnée pour compléter l'état de l'art du domaine. Enfin, certaines expériences portant sur les défauts sont rappelées.

Chapter 1

Introduction

1.1 General Ideas

Silicon (Si), the most common metalloid and the eight most common element in the universe by mass is one among the most important material for industrial use. It is the principal component of most semiconductor devices, most importantly integrated circuits or microchips. Silicon is widely used as a semiconductor because it remains more of a semiconductor at higher temperatures than another material of the same family, germanium, and also because its native oxide is easily grown in a furnace and forms a good semiconductor/dielectric interface. In the form of silica and silicates, silicon comprises useful glasses, cements, and ceramics. It is also a constituent of silicones, a class-name for various synthetic plastic substances made of silicon, oxygen, carbon and hydrogen. In naturally found Si and also for the industrial uses one often comes across defects in crystalline structure of the material and hence the study to know more about the pros and cons of those defects came into practice. There are several phenomena such as the electrical transport and phototransport, the light absorption and emission etc., for which the investigation of defects is essential. Sometimes the defects are useful and sometimes they have to be avoided because they make troubles. In bulk semiconductors, there are various specific applications like the radiation detectors where the defects are very useful. Since a long time

Silicon is used in radiation detectors and electronic devices. Nowadays, these devices work on submicron technology and they are parts of integrated circuits with large to very large scale integration. Silicon and silicon based devices are heavily worked upon in great theoretical and experimental detail, in many fields of physics including particle physics experiments, nuclear medicine, reactors and space. Defects in the material represent a limiting factor in the operation of devices. In spite of the huge research being put into by the scientific community till date, there are a lot of aspects not clarified, related to the behavior of impurities, defects, vacancies in Silicon. And hence a global understanding of their local structure and properties became increasingly important due to the reduction in chip sizes and to the increase of the operation speed. The study of effects of point defects on electronic, structural and vibration properties of bulk semiconductors, and also on low size semiconductor structures is a thematic of high interest. This study will bring contributions to the fabrication of Si based smart materials for photonics, MOS and nanowires based devices etc. The fabrication of new materials will open up new horizons and enable path-breaking advances in science and technology.

In bulk semiconductors various defects (sometimes called trap defects), like the point defects, impurities or local stresses, are located in the volume of the material. In nanocrystalline semiconductors the trapping phenomena are dominated by the traps located at the surface or interface, due to the very big area/volume ratio (of the order of $10^8 m^{-1}$ for nanocrystals). These traps are produced by the adsorption, dangling bonds, and the internal stresses (induced by misfit)[1]. Experimental methods like the photo-induced current transient spectroscopy (PICTS), the thermally stimulated currents (TSC), the thermally stimulated depolarization currents (TSDC), and the optical charging spectroscopy (OCS) are in practice to study those defects. In theory as well scientists are making headway through the calculations of the stability, energetics of formation, migration, electrostatics etc. of all such defects. Before going into the further discussion about the defects and their respective analyses, one may feel the need to classify broadly the types of defects that are common in Silicon.

1.2 Types of defects

In reality there is no existence of a perfect crystal. All crystals have some defects. These defects do in general contribute to various mechanical and electronic properties of the material. In fact a part of modern electronic engineering is based on the manipulation of these defects for efficient use of the material. Grossly these defect types in silicon crystals can be grouped as following :

- Point defects. (vacancies, interstitials, impurities etc.)
- Linear defects (dislocations etc.).
- Planar defects (grain boundaries, stacking faults etc.)

1.2.1 Point defects

When in the lattice structure of a material, an atom is missing or is in an irregular place, then that material is said to have point defects. This class of defects includes self interstitial atoms, interstitial impurity atoms, substitutional impurities and vacancies. A self interstitial atom is an extra atom that has crowded its way into an interstitial void in the crystal structure. A substitutional impurity atom is an atom of a different type than the bulk atoms, which has replaced one of the bulk atoms in the lattice. Interstitial impurity atoms are much smaller than the atoms in the bulk matrix and they are found to fit in the inter-atomic space between the bulk atoms of the lattice structure. Vacancies are basically the empty spaces where an atom should be, but is missing. They are common in metals and semiconductors, especially at high temperatures when atoms are found to change their positions pretty often leaving behind empty lattice sites. In most cases diffusion (mass transport by atomic motion) can only occur because of vacancies. The point defects are also responsible for the lattice strain in the crystal because of the deformation in the geometry around the defect itself. In the adjoining Figure 1.1, an example of the occurence of all the point defects discussed here, is schematically described. The vacancies can be charged giving rise

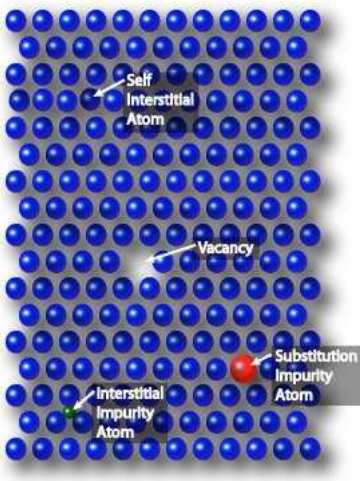

Figure 1.1: Various point defects in the bulk material.

to a special sub-branch of defects known as the *charged defects*. Even doping the host material with foreign atoms (technically impurities) produce charged defects. The cases of doped Silicon crystals can be considered as an example, where donor atoms provide excess electrons to form n-type silicon and acceptor atoms provide a deficiency of electrons to form p-type silicon. It is also worth mentioning here that combination of the point defects, eg. *a vacany + an interstitial* can give rise to another category of charged defects. Those defects can influence the formation of cluster defects in the bulk material. In this regard it is worth mentioning a special type known as the Frenkel defects. A Frenkel defect, Frenkel pair, or Frenkel disorder is a type of point defect in a crystal lattice where the defect forms when an atom or cation leaves its place in the lattice, creating a vacancy, and becomes an interstitial by lodging in a nearby location not usually occupied by an atom. Frenkel defects occur due to thermal vibrations, in principle there will be no such defects in a crystal at 0 K.

1.2.2 Linear defects

These defects are found in the material when an array of atoms is displaced in the crystal structure. The presence of such dislocations affect the physcial properties of the material to a pretty large extent, in fact the motion of the dislocations are the cause for the plastic deformations to occur in the material. The dislocations can be broadly devided into *Edge dislocations* and *Screw dislocations*. An edge dislocation is said to have occured where an extra half-plane of atoms is introduced half way in the middle through the crystal, disrupting the symmetry of nearby planes of atoms. The dislocation is called a line defect because the locus of defective points produced in the lattice by the dislocation lie along a line. The inter-atomic bonds are significantly distorted only in the immediate vicinity of the dislocation line. The screw dislocation is not very straightforward to understand. The motion of a screw dislocation is also a result of shear stress, but the defect line movement is perpendicular to direction of the stress and the atom displacement, rather than parallel. Figure 1.2 describes the two different dislocations schematically. The edge dislocations allow deformation to occur

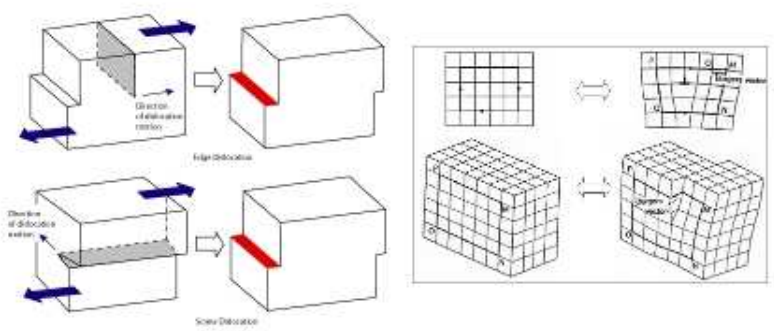

Figure 1.2: Edge and Screw dislocations.

at much lower stress than in a perfect crystal. One can understand that

fact by studying the movement of the edge dislocation. Dislocation motion is analogous to movement of a caterpillar. A schematic diagram in Figure 1.3 shows the movement of the dislocation. As for the screw dislocations the

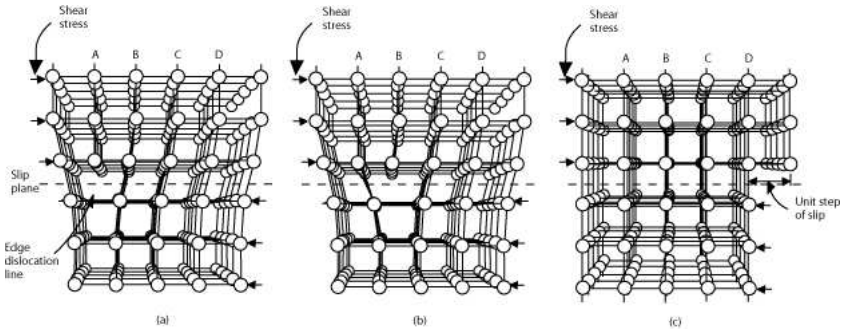

Figure 1.3: The movement of the edge dislocation.

dislocations move along the densest planes of atoms in a material, because the stress needed to move the dislocation increases with the spacing between the planes. FCC and BCC metals have many dense planes, so dislocations move relatively easy and these materials have high ductility.

1.2.3 Planar defects

Defects like the *Stacking faults, Twin boundaries, Grain boundaries* are examples of planar defects. A stacking fault is a one or two layer interruption in the stacking sequence of atom planes. Stacking faults occur in a number of crystal structures. For example we can consider the faults of hcp and fcc structures. Here the first two layers arrange themselves identically, and are said to have an AB arrangement. If the third layer is placed so that its atoms are directly above those of the first (A) layer, the stacking will be ABA. This indeed is the hcp structure, and it continues ABABABAB. However it is possible for the third layer atoms to arrange themselves so that they are in line with the first layer to produce an ABC arrangement which is that of the fcc structure. So, if the hcp structure is going along as ABABAB and suddenly switches to ABABABCABAB, there is a stacking fault present. Another type of planar defect is the grain boundary. The interface between

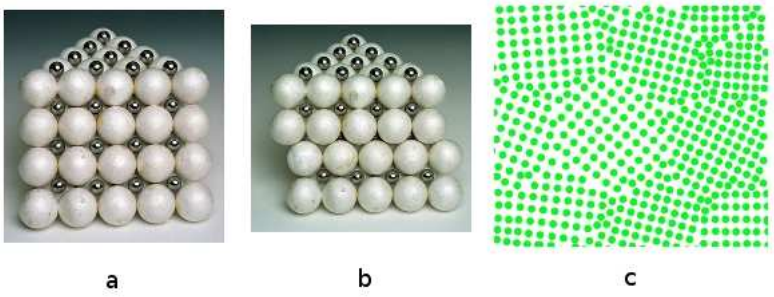

Figure 1.4: (a) Photograph showing a model of the ideal packing in the AB FCC structure, (b) Photograph showing a model of the AB FCC structure with a stacking fault (c) Differently oriented crystallites in a polycrystalline material forming boundaries.

two grains, or crystallites, in a polycrystalline material is known as the grain boundary. Grain boundaries are such defects in the crystal structure which are found to decrease the electrical and thermal conductivity of the material. Grain boundaries limit the lengths and motions of dislocations. It is known now that having smaller grains (more grain boundary surface area) strengthens a material. Different experimental procedures can be used to control the size of the grains.

1.3 A brief history of defects in bulk Si

Let us now focus on the study of defects in crystalline Silicon. Various experiments and theoretical calculations have revealed some interesting properties of the defects. In both forms of study there are frontiers which are difficult to conquer, mostly because of the complexity of the systems. In some cases the experiments are very difficult to carry out, whereas in some cases to construct the real theoretical picture of the system is extremely challenging. Some facts which will be mentioned in the following section are well researched and established. As for example we have known that the stability of crystalline silicon comes from the fact that each silicon atom can accommodate its four valence electrons in four covalent bonds with its four neighbors. The pro-

duction of primary defects or the existence of impurities or defects destroys this fourfold coordination. It has been established[3][4] that the structural characteristics of the *classical* vacancy in bulk Si are: the bond length in the bulk is 2.35 Å and the bond angle –109 degrees . The formation energy is 3.01 eV (p-type silicon), 3.17 eV (intrinsic), 3.14 eV (n-type). For interstitials, different theoretical works have reported the possibility of various structural configurations. They are a) the hexagonal configuration, a sixfold coordinated defect with bonds of length 2.36 Å, joining it to six neighbors which are fivefold coordinated; b) the tetrahedral interstitial is fourfold coordinated; has bonds of length 2.44 Å, joining it to its four neighbors, which are therefore fivefold coordinated; c) the split $-<110>$ configuration: two atoms forming the defect are fourfold coordinated, and two of the surrounding atoms are fivefold coordinated; d) the 'caged' interstitial contains two normal bonds, of length of 2.32 Å, five longer bonds in the range 2.55 2.82 Å, and three unbounded neighbors at 3.10 3.35 Å. The calculations [6]-[8] found that the tetrahedral interstitial and caged interstitial are metastable. For interstitials, the lowest formation energies (calculated theoretically) in eV are 2.80 (for p-type material), 2.98 (for n-type) and 3.31 in the intrinsic case respectively. Authors have reported that in silicon the vacancy takes on five different charge states in the band gap, viz. $V^{2+}, V^{+}, V^{0}, V^{-}$ and V^{2-}[9]. But about the charge states of the self-interstitial there are differences of opinions in reports by Lopez[10] et. al. The experimental examination of primary point defects buried in the bulk is difficult and for various defects this is usually indirect. In a series of theoretical studies[2] and correlated EPR and DLTS experiments of Watkins and co-workers[4], it became possible to solve some problems associated with the electrical level structure of the vacancy. In crystalline silicon bombarded with energetic projectiles, the divacancy center is being studied for quite some time now by numerous authors applying various experimental techniques, e.g. EPR [3], photoconductivity [11], infrared absorption [12], electron-nuclear double resonance (ENDOR) or deep level transient spectroscopy (DLTS) and at the room temperature it is considered as a stable defect. The undisturbed configuration of divacancy could be viewed as two vacant nearest neighbor lattice sites. Experiments by

Watkins et. al. with isochronal and isothermal annealing studies reveals that the divacancy anneals out at 570 K[3]. Since then many other experiments have tried to comment on the formation mechanism and charge states of the divacancy.
In 2002, in an important report, S. Goedecker, T. Deutsch and L. Billard [13] predicted the existence of a new type of primary defect in silicon and thus a new type of symmetry in the crystallography of the material. Their work proved the existence of a fourfold coordinated defect which is found to be more stable. Experiments by Lazanu and Lazanu [14] proved the existence of such defects. Lattice Monte Carlo calculations are done by Damien Caliste and Pascal Pochet[15] to study the diffusion of vacancies in bulk Si. They have reported the results of simulations of vacancy-assisted diffusion in silicon to show that the observed temperature dependence for vacancy migration energy is explained by the existence of three diffusion regimes for divacancies. The geometry and energetics of the normal divacancies and split divacancies are discussed as well. In a follow up work Damien et. al. have presented an analysis of stress-enhanced vacancy-mediated diffusion in biaxially deformed Si (100) films as measured by the strain derivative (Q') of the activation energy[16].

1.4 The Motivation

There are in fact two parts of this thesis. The first part deals with the accuracy of Hartwigsen-Goedeker-Hutter (HGH) pseudopotentials with Non Linear Core Correction (NLCC). The main idea is to use the pseudopotentials for further accurate calculations. One can argue of course the validity of such a job. We have tried to find out a less complex approach with the norm-conserving pseudopotentials to produce as accurate results as that of the Projector Augmented Wave[80] (PAW) approach or that of the all-electron calculations. The success of our approach would ensure a method other than the PAW method for accurate calculations of various physical quantities. This is an attempt to correct the otherwise implied linearization of the pseudopotential. Chapter 4 would deal in detail with this part of the

research. For the next and more important part of the research we wish to concentrate ourselves in the charged point defects in silicon nanoclusters. Up to now, as will be explained in Chapter 3, the charged defects have been simulated within the framework of Periodic Boundary Conditions (PBC). Indeed this PBC approach is good to simulate an infinite bulk. But, as will be shown in detail in the following chapters, this PBC approach comes with its own artifacts which can be difficult to deal with. The electrostatics, in particular for those systems is not simple to represent and a lot of mathematical jargon is needed to account for some other unwanted interactions. In our approach we have tried to find a method with which we can deal with isolated charged systems and also can comment on bulk properties even when we are working with Free Boundary Conditions (FBC). Our motivation is to find the correct electrostatics of the charged defects in the nanoclusters and its ability to extrapolate those results for the infinite bulk cases. Chapter 5 deals with this part of the research in detail. Before going into the details of the current research work it is handy to have an overview of some basic theoretical concepts.

Chapitre 2

Ce chapitre traite des différents concepts théoriques à la base de cette thèse. Une vue générale de la théorie de la fonctionnelle de la densité (DFT) dans ces différents aspects est décrite. J'aborde aussi les différentes fonctionnelles d'échange-corrélation (ECF) d'intérêt pour la thèse, ainsi que la théorie sous-jacente. La thèse utilisera par la suite une fonctionnelle GGA. Enfin, je traite aussi les différentes bases existantes pour résoudre les équations de Kohn-Sham (KS), montrant ainsi l'intérêt des ondelettes pour le traitement des défauts. Tous les calculs ayant été fait avec l'approximation des pseudo-potentiels, la théorie est abordée ici. La thèse est basée sur la forme des pseudo-potentiels de Hartwigsen-Goedecker-Hutter (HGH) pour le calcul des défauts abordé au chapitre 5, et les HGH avec correction non-linéaire de cœur pour le calcul des énergies d'atomisation décrites dans le chapitre 4.

Chapter 2

Some Theoretical Concepts : DFT and its components

2.1 Introduction

In this chapter we discuss in order of appearance the basic theoretical concepts of Density Functional Theory, along with its major components - the Pseudopotentials and the Exchange Correlation Functional. The different basis sets which can be used to solve the Kohn-Sham equations are also described with their respective pros and cons.

2.2 Density functional theory (DFT) (a brief overview)

Since its discovery almost four decades back, DFT, a theory of electronic ground state structure, has been one among the most important tools to understand the ground state properties of molecules, solids and clusters. Theoretical physicists and chemists find in it an altrenative to the traditional methods of quantum chemistry dealing with many-electron wave-function. DFT in its full glory is a thematic continuation of the previous approximate methods although itself being exact in principle. With a motive to reduce the number of parameters needed to describe the many body system, DFT works

centering around the electron density $\rho(\mathbf{r})$ of the electronic system. The main goal of almost all physical systems is to know its various physical properties and structure, and hence calculation of the total energy of the system is most important. Keeping in accordance with that goal, all the contributions to the total energy are expressed in terms of the electron density in the framework of DFT. In the following subsections various important structural parts of the DFT formalism are explained.

2.2.1 Hohenberg-Kohn theorems

Among the structural pillars of DFT Hohenberg-Kohn (HK) theorems [17] are of foremost importance. The first HK theorem proves that the ground state electron density ρ is sufficient to determine , in principle, the total energy of the system and hence any ground state property of the system without the knowledge of the many electron wave function can thus be obtained. The second theorem states that the ground state energy of the system is the minimal value of the energy functional of the electronic system. Both the two theorems are proven here in the following subsections.

First Hohenberg-Kohn theorem. *The ground state density $\rho(r)$ of a system of many interacting electrons moving in some external potential $v(r)$ determines this potential uniquely.*

Proof. [18] By *reductivo ad absurdum.* Let us consider two external potentials $v_1(\mathbf{r})$ and $v_2(\mathbf{r})$ having the same ground state electron density $\rho(\mathbf{r})$, with Hamiltonians H_1 and H_2 respectively, and non-degenerate ground states $|\Psi_1\rangle$ and $|\Psi_2\rangle$, therefore

$$H_1 |\Psi_1\rangle = E_1^0 |\Psi_1\rangle \tag{2.1}$$

$$H_2 |\Psi_2\rangle = E_2^0 |\Psi_2\rangle \, . \tag{2.2}$$

Let us apply the variational principle at this point

$$E_1^0 < \langle\Psi_2| H_1 |\Psi_2\rangle = \langle\Psi_2| H_2 |\Psi_2\rangle + \langle\Psi_2| H_1 - H_2 |\Psi_2\rangle \tag{2.3}$$

$$< E_2^0 + \int \rho(\mathbf{r}) \left[v_1(\mathbf{r}) - v_2(\mathbf{r})\right] d\mathbf{r} \, . \tag{2.4}$$

Evidently by interchanging subscripts 1 and 2 in the above inequality another inequality can be formed of similar structure. By adding both inequalities we can get

$$E_1^0 + E_2^0 < E_2^0 + E_1^0 \tag{2.5}$$

which is obviously not true. Hence by contradiction to our initial assumption we can conclude that **there is one and only one external potential associated with the ground state electronic density.** □

Since $\rho(\mathbf{r})$ is known for the system, all other ground state properties like the particle number, and the external potential, the total energy $E[\rho]$, the kinetic energy $T[\rho]$, the potential energy $V[\rho]$, etc. can be calculated directly.

Second Hohenberg-Kohn theorem. *If any electron density, given by,* $\widetilde{\rho}(\mathbf{r})$ *is such that* $\int \widetilde{\rho}(\mathbf{r})dr = N$ *and* $\widetilde{\rho}(\mathbf{r}) \geqslant 0$ *then*

$$E_0 \leqslant E_v[\widetilde{\rho}] = T[\widetilde{\rho}] + V_{ne}[\widetilde{\rho}] + V_{ee}[\widetilde{\rho}] \equiv \int v(\mathbf{r})\widetilde{\rho}(\mathbf{r})\, d\mathbf{r} + F_{HK}[\widetilde{\rho}]\ . \tag{2.6}$$

where E_0 is the ground state energy, V_{ne} and V_{ee} are potentials due to nucleus-electron and electron-electron interactions. F_{HK} is the universal functional as it describes a treatment of the kinetic and internal potential energies which is same for all systems.

Proof. According to the first HK theorem any electron density $\widetilde{\rho}(r)$ uniquely determines the external potential $v(\mathbf{r})$ consequently with its own Hamiltonian and the ground state wave function $\langle\widetilde{\Psi}|$ associated with this Hamiltonian. Let $\langle\Psi|$ describe the ground state of a system with density ρ and Hamiltonian H. According to the Rayleigh-Ritz variational principle, for any electronic state $\langle\widetilde{\Psi}|$

$$\left\langle\widetilde{\Psi}\right| H \left|\widetilde{\Psi}\right\rangle \geq \langle\Psi| H |\Psi\rangle = E[\rho] \tag{2.7}$$

and

$$\left\langle\widetilde{\Psi}\right| H \left|\widetilde{\Psi}\right\rangle = \int v(\mathbf{r})\widetilde{\rho}(\mathbf{r})\, d^3\mathbf{r} + T[\widetilde{\rho}] + V_{ee}[\widetilde{\rho}] = E_v[\widetilde{\rho}]\ . \tag{2.8}$$

Therefore

$$E_v[\widetilde{\rho}] \geq E_v[\rho] \tag{2.9}$$

□

2.2.2 The Kohn-Sham (KS) equations

In the framework of DFT KS equations [18] are essentially Schroedinger equations of a system of noninteracting particles that would generate the same density as one given system of interacting particles. To that end we need to derive the equations for the single particle system that yields the density $\rho(\mathbf{r})$. To start with let us focus in deriving the equations for a system of noninteracting particles. For a noninteracting system, the total energy of the system can be written as

$$\tilde{E}[\rho] = T_s\left[\tilde{\rho}\right] + \int v(\mathbf{r})\tilde{\rho}(\mathbf{r})\,, \tag{2.10}$$

where v is the net potential and $T_s\left[\tilde{\rho}\right]$ is the kinetic energy of the ground state of the system of *noninteracting* electrons having a density $\tilde{\rho}(\mathbf{r})$. The density of the system is given by

$$\tilde{\rho}(\mathbf{r}) = \sum_{i=1}^{N} \left|\tilde{\varphi}_i(\mathbf{r})\right|^2 . \tag{2.11}$$

The number of occupied states N being constant, let us consider the variation in density as

$$\delta\tilde{\rho}(\mathbf{r}) = \sum_{i=1}^{N} \delta\tilde{\varphi}_i{}^*(\mathbf{r})\tilde{\varphi}_i(\mathbf{r}) \tag{2.12}$$

Since the density in equation 2.11 is stationary with respect to the given variation (the total number of particles being constant), the integral of the variation of density is evidently zero.

$$\int \delta\tilde{\rho}(\mathbf{r})d\mathbf{r} = \int \sum_{i=1}^{N} \delta\tilde{\varphi}_i{}^*(\mathbf{r})\tilde{\varphi}_i(\mathbf{r})d\mathbf{r} = 0\,. \tag{2.13}$$

Let us now apply the trick of Lagrange multiplier. For this case with the lagrangian multiplier ϵ, the variation in the energy functional takes the form

as

$$\delta\tilde{E}[\tilde{\rho}(\mathbf{r})] = \int \delta\tilde{\rho}(\mathbf{r}) \left\{ v(\mathbf{r}) + \frac{\delta}{\delta\tilde{\rho}(\mathbf{r})} T_s[\tilde{\rho}(\mathbf{r})] - \tilde{\epsilon} \right\} d\mathbf{r} = 0\,. \tag{2.14}$$

The system we have at hand is of *noninteracting* particles. Hence we can write the ground state energy eigenvalue of the system as

$$\tilde{E} = \sum_{i=1}^{N} \tilde{\epsilon}_i \tag{2.15}$$

and obtain as single-particle equations

$$\left[-\frac{1}{2}\nabla^2 + v(\mathbf{r}) - \tilde{\epsilon}_i \right] \tilde{\varphi}_i(\mathbf{r}) = 0 \tag{2.16}$$

The objective is to find equations for the states φ_i, but it must be kept in mind that these equations (2.16) are valid only for *noninteracting* particles. Obviously they yield the density $\tilde{\rho(\mathbf{r})}$ of a system of *noninteracting* particles. Whereas in reality the quantity we are interested in is the density $\rho(\mathbf{r})$ of a system of interacting particles. In the framework of DFT equation (2.10) needs to be rewritten as

$$E[\rho] = F_{HK}\,[\tilde{\rho}] + \int v_{ext}(\mathbf{r})\tilde{\rho}(\mathbf{r})\,, \tag{2.17}$$

where v_{ext} is the external potential and $F_{HK}\,[\rho]$ is the density functional, which we can split into expressions like

$$F_{HK}\,[\rho] = T_s\,[\rho] + \frac{1}{2}\int\int \frac{\rho(\mathbf{r})\rho(\mathbf{r}')}{|\mathbf{r}-\mathbf{r}'|} d\mathbf{r}d\mathbf{r}' + E_{XC}\,[\rho]\ , \tag{2.18}$$

In 2.18, $T\,[\rho]$ is the *noninteracting* part of the kinetic energy of this many electron system we are dealing with

$$T_s\,[\rho] = \sum_i \langle\varphi_i| -\frac{1}{2}\nabla^2_{\mathbf{r}}|\varphi_i\rangle\,. \tag{2.19}$$

The second term in equation 2.18 describes the classical electrostatic interaction between the noninteracting particles. This is the Hartree energy of

the system. $E_{XC}[\rho]$ is the exchange-correlation energy, which takes in account the entire electron-electron interaction effect beyond the Hartree term viz. *the exchange energy due to the Pauli exclusion principle*, *the correlation energy* and *the difference in kinetic energy between an interacting and a noninteracting system.* In practice the second and third term are collectively considered with the external potential as the effective Kohn-Sham potential

$$v_{eff}(\mathbf{r}, \rho(\mathbf{r})) = v_{ext}(\mathbf{r}) + \int \frac{\rho(\mathbf{r}')}{|\mathbf{r} - \mathbf{r}'|} d\mathbf{r}' + \frac{\delta E_{XC}[\rho(\mathbf{r})]}{\delta \rho(\mathbf{r})} \,. \tag{2.20}$$

The exchange-correlation potential is described by the third term as

$$v_{xc}(\mathbf{r}) = \frac{\delta E_{xc}[\rho]}{\delta \rho} \,. \tag{2.21}$$

Hence equation 2.17 can alternatively be written as

$$E[\rho] = T_s[\rho] + \int v_{eff}(\mathbf{r}) \rho(\mathbf{r}) \,, \tag{2.22}$$

The particles described by equation 2.22 and 2.10 are of course different yet since those two equations are essentially similar they will yield similar single particle equations. Finally we can write the most appropriate form of the Kohn-Sham equations as

$$\left[-\frac{1}{2} \nabla^2 + v_{eff}(\mathbf{r}) \right] \varphi_i = \epsilon_i \varphi_i \,, \tag{2.23}$$

φ_i and ϵ_i being the single particle orbitals and energies. At this point it is pretty clear that the ground state electron density can be computed from the self-consistent solution of the KS equations as in 2.23 only if *the expression for the exchange-correlation potential is known.* In practice, the density is calculated with the formula in equation 2.24 and consequently the obtained density is inserted in the exchange-correlation potential as in equation 2.21. Then the new eigenstates and new electron density of the

system are calculated, until the required convergence is reached.

$$\rho(\mathbf{r}) = \sum_{i=1}^{N} |\varphi_i(\mathbf{r})|^2 \tag{2.24}$$

It is noteworthy here that the KS equations as in equation 2.23 yield eigenstates φ_i of *fictitious* particles which only have the same density as the real particles. Hence it must be kept in mind that the ground state energy of the real system is not the simple sum of the Kohn-Sham single-particle eigenvalues as for noninteracting particles 2.15. Let us now have a look at the ground state energy (of the *real* system). It would look like

$$E = \sum_{i=1}^{N} \epsilon_i + E_{xc}[\rho(\mathbf{r})] - \int v_{xc}(\mathbf{r})\rho(\mathbf{r})d\mathbf{r} - \frac{1}{2}\int \frac{\rho(\mathbf{r})\rho(\mathbf{r}')}{|\mathbf{r}-\mathbf{r}'|}d\mathbf{r}d\mathbf{r}'. \tag{2.25}$$

KS DFT is a technique to describe the ground state energy and density, more to say almost all ground state properties of a many body system in terms of single particle equations and states. It is trap that one may find himself in if one believes, that in this formalism, real electrons are being described as independent particles experiencing an external field of the ions and of all other electrons. In reality the KS equations are merely the equations of noninteracting *fictitious* particles, whose density is the same as the density of real electrons in the ground state. Hence it can be said that the eigenstates of the KS equations do not have a direct physical meaning. However, in a system of N occupied states the N-th KS eigenvalue, ϵ_N, in equation (2.23) finds one a physical interpretation [20]

- The ionization potential (IP) of a finite system is given by

$$\epsilon_N = -IP \tag{2.26}$$

- And the same is the chemical potential for extended systems μ

$$\epsilon_N = \mu \tag{2.27}$$

It depends on the approximation used for the exchange-correlation functional/potential how close ϵ_N comes to the exact ionization potential or chemical potential [21].

2.3 Different Basis Set Approaches

As one can expect there are different approaches to solve the KS equations. The approaches are based on the basis sets on which this KS equations are expanded and then solved accordingly. Within this chapter I would discuss the three main approaches in terms of basis sets viz. the localized basis set approach, the plane wave approach and the wavelet basis set approach.

2.3.1 Atomic Basis Sets

Since the first efforts to solve the KS equations the use of atomic basis sets has been serving the cause to a very good effect. In this approach the molecular orbitals (MO) are expressed as a linear combination of atomic orbitals (LCAO). The basic strength of the LCAO approach is its general applicability as in reality it can work on any molecule with any number of atoms. To take the LCAO concept another step ahead to facilitate the calculations we can use a larger number of atomic orbitals (AO)(e.g. a hydrogen atom can have more than one s AO, and some p and d AOs, etc.). This helps us to achieve a more flexible representation of the MOs and therefore more accurate calculated properties according to the variation principle. One can also use AOs of a particular mathematical form that simplifies the computations (but are not necessarily equal to the exact AOs of the isolated atoms). These AOs are called the basis functions, or more precisely the localized atomic basis functions. Instead of having to calculate the mathematical form of the MOs (impossible on a computer) the problem is reduced to determining the MO expansion coefficients in terms of the basis functions. Functions that resemble hydrogen AOs (Slater functions in other words) are very suitable for expanding MOs because they have the correct shape (a) near the nucleus (shape of a cusp) and also (b)far from the nucleus (decay like $\exp -ar$). The

main reason for the preference of the Gaussian functions is the fact that they allow for efficient computation of molecular integrals. In quantum chem-

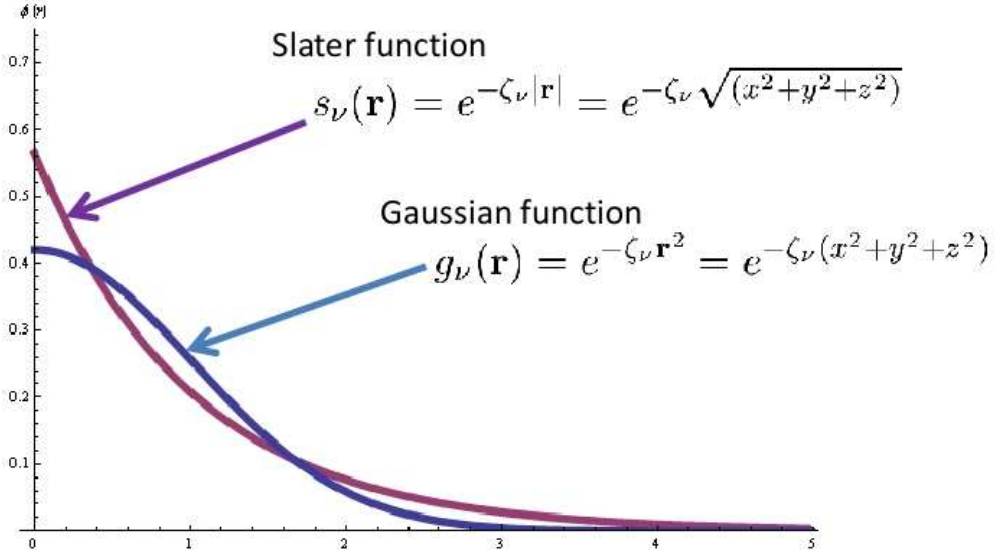

Figure 2.1: Illustration of the simplicity of the Gaussian functions over the slater functions

istry terminology a single Gaussian function is called a primitive Gaussian function, or primitive GTO (Gaussian Type Orbital). Some programs use cartesian primitive GTOs while the others use spherical primitive GTOs. In mathematical terms spherical and cartesian functions are the same for up to $l = 1$ (p functions) but differ slightly for $l = 2$ or higher. In practice, fixed linear combinations of *primitive* Gaussian functions are used which are called *Contracted Gaussians* (CGs). The simplest kind of CGs are the STO-nG basis sets . These basis sets attempt to approximate Slater-type orbitals (STOs) by n primitive Gaussians. The STO-nG basis sets are not that satisfactory as they include only one CG per atomic orbital. Improved basis sets are obtained by including more than one CG per atomic orbital, e.g.: DZ ("double zeta"), TZ ("triple zeta"), QZ ("quadruple zeta"). Or the improvement can also be achieved by the use of one CG per *core* atomic orbital and more than one for the valence atomic orbitals, e.g. *SV, 3-21G, 4-31G, 6-31G, 6-311G*. Increasing the number of CGs per atomic orbital will not

actually give a good quality basis set because in reality there are other types of CGs which are to included. For example one can include CGs of angular momentum higher than in the valence orbitals of each atom. These *polarization functions* enhance the *flexibility* of atoms to form chemical bonds in any direction and hence improve the calculated molecular structures. Few examples of such type are DVP, TZP, cc-pVDZ, cc-pVTZ etc. One can also take in account the CGs which extend further from the nucleus than the atomic orbitals. Such *diffuse functions* improve the predicted properties of species with extended electronic densities such as anions or molecules forming hydrogen bonds. Basis sets are considered *balanced* when they include both polarization and diffuse functions. Examples of these types comprises 6-31+G*, 6-311++G**, aug-cc-pVDZ etc. But completeness for these types of basis sets also calls for it to be infinite which is computationally unachievable. Indeed the atomic basis sets give out the real physics of the molecules but the two point integrations are exceedingly difficult to calculate with such basis sets. Again there is a problem of physical convergence of the computed results with these basis sets. In principle more informations can be put in to the computational structure but to need the complete picture what we need is an infinite basis set of this kind. Which of course is not possible to realize in reality.

2.3.2 Plane Wave Basis Sets

This approach is one where the Fourier representation of the equations bear a heavy significance. In reality most computational operations are easy to work with in the Fourier space which hands over an advantage to the plane wave basis sets in DFT calculations. According to the Bloch's theorem of solid state physics, the electronic wave functions at each k point can be expanded in terms of a discrete plane wave basis set. In principle, an infinite plane-wave basis set is required to expand the electronic wave functions. However, the coefficients for the plane waves with small kinetic energy are more important than those with large kinetic energy. Thus one can understand that there is a possibility for the plane-wave basis set to be truncated to include only plane

waves that have kinetic energies less than some particular cutoff energy. The basis set would be infinite if a continuum of plane-wave basis states were required to expand each electronic wave function, irrespective of the small magnitude of the cutoff energy. Thus one feels a need to make this apparently infinite basis set to a finite one. Application of the Bloch theorem allows the electronic wave functions to be expanded in terms of a discrete set of plane waves. To that end if one introduces a cutoff energy to the discrete plane-wave basis set we can have a finite basis set. Hence one can say that to achieve completeness plane wave basis sets should be infinite as well but with the cutoff approximation appropriately accurate results can be obtained. An error will be there for sure in the computed total energy due to the truncation of the plane-wave basis set at a finite cutoff energy. However, it is possible to reduce the magnitude of the error by increasing the value of the cutoff energy. In principle, the cutoff energy should be increased until the calculated total energy has reached convergence. One of the difficulties associated with the use of plane-wave basis sets is that the number of basis states changes discontinuously with cutoff energy. Generally these discontinuities are found to occur at different cutoffs for different k points in the k-point set. Another important aspect is that at a fixed-energy cutoff, a change in the size or shape of the unit cell will cause discontinuation in the plane-wave basis set. This problem is generally taken care of by using denser k-point sets, so that the weight attached to any particular plane-wave basis state is reduced. However, the problem is still present even with quite dense k-point samplings. It can be handled by applying a correction factor which manages to account for the difference between the counts approximately number of states in a basis set with infinitely large number of k points and the number of basis states actually used in the calculation [56]. In thsi approach though one needs to compute the coefficients which are in general large in number. This aspect raises a question about the speed of the process for calculations of very large systems. In reality this is an order N method. Very large systems can be tackled if we can use the plane wave DFT codes with parallel computation. But it is very difficult to parallelize the plane wave computations mainly because of the complexities raised by Fast Fourier Transformation (FFT).

2.3.3 Wavelet Basis Sets

A novel approach to solve the KS equations were shown to be very successful by Genovese and his colleagues[43]. They have used the Daubechies wavelets as a powerful systematic basis set for electronic structure calculations and have shown that they are good because they are orthogonal and localized both in real and Fourier space. Daubechies wavelets have been found to have all the properties that a DFT program would like to have of a basis set used for the simulation of isolated or inhomogeneous systems. They form a systematic orthogonal and smooth basis, localized both in real and Fourier spaces and that allows for adaptivity. Hence a DFT approach based on such functions will be very good to satisfy the requirements of precision and localization found in many applications. A wavelet basis comprises a family of functions generated from a mother function and its translations on the points of a uniform grid of spacing h. Here the number of basis functions is increased by decreasing the value of h (which is an analog to the cutoff energy for the case of plane wave basis sets). Because the basis set in systematic , the numerical description is reported to be more precise. The degree of smoothness determines the speed with which one converges to the exact result as h is decreased. The degree of smoothness increases as one goes to higher order Daubechies wavelets. In the method used for the DFT code BigDFT (the one which is used for the calculations in this thesis) Daubechies wavelets of order 16 are used. A very high rate of convergence is achieved in comparison to other finite difference, finite element, or real space methods[57][58][59]. Luigi et. al. have discussed the need of the localization of the basis sets in real space as essential for molecular systems. This is becaude for basis sets that are not localized in real space are wasteful in the context of molecular systems. For example, with plane waves one has to fill an orthorhombic cell into which the molecule fits. There can be regions of the cell that may contain no atoms and hence no charge density. But the plane wave approach cannot be used to utilize this scenario. Since Daubechies wavelets have a compact support, one can consistently define a set of localization parameters, which allows the researchers to put the basis

functions only on the points that are very close to the atoms. The computational volume in this method is thus given only by the union of spheres centered on all the atoms in the system. Real space localization is also necessary for the implementation of linear scaling algorithms. Hence this family of basis set is a worthy contender for developing such algorithms. A technical fact can be looked into at this point. For a given system, the convergence rate of the minimization process depends on the highest eigenvalue of the Hamiltonian operator. Since the high frequency spectrum of the Hamiltonian is dominated by the kinetic energy operator, high kinetic energy basis functions are therefore also approximate eigenfunctions of the Hamiltonian. A function localized in Fourier space is an approximate eigenfunction of the kinetic energy operator. By using such functions as basis functions for the KS orbitals, the high energy spectrum of the Hamiltonian can thus easily be preconditioned. It is of course known that a high degree of adaptivity is necessary for all-electron calculations since highly localized core electrons require a much higher spatial resolution than the valence wave function away from the atomic core. This fact is also discussed in the previous paragraphs. The important fact is that pretty high adaptivity can be obtained with a wavelet basis. In BigDFT use of pseudopotentials is undertaken to a very good effect. This is because such pseudopotentials are the easiest way to incorporate the relativistic effects that are important for heavy elements. The use of pseudopotentials readily reduces the need for adaptivity and one has therefore only two levels of adaptivity. Now one will have a high resolution region that contains all the chemical bonds and a low resolution region further away from the atoms where the wave functions would decay exponentially to zero. In the low resolution region each grid point carries a single basis function. In the high resolution region it carries in addition seven wavelets. In terms of degrees of freedom, the high resolution region is therefore eight times denser than the low resolution region. In comparison with a plane wave method this wavelet method is therefore particularly efficient for open structures with large empty spaces and a relatively small bonding region.

2.4 Approximations to the Exchange-Correlation Potential

In this section we talk about the approximation which is inherent to the DFT methods. It is the approximation to the exchange-correlation potential.
In equation (2.21)the exchange correlation potential is defined as

$$v_{xc}(\mathbf{r}) = \frac{\delta E_{xc}\,[\widetilde{\rho}]}{\delta \widetilde{\rho}}\,. \tag{2.28}$$

Although the KS equations appear very promising yet without the explicit knowledge of the exchange correlation functional the KS equations cannot be solved exactly. Among the cons of DFT finding a good approximation to the exchange correlation potential is of prime importance. In this section two very important approaches for the approximation to the potential are discussed.

2.4.1 The Local Density Approximation (LDA)

In the framework of LDA [19] the electron density of local area of the inhomogeneous system is approximated with the same density as that of a homogeneous electron gas in the same extremity. If we take ϵ_{xc} to be the exchange correlation energy per electron of a homogeneous electron gas of density ρ, then the real exchange correlation energy functional can be approximated by

$$E_{xc}[\rho] \approx E_{xc}^{LDA}[\rho] \equiv \int \rho(\mathbf{r})\epsilon_{xc}(\rho(\mathbf{r}))\,d\mathbf{r}\,. \tag{2.29}$$

the expression for v_{xc} can be obtained by taking the functional derivative of E_{xc} with respect to ρ

$$v_{xc}^{LDA} = \frac{\delta E_{xc}}{\delta \rho} = \epsilon_{xc}(\rho) + \rho\frac{\partial \epsilon_{xc}}{\partial \rho} \tag{2.30}$$

and, since the system is not homogeneous, $\rho = \rho(\mathbf{r})$. It is assumed hereby that ϵ_{xc} can be calculated accurately for the homogeneous electron gas. In fact, ϵ_{xc} can be divided into exchange and correlation parts $\epsilon_{xc} = \epsilon_x + \epsilon_c$. The exchange part is known analytically and given by

$$\epsilon_x = \frac{3}{4}\left(\frac{3\rho(\mathbf{r})}{\pi}\right)^{1/3} \tag{2.31}$$

and the *LDA* exchange potential is given as

$$v_x(\mathbf{r}) = -(\frac{3}{\pi}\rho(\mathbf{r}))^{1/3}\,, \tag{2.32}$$

while for the correlation part one has to fall back on the Perdew-Zunger parametrization of quantum Monte-Carlo data for the electron gas [23]. It is obvious from the discussion till here that for a homogeneous electron gas, the LDA exchange-correlation functional is exact. Despite the fact that for most applications, especially for isolated systems, the electron density differs by a fair margin from that of a homogeneous electron gas, the approximation still produces acceptable and good results. This can be understood from the explanation that the LDA satisfies the sum rule which expresses normalization of the so-called exchange correlation hole [18]. In other words, given that an electron is at the position $\mathbf{r}$, the electron density for the other electrons is depleted near $\mathbf{r}$. A 'hole' in the density distribution $\rho(\mathbf{r}')$. is dug by the electron at position $\mathbf{r}$ due to Pauli principle and electron-electron interaction. It is thus normalized as

$$\int \rho_{xc}(\mathbf{r}, \mathbf{r}')d\mathbf{r}' = -1 \tag{2.33}$$

2.4.2 Overview of the performance of LDA

In a report[29] results showing the success of LDA formalism have listed. In a thumbnail representation, the success story of LDA can be tabulated as the following,

- Binding energies are often better than 1 eV but in some s–d bonded

systems the error can be twice or even three times as large. There is a systematic over binding.

- Equilibrium distances are generally accurate to within 0.1 Å, They are systematically too short. Hence in general it can be said that geometries are accurately computed within this framework.[22]

- Vibrational frequencies are accurate to within 10–20 %. There exist occasional cases with larger errors.

- Charge densities are better than 2 %.

- LDA results are nearly always much better than those of the Hartree–Fock (HF) approximation.

As for the validity of the above observations we can have a look at the following tables in figure 2.2 taken from the works of Muller, Jones and Harris[30]. The results shown here, however, also indicate some problematic deficiencies. Most notable is the systematic overbinding predicted by the LDA, particularly for the s-d bonded systems. Although the overbinding is to a much lesser extent yet is reflected in a small but relatively systematic underestimate of the bonding distances. The following small list gives instances of systems for which the LDA poses some serious problems.

- The transition-metal oxides FeO and CoO are erroneously predicted to be metallic. But, MnO and NiO come out as anti-ferromagnetic insulators in accordance with experiment[31].

- Solid Fe is predicted to be an fcc paramagnet [32] but is a bcc ferromagnet at low temperatures.

- In many semiconductors, the LDA gives the metal-insulator transition at much too large volumes[33].

- The LDA predicts the wrong dissociation limits for a large number of molecules[34].

- The LDA predicts incorrect ground states for many atoms[35].

Table I. Total energies (in eV) of a few atoms.

Atom	LDA	exp
H	13.3	13.6
H^-	14.4	14.4
Al	6567	6592

Table II. Ground-state properties of the molecules H_2O, NH_3, and CO_2, as obtained from the LDA and from experiment. The results are taken from the work by Müller, Jones, and Harris [55]. We assume that the numerical errors involved in obtaining the LDA results are negligible in comparison to the deviation between theory and experiment. The equilibrium distances in Table II are probably exceptions to our assumption because they do not conform to the general expectations of bond distances being too short within the LDA.

	H_2O		NH_3		CO_2	
	LDA	exp	LDA	exp	LDA	exp
d	1.84	1.81	1.94	1.91	2.21	2.20
θ	106	105	108	107	180	180
ω_a	3680	3657	3335	3337	1420	1388
ω_b	1590	1595	820	950	730	667
μ	0.732	0.730	0.564	0.583	0	0

d is the equilibrium distance in atomic units.
θ is the equilibrium bond angle in degrees.
ω_a is the stretching frequency in cm^{-1}.
ω_b is the bending frequency in cm^{-1}.
μ is the dipole moment in atomic units.

Figure 2.2: Ground-state properties of the molecules H_2O, NH_3, and CO_2, as obtained from the LDA and from experiment. It is assumed that the numerical errors involved in obtaining the LDA results are negligible in comparison to the deviation between theory and experiment. The equilibrium distances in Table II are probably exceptions to the assumptions because they do not conform to the general expectations of bond distances being too short within the LDA.

- The LDA gives unstable negative atomic ions in many cases when these are stable[35].

2.4.3 Generalized Gradient Approximations (GGA)

As stated in the previous section, we can understand that although LDA is quite adequate for some cases, yet for most systems a higher accuracy is desired. An error in a binding energy of the order of 20 % or 1 eV is, e.g., not acceptable in the study of chemical reactions. In this field what would be great is the binding-energy errors being of the order 0.05 eV or less. The simplicity of DFT calculational methods as compared to traditional many-body techniques has, however, spawned considerable efforts to improve on

the LDA. Attempts to go beyond the LDA are based either on an improved description of the exchange-correlation hole in real space or on a description of exchange-correlation energies in reciprocal space usually leading to so-called generalized gradient approximations (GGA). In recent years, the largest effort has gone into the reciprocal-space approach which so far has been the most successful ab initio DFT method. It is common and intuitive to consider GGA corrections as some sort of next order corrections to the LDA. In this framework a functional dependence on the gradient of the density is added to ϵ_{xc}, i.e.,

$$E_{xc}^{GGA}[\rho] = \int d^3\mathbf{r}\, \rho(\mathbf{r})\epsilon_{xc}\left(\rho(\mathbf{r}), \nabla\rho(\mathbf{r})\right) d\mathbf{r}\,. \tag{2.34}$$

As reported in [18], compared to the LDA approximation, the error for ion-

The errors (in eV) in the binding energies of the first-row dimers as obtained from different density functionals defined below. Δ is the average absolute error for each functional.

	Li_2	Be_2	B_2	C_2	N_2	O_2	F_2	Δ
LDA	−0.1	0.5	0.8	1.0	1.7	2.4	1.7	1.2
LPM	−0.5	0.3	0.2	−0.2	0.3	1.2	0.7	0.5
PW86	–	–	0.2	−0.1	–	0.7	0.5	0.4
PW91	−0.1	0.3	0.3	−0.1	0.7	1.0	0.7	0.5
B86	−0.1	0.1	−0.5	−0.8	0.2	0.2	0.0	0.3
B I	−0.1	0.1	−0.3	−0.7	0.3	0.3	0.2	0.3
B II	−0.3	–	–	–	0.4	0.8	0.5	0.5
B III	−0.3	–	–	–	−0.1	0.2	−0.1	0.2

LDA the local-density approximation.
LPM the functional by Langreth, Perdew, Mehl and Hu
PW86 the older functional by Perdew and Wang
PW91 the functional by Perdew *et al.* preceding the PBE
B86 an older exchange approximation by Becke plus correlation from Stoll *et al.*
B I the functional of "Becke: Thermo-chemistry I"
B II the functional of "Becke: Thermo-chemistry II"
B III the functional of "Becke: Thermo-chemistry III"

Figure 2.3: The errors (in eV) in the binding energies of the first-row dimers as obtained from different density functionals defined below. Δ is the average absolute error for each functional.

ization energies is reduced by factors of 3-5 for the GGA corrections. In the DFT community one can find several different GGA functionals. An illustrative comparison is made in [24]. The table in Figure 2.3 from the article of Von Barth[29] gives a comparative idea of the accuracy of the corrective functionals as well. Perdew, Burke, and Ernzerhof[25] have described a functional form (PBE) that has several attractive features. The accuracy of the

PBE functional for atoms and molecules has been compared with results of other popular functionals like LSD, BLYP, and B3LYP[40] by Ernzerhof and Scuseria[26]. The PBE functional performed as well as B3LYP for the properties considered by these authors. Generalized gradient approximations generally lead to improved bond angles, lengths, and energies. In particular, the strengths of hydrogen bonds and other weak bonds between closed shell systems are significantly better than local density results. However, the self interaction problem remains, and some asymptotic requirements for isolated atoms are not satisfied.

2.4.4 Meta-GGA

Following the development of GGA, the next steps in the gradient approximations were taken with a view to incorporate the kinetic energy density. A version based on the PBE form was described by Perdew et.al.[28]. This form includes the kinetic energy density for the occupied Kohn Sham orbitals. However, this and other forms initially developed included parameter(s) found by fitting to experimental data. This last feature was avoided in the recent work of Tao, Perdew, Staroverov and Scuseria[37][36] whose form satisfied the requirement that the exchange potential be finite at the nucleus for ground state one and two electron densities. Extensive numerical tests for atoms, molecules, solids, and jellium surfaces showed generally very good results.

2.4.5 Hybrid Schemes : Combination of Hartree-Fock and DFT

In many reports it is mentioned just how poor the exchange energy differences could be between states whose wave functions have different nodal structures. It has also been noted for many years[38] that errors in the local density descriptions of exchange and correlation tend to balance. Probably the final step in constructing the correct functional is to come up with the Hybrid Functional. Hybrid functionals are a section of approximations to the

functional in DFT that blend a portion of Exact Exchange from Hartree-Fock (HF) theory with exchange and correlation from other sources (ab initio, such as LDA, or empirical). This suggests that a combination of Hartree-Fock exchange and DFT calculations could be useful as in the following expression,

$$E_{XC}^{hybrid} = \alpha E_X^{HF} + E_C, \tag{2.35}$$

where α can be chosen to satisfy the particular criteria. A formal justification for such hybrid schemes was given by Gorling and Levy[39]. Among the ones which are used a lot these days in the community B3LYP[40] is one. Hybridization with HF provides a simple scheme for improving many molecular properties, such as atomization energies, bond lengths and vibration frequencies. It is to be noted here that those calculations which are done with the first generation functionals enjoy a further improvement in accuracy. Enrique R. Batista[41] and his co-workers made a benchmark calculations as to have a comparative idea about the performance of the exchange correlation functionals. According to their report the Diffusion Monte Carlo (DMC) methods give the highest accuracy in terms of the calculations of interest. Hence their comparing standard for all the exchange-correlation functionals is the set of results from DMC. It goes without saying that DMC is very expensive as far as computation time is concerned. It is an attempt to summarize the comparative performances of the hybrid pseudopotentials. According to their report[41] the Heyd-Scuseria-Ernzerhof [42](HSE) functional has been found to be in excellent agreement with their DMC benchmark (Figure 2.4). A comparative idea has been put into paper between the various hybrid functionals like Perdew-Wang-91(PW91)[27], Tao-Perdew-Scuseria-Staroverov [37](TPSS) and the previously mentioned functionals. The comparative idea shows that the hybrid functional like HSE significantly improves the agreement between DFT and DMC (DMC being established as the most accurate of all). This part of the research is still pretty open and further works are still going on in trying to figure out the correct functional. As for concluding remarks we can have a look at figure 2.5 where the Jacob's ladder is given describing the order of accuaracy for different functionals in practice.

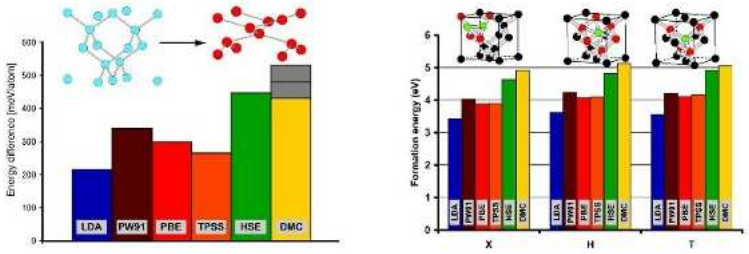

Figure 2.4: (a)Difference in energy per atom in the diamond phase and in β tin phase of Si. The HSE functional agrees with the DMC results while the other functionals underestimate the energy difference (b)Formation energy of the three lowest energy single interstitials in silicon (X, H, and T).Comparison to the DMC results demonstrate a steady improvement of the accuracy of the functionals as the order of density expansion increases, with quantitative agreement for the hybrid HSE functional.[41]

The development of approximations to the exchange-correlation functionals over the past 20 years has improved the performance of DFT calculations, and many scientists in the community think that progress up the Jacob's ladder will continue until energy differences can be determined to within 1 kcal/mol ("chemical accuracy"). Of course the numerical cost increases as one climbs, and this may not necessarily bring more information.

2.5 Pseudopotentials

Pseudopotentials were originally introduced to simplify electronic structure calculations by eliminating the need to include atomic core states and the strong potentials responsible for binding them. Most physical and chemical properties of crystals depend to a very good approximation only on the

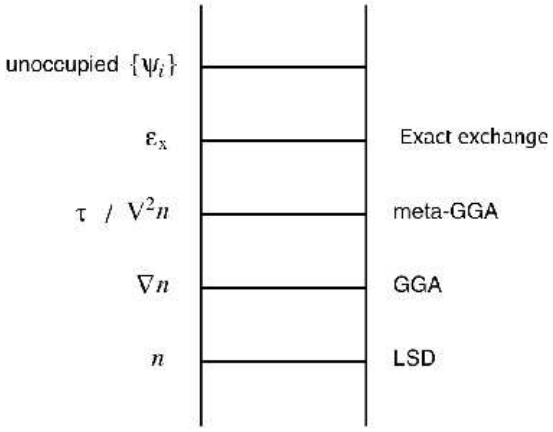

Figure 2.5: Jacob's ladder of DFT schemes according to Perdew and collaborators.

distribution of the valence electrons. The core electrons do not participate in the chemical bond. They are strongly localized around the nucleus, and their wave functions overlap only very little with the core electron wave functions from neighboring atoms. Hence, the distribution of the core electrons basically does not change when the atoms are placed in a different chemical environment. It is thus justified to assume the core electrons to be "frozen" and to keep the core electron distribution of the isolated atom in the crystal environment. This is essentially a non-technical description of the otherwise technical approach known as Frozen Core approximation. The first advantage of the frozen–core approximation is that now less electrons have to be treated and less eigenstates of the Kohn–Sham equations have to be calculated. Secondly the total energy scale is largely reduced when the core electrons are removed from the calculation which makes the calculation of energy differences between atomic configurations numerically much more stable and tractable. Figure 2.6 is the schematic illustration of an atomic all–electron wave function and the corresponding atomic pseudo wave function together with the respective external Coulomb potential and pseudopotential. Φ_{PS} and V_{PS} are the pseudo wave function and the pseudopotential, where as the solid line is Φ_{AE}, the actual wave function. In the scope of the present thesis

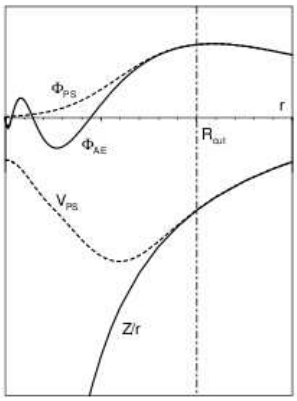

Figure 2.6: Schematic illustration of an atomic all–electron wave function (solid line) and the corresponding atomic pseudo wave function (dashed line) together with the respective external Coulomb potential and pseudopotential.

let me discuss some of the important classes of pseudopotentials. depending on the properties they exhibit they can classified and used in various schemes.

2.5.1 Normconserving Pseudopotentials

The pseudopotentials we use today are constructed from ab initio calculations for isolated atoms. The Kohn-Sham equations for a single atom are to be solved for a single atom of the chemical species for which we would like to generate a pseudopotential. This can be done without much of a problem since due to the spherical symmetry of atoms the wave functions can be written as a product of a radial function and a spherical harmonic. The Schroedinger equation then reduces to one dimensional differential equations for the radial functions which can be integrated numerically. Figure 2.6 represents such a typical result for a radial function from such an "all–electron" atom calculation together with the corresponding external Coulomb potential. The aim now is to replace the effective all–electron potential within a given sphere with radius R_{cut} by a much weaker new potential with a node less ground state wave function to the same energy eigenvalue as the original all–electron state which matches exactly the all–electron wave function

outside R_{cut}. An important aspect here is to understand why should this happen at all? We can notice that the radial Schroedinger equation for a constant potential and fixed energy E to the angular momentum l is a one-dimensional ordinary linear second order differential equation which has two linear independent solutions. But only one of the two solutions, $\Phi_l(r)$, is regular for $r \to 0$. We have to see that if we do not change the logarithmic derivative

$$L_l(E) = \frac{d}{dr} ln\Phi_l(r;E)|_{R_{cut}} = \frac{\Phi_l'(R_{cut};E)}{\Phi_l(R_{cut};E)} \tag{2.36}$$

while changing the potential inside the atomic sphere, then the wave functions outside the sphere remain unchanged. For the energy of the eigenstate of our all electron calculation E_l^{AE} the procedure is as explained in the following section. The all electron wave function Φ_l^{AE} inside the sphere is replaced by an arbitrary smooth nodeless function Φ_l^{PS} with the equivalent logarithmic derivative at R_{cut} as the original all electron function. Since Φ_l^{PS} is nodeless by construction the radial Schroedinger equation can be readily inverted with this new function and with the eigenvalue E_l^{AE} of the all electron calculation to get the potential that has exactly the required property for the more complicated case at hand. A lot of recipies are in publication with which this can be implemented[44][45][46][47][48][49][51]. One further important requirement is the essential normconserving condition. In simple words this means that the all electron and the pseudo wave function inside the atomic sphere must have the same norm to guarantee that both wave functions generate identical electron densities in the outside region. In addition to this condition, the additional degrees of freedom in generating a suitable pseudopotential can be employed to make the pseudo wave functions as smooth as possible[52]. Evidently till now the above arguments claim the existence of the logarithmic derivative of the effective all electron potential only for the reference energy E_l^{AE}. Now however, if the chemical environment of the atom in consideration is changed, evidently the eigenstates will be at a slightly different energy. Hence of course, for a pseudopotential to be useful it has to be able to reproduce the logarithmic derivative of the all electron potential over a whole energy range. The transferability of the pseudopotential

to other chemical environments depends on this width of the energy range. As reported in various articles, in particular the normconserving condition guarantees such a transferability. And again, the pseudopotential should be as *soft* (technical in sense) as possible. The term *soft* means that the number of plane waves required to expand the pseudo wave functions should be as small as possible. Both properties, transferability and softness, are closely related to the cutoff radius R_{cut}, and compete with each other. Reports claim that low cutoffs give pseudopotentials with a very good transferability[50]. However, increasing R_{cut} makes the pseudopotentials softer. Usually compromising balance between the two requirements is to be struck with. An upper limit for R_{cut}, is given by half the distance to the next nearest atom in the configuration for which one may want to apply the pseudopotential. If this value is exceeded, we can see that there will not be any region between the neighboring atoms left where we will recover the true all electron wave functions. Hence, we can not expect anymore to get an accurate description of the chemical bond between the two atoms.

2.5.2 Fully Nonlocal Pseudopotentials

From (2.36) it is evident that the logarithmic derivative depends on the angular momentum l and hence a separate pseudopotential $V_l^{PS}(r)$ for each value of l needs to be constructed. This would call for the fact that, the full pseudopotential for our atom therefore has to be a nonlocal operator. The following equation describes the way in which it is done.

$$\hat{V}_{PS} = V_{loc}^{PS}(r) + \sum_l V_{nl,l}^{PS}(r)\hat{P}_l, \quad V_{nl,l}^{PS}(r) = V_l^{PS}(r) - V_{loc}^{PS}(r). \tag{2.37}$$

The pseudopotential $V_l^{PS}(r)$ pertaining to one specific angular momentum (usually the highest value of for which a pseudopotential has been generated) is taken to be the local part of the pseudopotential. The nonlocal components $V_{nl,l}^{PS}(r)$ are defined as the difference between the original l dependent $V_l^{PS}(r)$ and this local part of the pseudopotential. As we know by now that all $V_l^{PS}(r)$ are identical beyond R_{cut}, hence we understand here that the nonlo-

cal components of the pseudopotential are strictly confined within R_{cut}. $\hat{P}_l$ is a projection operator which picks out the l^{th} angular momentum component from the subsequent wave function. This construction guarantees that when the full pseudopotential operator V_{PS} is applied to a general wave function each angular momentum component of the wave function experiences only its corresponding part $V_l^{PS}(r)$ of the potential. Since the projection operators act only on the angular variables of the position vector $\mathbf{r}$ the pseudopotential is still a local operator with respect to the radius . The form (2.37) is therefore called a semilocal pseudopotential. As reported, for numerical efficiency however, it would be better to have the pseudopotential in a fully nonlocal form as described in the article by Kleinman and Bylander[53]. In the following section the technique as shown by Vanderbilt[54] to construct a fully nonlocal pseudopotential, is discussed.

2.5.3 Vanderbilt Ultrasoft Pseudopotentials

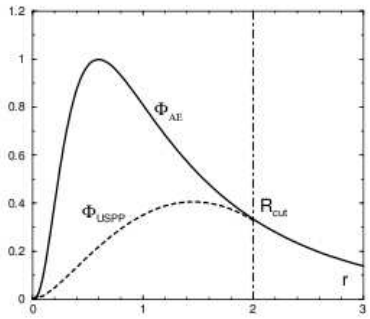

Figure 2.7: Illustration of a strongly localized valence wave function inside the atomic core region and the modified wave function in the Vanderbilt ultrasoft pseudopotential scheme.

The general view is that it is very difficult to treat within a pseudopotential scheme all elements with nodeless valence states (in particular those with $2p$ and $3s$ valence electrons). For those elements the pseudo and the all electron wave functions are almost identical. Since these valence electrons are strongly localized in the ionic core region, many plane waves are required for

a good representation of their wave function which often makes calculations for such elements highly expensive. In consequent works[54][55] Vanderbilt has introduced a new type of pseudopotentials the so-called ultrasoft pseudopotentials, in which the normconserving requirement has been relaxed. Instead of representing the full valence wave function by plane waves, only a small portion of the wave function is calculated within the Vanderbilt ultrasoft pseudopotential scheme (as shown in figure 2.7). This allows to reduce substantially the plane wave cutoff energy in the calculations. However there is a price to pay in terms of complications in calculations. It is because now the Fourier representation of the Kohn Sham equation becomes more complicated. First, when the electron density is calculated the part of the electron distribution has to be added back (which is represented by the difference between the solid and the dashed line in figure 2.7, the so-called augmentation charges). Secondly, due to the relaxation of the normconserving condition, the Bloch eigenstates will not be not orthonormal anymore. An overlap matrix has to be introduced and the eigenvalue problem of the Fourier representation of the Kohn Sham equations will transform into a generalized eigenvalue equation. Next, the nonlocal part of the pseudopotential becomes density–dependent now. Lastly ,due to these modification additional terms in the force calculations have to be evaluated. However, the report claims that the gain in computational cost by lowering the plane wave cutoff energy outweigh in many cases the additional computational effort which is required by these modifications.

With all those theoretical concepts discussed it is now time to talk about the present day theoretical models with which people are trying to tackle the probelm of charged defects in solids. It is also important to know the experimental techniques involved in the study of point defects. With that view we move on to the next chapter.

Chapitre 3

Dans ce chapitre, les différentes techniques utilisées pour traiter les défauts chargés dans les solides sont abordées en détails. Je commence avec les techniques expérimentales déjà utilisées dans le silicium depuis plusieurs années, et détaille les approches utilisées pour chaque type de défauts. Ensuite, j'aborde les différentes méthodes théoriques. Les différences dans le traitement de l'électrostatique sont rapportées et les avantages et inconvénients des différentes méthodes sont prises en considération, montrant la motivation de d'avoir une autre méthode. Parmi les méthodes décrites, on trouvera celle de Makov-Payne, celle de Schultz, celle de Freysoldt ou celle de Dabo.

Chapter 3

State of the Art: Experiments and Theory

3.1 Introduction

The success of the Density Functional Theory (DFT) as a tool for ab initio calculation of various properties of solids has inspired scientists to use it even to study defects (both charged and uncharged) in metals and semiconductors. In this chapter I wish to give a moderate review of the most widely used and successful techniques in calculating the potential and consequently the energies and forces of systems with charged defects. To model a localised defect nested in the bulk host, the supercell approximation is employed by most of the calculations. Reports of increasing usage of this method to predict the structures of crytalline solids and even an extension to the aperiodic systems of defects and molecules are found since a long time now [60][61][62]. According to the available reports it is easier to deal with the uncharged point defects in metals and semiconductors with this method than to deal with defects in ionic insulators. In reality all the approximations that goes into the calculations viz. the used pseudopotentials, the choice of exchange-correlation functionals or the shape and size of the supercell, can account for a difference in the predicted physical properties. Among the few important causes for this trouble at hand are the defect defect interaction

due to localised charge and the self interaction of the strongly localised defect states. Hence it is arguably evident that the formation energies thus inferred through this periodic techniques may not find a strong ground in terms of theoretical completeness and comparison with the experimental results. In this chaper I would discuss in brief the various modifications in the calculations undertaken so as to find the correct way to calculate the formation energies of the charged defects in bulk systems. It is notworthy here to mention that broadly we can tackle the problem at two different points in the run of calculations. We can either start off with fixing the potential of the system with physical arguments and consequently generate an accurate density for the self-consistent loop in the DFT calculations or we can incorporate correction terms to the finally calculated total energies. It is worth mentioning at this point that the total energies that are calculated from an inaccurate and approximate potential are bound to deviate from the true values (experimental in all physical cases). We will have an overview in this chapter of all the formalisms and derivations of various correction factors.

3.2 Experimental Methods To Study Point Defects

Before taking a plunge into the various theoretical methods of modern day to handle the charged point defects it can be a interesting as well to know few important experimental techniques that are used in abundance to study point defects. The most popular set of experiments which where done to study the defects in silicon were done by Corbett and Watkins[3][63]. Those experiments were carried out with the methods known as Electron Paramagnetic Resonance (EPR) or Electron Spin Resonance (ESR). The theory of such experiments is based on the fact where the atoms of a solid exhibit paramagnetism as a result of unpaired electron spins. Here transitions can be induced between spin states by applying a magnetic field and then supplying electromagnetic energy, usually in the microwave range of frequencies. The resulting absorption spectra are described as electron spin resonance (ESR)

or electron paramagnetic resonance (EPR). ESR has also been used as an investigative tool for the study of radicals formed in solid materials, since the radicals typically produce an unpaired spin on the atom from which an electron is removed. The study of the ESR spectra has been very effective for the radicals produced as radiation damage from ionizing radiation. Study of the radicals produced by such radiation gives information about the locations and mechanisms of radiation damage. The interaction of an external

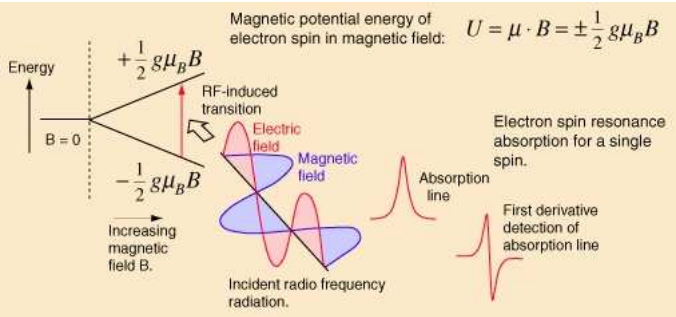

Figure 3.1: Schematic diagram of the theory behind the ESR experiment.

magnetic field with an electron spin depends upon the magnetic moment associated with the spin, and the nature of an isolated electron spin is such that two and only two orientations are possible. The application of the magnetic field then provides a magnetic potential energy which splits the spin states by an amount proportional to the magnetic field which is nothing but the Zeeman effect. Then radio frequency radiation of the appropriate frequency can cause a transition from one spin state to the other. The energy associated with the transition is expressed in terms of the applied magnetic field B, the electron spin g-factor g, and the constant μ_B which is called the Bohr magneton. In their work Corbett and Watkins studied the EPR spectrum of the silicon vacancies and reported the geometry, energy of formation and stability of the different types of point defects (vacancies). Another technique which they used was the Electron-Nuclear Double Resonance (ENDOR). ENDOR is a magnetic resonance spectroscopic technique for the determination of hyperfine interactions between electrons and nuclear spins. There are two principal techniques. In continuous-wave ENDOR the intensity of an electron

paramagnetic resonance signal, partially saturated with microwave power, is measured as radiofrequency is applied. In pulsed ENDOR the radiofrequency is applied as pulses and the EPR signal is detected as a spin-echo. In each case an enhancement of the EPR signal is observed when the radiofrequency is in resonance with the coupled nuclei. George Feher[64] introduced this technique in 1956 so that interactions which are not accessible in the EPR spectrum could be resolved.

A method to calculate the formation energies of the point defects is to directly calculate the type and concentration of the defects. This was put forward by the works of R. O. Simmons and R. W. Balluffi[65]. Here it is necessary to measure the change of the lattice constant a, i.e. Δa, and the change in the specimen dimension, Δl, (one dimension is sufficient) simultaneously as a function of temperature. Which in other words is also called the *differential thermal expansion method*. Here l is the length of the specimen which can be thought as a function of the temperature and the defects i.e. l(T, defects). The basic idea is that $\Delta l/l$–$\Delta a/a$ contains the regular thermal expansion and the dimensional change from point defects, especially vacancies. This is so because for every vacancy in the crystal an atom must be added at the surface; the total volume of the vacancies must be compensated by an approximately equal additional volume and therefore an additional Δl. If we subtract the regular thermal expansion, which is simply given by the change in lattice parameter, whatever is left can only be caused by point defects. The difference then gives directly the vacancy concentration. Some of the other direct methods for measuring point defect properties can be classified as the following.

- There can be measurements of the resistivity. This method is pretty suitable to ionic crystals if the mechanism of conduction is ionic transport via point defects. But one may never know for sure if what is being measured is actually the intrinsic equilibrium because "doping" by impurities may have occurred.

- Measuring specific heat as a function of T is another method. While there should be some dependence on the concentration of point defects,

it is experimentally very difficult to handle with the required accuracy.

- Measuring electronic noise can also be a direct method in this category. This is a relatively new method which relies on very sophisticated noise measurements. It is more suited for measuring diffusion properties, but might be used for equilibrium conditions, too.

All the methods described above are for the equilibrium point defects. One must undertake Quenching Experiments for the non-equilibrium point defects. The basic idea behind these techniques is simple. If one has more point defects than what one would have in thermal equilibrium, it should be easier to detect them. There are several methods, the most important one being quenching from high temperatures. The general methodology is as follows.

- A wire of the material to be investigated is heated to some desired (high) temperature T in liquid and superfluid He II (i.e. a liquid with somewhat large heat conduction) to the desired temperature (by passing current through it). Surprisingly this is easily possible because the He-vapor produced acts as a very efficient thermal shield and keeps the liquid He from exploding because too much heat is transferred.

- After turning off the heating current, the specimen will cool extremely fast to He II temperature ($> 1K$). There is not much time for the point defects being present at the high temperature in thermal equilibrium to disappear via diffusion; they are, for all practical purposes, *frozen-in*. The frozen-in concentration can now be determined by e.g. measuring the residual resistivity of the wire.

- The residual resistivity is simply the resistivity found around 0 K. It is essentially dominated by defects because scattering of electrons at phonons is negligible.

A relatively new way of looking at point defects is to use the scanning tunneling microscope (STM) and to look at the atoms on the surface of the sample. This idea is not new actually. Before the advent of the STM field ion

microscopy was used with the same intention, but experiments were (and are) very difficult to do and severely limited. One idea is to investigate the surface after fracturing the quenched sample in-situ under ultra-high vacuum (UHV) conditions. This would give the density of vacancies on the fracture plane from which the bulk value could be deduced. Although in these experiments the vacancies can be seen, but there are other problems to tackle with. The image changes with time - the density of point defects goes up.
In a nutshell I have tried to give an overview of the experimental techniques that are involved in detecting the various properties of defects in the solids. From the next section we would concentrate only on the theoretical models to study defects in general.

3.3 Theoretical Methods To Study Point Defects

3.3.1 Treatment of Makov and Payne

In their article G.Makov and M.C.Payne[66] explained in length the technique of using Periodic Boundary Conditions (PBC) for different cases of practical theoretical interest. They have argued the validity of using PBC for calculations in solids on grounds like (i) ease of implementation in the calculation (ii) compatibility with plane-wave expansions and consequent simple calculations of forces in molecular dynamics simulations. (iii) availability of an unified scheme for both periodic and aperiodic systems. In the article they have proposed a detailed description of the electrostatics of the system dealt with. The need for the correct electrostatics is felt as the convergence of the total energy, with the increase of the size of the supercell, is determined by the longest-ranged forces. Those forces are indeed electrostatic in nature. The elastic forces can also be long ranged in solids and they are also treated in the similar fashion in this particular report. In principle this work is a continuation of the works by Leeuw[67] et al. The idea is to calculate the total energy as correctly as possible because all the other physical quantities

are derived from the energy via the variational principle. For aperiodic systems using PBC, one is only interested in the energy, E_0 in the limit $L \to \infty$, where L is the linear dimension of the supercell. The energy calculated for a finite supercell $E(L)$ differs from E_0, because of the spurious interactions of the aperiodic charge density with its images in the neighbouring cells. The first case to investigate is the case with Neutral molecular species.

Neutral molecular species

Here for simplicity it is considered that the entire molecular charge density is contained in the supercell. In practice, the electron density decays exponentially away from the molecular species and the supercell need only be large enough for the density at the surface of the cell to be in this regime. As reported the energy is absolutely convergent for the isolated molecule which has no dipole moment. A careful conjecture about the nature of the asymptotic behaviour of the energy would show that the energy will be,

$$E(L) = E_0 + O(L^{-5}). \tag{3.1}$$

For an isolated neutral molecule that has a dipole moment the scenario is of course different as the order of summation of the electrostatic sum should be chosen with a bit more care. For an infinite lattice as considered in this type of formalism that sum is not well defined. Hence the choice of the summation area should be more of convenience with respect to the extent of the dipole moment. In this case of course one finds the presence of a dipole dependent term. It is also to be noted that for an aperiodic system, the absence of this term will not change the value of energy in the limit $L \to \infty$, as the extra term is $O(L^{-3})$. The results (figure 3.2) of a calculation from their article show that energy calculated without the dipole term converges slowly in comparison to the one, done with the dipole term. Another interesting observation can be mentioned here. In general the dipole moment is reported to be ill defined in PBC[68]. In principle, in a periodic solid, all choices of supercell geometry relative to the charge distribution should give the same energy. The electrostatic energy functional as menthioned in [66] infers that

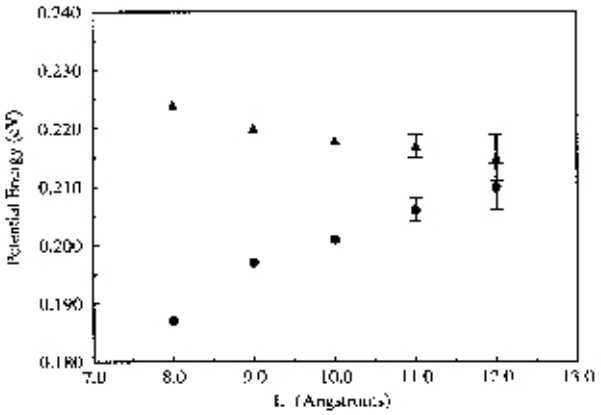

FIG. 2. The potential energy of stretching a NaCl molecule by 0.3 A from equilibrium calculated for cubic supercells of side L. The triangles refer to the electrostatic energy functional in Eq. (8), while the filled circles refer to the same functional without the dipole term.

Figure 3.2: The energy calculated without the dipole term converges slowly in comparison to the one, done with the dipole term

different choice of the supercell will give different values of the dipole moment. This is the manifestation of the fact that an infinite periodic solid with a dipolar basis will not have a well defined energy. The limit $L \to \infty$ dictates the choice of the necessary supercell geometry. The supercell then must create the picture of the aperiodicity in the cell as it would be in the bulk. This is indeed necessary for the dipole moment to be invariant. For the case considered in [66] the shape of the supercell is chosen to be a cube as the result implies that dipoles on a cubic lattice do not interact and hence the convergence of the energy would be $O(L^{-5})$.

Nonneutral molecular species

Systems dealing with charged impurities or vacancies in crystalline solids would call for total energy calculations in a periodically repeated electrically charged system. And of course the value of the total electrostatic energy diverges. In this scenario what is considered is the original charged system

immersed in a Jellium background, so the net charge is zero[62]. Then again one can fall back to the procedure undertaken previously for the neutral molecular species. The interaction between the Jellium background and the charged species will decrease with the cell size and hence the convergence will be slow, having a form of a power law in L. Evidently the charge density of the immersed system consists of the density of the charged species and Jellium density. This density again can be thought of as a contribution of two charge densities giving rise to self interactions and an interaction with each other. If we consider a charge placed at a particular point inside the supercell, the self interaction of that charge will give rise to the term more well-known as the Madelung energy of a lattice of point charges immersed in a neutralizing Jellium.

$$E_{Madelung} = -\frac{q^2\alpha}{2L}, \tag{3.2}$$

where α is the lattice dependent Madelung constant. The mutual interaction of the charge densities will also give rise to a very important term. As the Jellium density depends on the supercell size hence this energy does not converge as the previous one. The form includes a quadrupole term signifying the interaction between the neutral defects. At the end what we get are two correction factors. The assymptotic result for the total electrostatic energy of a charged species on a cubic lattice finds the form as

$$E = E_0 - \frac{q^2\alpha}{2L} - \frac{2\pi qQ}{3L^3} + O(L^{-5}), \tag{3.3}$$

where Q is the quadrupole moment and E_0 is the desired electrostatic energy of the isolated species. Results with ionization potential of a Mg atom are shown in Figure 3.3. With all the corrections applied, it is evident that the convergence is faster.

Aperiodic system in condensed matter

For aperiodic system in condensed matter the electrostatic energy can be considered to be the sum of three major interactions. (1) The periodic charge density interacting with itself. This is independent of L. (2) Interaction

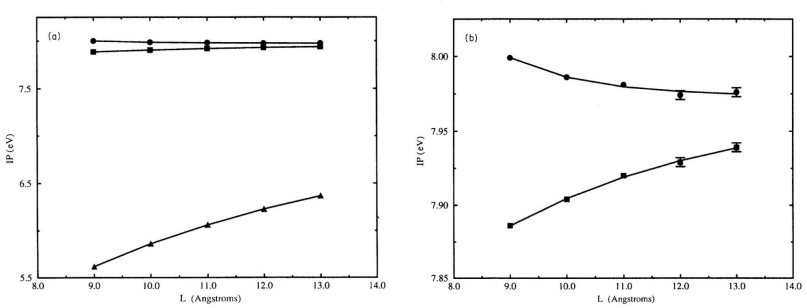

Figure 3.3: (a)The ionization potential of a Mg atom calculated in cubic supercells of side L (triangles), The same after including Madelung correction (squares), The same after the entire correction factor is applied (circles) (b) Expanded section of (a)

between periodic and aperiodic charge densities. This is also independent of L.(3) The L dependent aperiodic densities located in different supercells. Here also the main motive is to chalk out the asymptotic dependence of the aperiodic density and its multipoles on the supercell dimensions. The first source of L dependence is the one already discussed above, the case of changes in the charge distribution induced by the interactions of the aperiodic charge with its images. The second reason for the L dependence is the dielectric response of the periodic medium to the aperiodic density. This is treated nonelectrostatically and a correction factor containing the dilectric constant is incorporated in the spirit of the arguments of Leslie and Gillan. The term contains a quadrupole moment which is an artifact of the aperiodic density whereas the dielectric constant is coming from the periodic density. With this correction the final form of the total electrostatic energy becomes

$$E = E_0 - \frac{q^2\alpha}{2L\epsilon} - \frac{2\pi qQ}{3L^3\epsilon} + O(L^{-5}). \tag{3.4}$$

In this case though, Q is the second radial moment only of that part of the aperiodic density that does not arise from the dielectric response or from the the Jellium. It is worthy of mention here that both Q and ϵ are properties of the aperiodic density and the periodic density respectively.

3.3.2 Treatment of Schultz

A careful analysis by Peter A. Schultz[69] deals with some of the problems in the Makov Payne formulation and employs a different method to avoid them. Schultz concludes in his analysis that the Jellium approach fails to represent the topology of the local electrostatic potential accurately. In fact he mentions in his article that the inaccuracy is to such an extent that for typical semiconductors with sufficient band-gap energies the results obtained in the Jellium approach are delusive. It is reported that tails of the potentials generated by local electrostatic moments of the defect overlap cell boundaries, corrupting the local potential of the "isolated" defect. For supercells separated by vacuum gaps, e.g. molecules or repeated slabs, it is possible to avoid, rigorously, the error of interacting multipole moments. He proposes a technique as a generalisation of the Local Moment Counter Charge (LMCC) method [70] to calculate a more accurate electrostatic potential within the supercell. In this article the error in the predicted potential of the Jellium approach in comparison to his LMCC method is also reported. The main problem is that the local potential incorporates an error with the potential tails of the periodic image charges which the compensating Jellium charge does not take into account. The results show that the error in the potential for semiconductors like charged Si and Ge are in the order of their band-gaps viz. 1.00 eV for Si 64 atom cubic supercell and 0.62 eV for Ge 216 atom cubic supercell. Increasing the cell size to reduce the Jellium potential error is considered impractical in this article. In Figure 3.4 the error in the computed electrostatic potential in a supercell calculation using jellium as the neutralizing agent has been shown. As reported for vacuum gap supercells, the LMCC method[70] is an alternate solution to Poisson's equation that exactly removes the spurious effects on the potential (and energy) of multipole moments in the supercell. According to this formulation of Schultz, a model density composed of a Gaussian array of charges is constructed in conformity to the moments of the local system. Hence the system's total charge distribution comprises two parts, one part from this model density, and another remaining half, which is devoid of any moments. Hence the potential for this

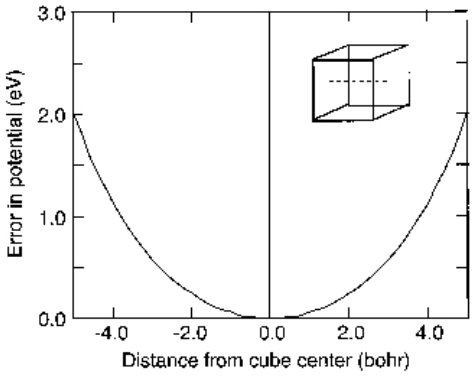

Figure 3.4: Error in the computed electrostatic potential in a supercell calculation using jellium as the neutralizing agent. The exact potential is computed analytically for a Gaussian density distribution in a cube, and using an FFT after neutralization by jellium. The difference is plotted along a line connecting the centers of opposite faces and going through the center of the cell (inset).

part can easily be calculated with sufficient accuracy employing PBC and Fast Fourier Transformation (FFT). The model density is treated as isolated and only then the potential is calculated. Evidently the total potential is the sum of these two, viz. the PBC potential and the Local Moment(LM) potential,

$$\phi(r) = \phi'_{PBC} + \phi_{LM} \tag{3.5}$$

The idea is to create an isolated defect or molecule and blending the boundary conditions to achieve the solution to the Poisson's equation. For charged defects in Si the potential ϕ_{LM} is found to be discontinuous and this phenomenon needs to be avoided. The $\frac{q}{r}$ long range asymptotic potentials misalign at cell boundaries. Again if the LMCC charge cannot be fixed by symmetry, the multipole moments of the defect are to be exactly determined. In reality these are ill defined in bulk. Lastly the interaction of the LMCC charge with the bulk material is to be taken into account. The potential of an isolated charged defect extends outside the local cell volume and interacts with bulk, but the LMCC potential is truncated at the cell boundary. The Wigner-Seitz cell geometry around the position of each LMCC charge takes

care of the discontinuity in the potential. The multipole moments of the defect can be calculated in two halves, contributions coming from the sum of the spherical(momentless) atom charge distributions and the cell-dependent moments of the perfect crystal reference and the defects. The last part of this technique involves the interaction of the local charge with the bulk medium. Schultz shows two Madelung integrals accounting respectively for (i)the interaction between the LMCC and the potential from the crystal density and (ii) the interaction between the LMCC potential and the crystal density in WS volume.

$$E_M = \int n_{LM}(r)\delta\phi^{ref}(r) - \int_{WS} \phi_{LM}(r)\delta\rho^{ref}(r). \tag{3.6}$$

The first term is a Madelung integral over all space between the LMCC and the potential $\delta\phi^{ref}(r)$ from the crystal density $\delta\rho^{ref}(r)$ The second term subtracts a local Madelung integral of the LMCC potential and a crystal density in the WS volume. The energy of the dielectric response of the bulk is calculated in same spirit as in the approach of Leslie and Gillan[71]. The claim in this method is that it eliminates the spurious interaction of charges between supercells and helps to compute the properties of charged defects in bulk systems with the help of correctly computed electrostatic potential. Results from three series of calculations are presented in the paper (figure 3.5): a 1D single strand of alternating Na and Cl, a 2D square single sheet of NaCl, and 3D bulk NaCl. Also from Figure 3.4 it is to be noted that the resulting energy error in the jellium-based calculation is not linear in the charge. Doubling the charge doubles the error in the computed potential, and the energy is the integral of these two. Hence, the error in total energy calculations scales at least as q^2 , even neglecting the consequences of screening. If results for singly charged systems bear uncertainties on the order of a band-gap energy, results for multiply charged defects will be much worse. In this study though the first principle calculations of total energetics of charged vacancies in NaCl that accurately embody the correct electrostatic interactions appropriate to isolated defects is reported with some criticism of the Makov Payne formalism. It is demonstrated that the standard recipe

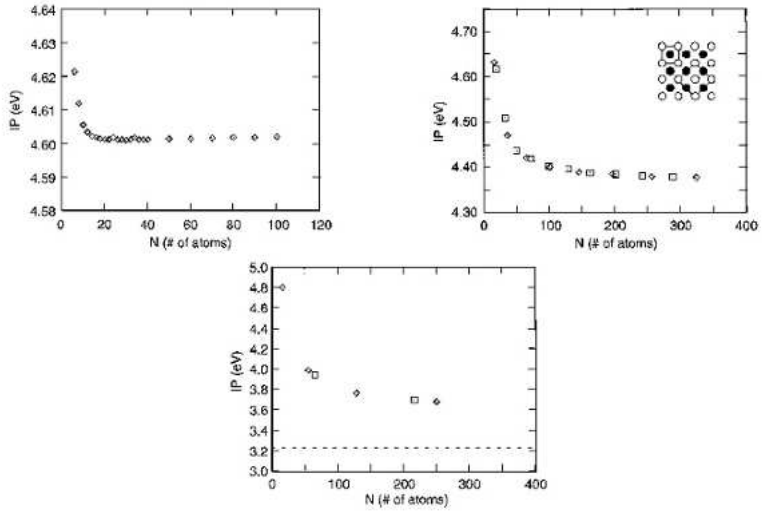

Figure 3.5: (a) The computed IP for a chlorine vacancy in a 1D NaCl chain, as a function of cell size. (b) The computed ionization potential for a chlorine vacancy in a 2D square NaCl sheet, as a function of cell size. Points from polar NXN cells (inset: smaller $1X1$ two atom cell) are plotted with squares, and nonpolar $N\sqrt{2}XN\sqrt{2}$ cells (inset: larger rotated four-atom $\sqrt{2}X\sqrt{2}$ cell) with diamonds. (c) The computed ionization potential for a chlorine vacancy in bulk NaCl, as a function of cell size. Points from nonpolar cubic cells are plotted with squares, and points from polar fcc cells with diamonds. The dashed line denotes the extrapolated asymptotic limit of the IP.

for studying charged defects in bulk systems, using jellium as a neutralizing agent in supercell calculations, incorporates an error in the computed electrostatic potential comparable to the energy scale of physical interest. The generalized LMCC approach presented here claims to eliminate the unphysical interaction of charges between supercells and enables the computation of the properties of charged defects in bulk systems using the correct local electrostatic potential.

3.3.3 Treatment of Freysoldt, Neugebauer and Van de Walle

In their report Freysoldt[72] et. al. argues against the formalisms of the correction factors of Makov and Payne and even the potential correcting schemes Schultz. They argue that for realistic defects in condensed systems, however, the quadrupole moment correction term as stated in previous works [66] do not always improve the convergence[73][74][75]. They have shown that the Madelung correction greatly overshoots for small supercells. Alternatively they have also argued against the technique of Schultz type formulation where several scientists have suggested to truncate or compensate the long-range tail of the bare Coulomb potential during the computation of the electrostatic potential itself in order to remove the unwanted interactions. According to Freysoldt[72] et. al. this scheme when applied to solids suffers from ignoring the polarization outside the supercell. In their approach they put forth a new idea which they claim (i) is based on a single supercell calculation, (ii) does not rely on fitted parameters, (iii) derives from an exact expression applying well-defined approximations, and (iv) sheds light on the problems encountered in previous schemes. The central idea of this type of method revolves around the accurate calculation of the potentials and proper treatment of the defect-defect interactions. The creation of the charged defects is broken into three building steps which would account for the final expression of the energy. First the charge for a single defect is introduced by adding or removing electrons. At the same time all the other electrons are frozen. This step results in an unscreened charge density. Obviously enough the following step would incorporate all the other electrons to screen this introduced charge. Lastly an artificial periodicity is imposed upon along with the addition of a compensating homogeneous background charge. With all these inputs and considering the unscreened defect charge to be fully contained in a convenient zone of the supercell the screened lattice energy of the charge with the compensating background is formulated out. Here one must take care that when the electrons are allowed to screen the introduced charge, the electron distribution forces an alteration in the elec-

trostatic potential V_{defect} with respect to the neutral defect, which is given by,

$$V_{q/0}(r) = V_{defect_q} - V_{defect_0}. \tag{3.7}$$

The resulting potential then is (up to an additive constant) a superposition of the potentials $V_{q/0}(r+R)$, where R is a lattice vector. Now this $V_{q/0}$ in the reciprocal space would be easily formulated with the Fourier transformation. Hence the periodic defect potential is obtained from a Fourier series as $\tilde{V}_{q/0}(r)$. The interaction energy associated with the artificial potential due to the periodic repetition of the charge comes out to be

$$E^{inter} = \frac{1}{2}\int_{\Omega} d^3r[q_d(r)+n][\tilde{V}_{q/0}(r) - V_{q/0}(r)], \tag{3.8}$$

where n is the homogeneous background charge $-q/\Omega$ (Ω being the volume of the supercell), $q_d(r)$ is the unscreened charge density and $\tilde{V}_{q/0}(r) - V_{q/0}(r)$ is the artificial potential due to the periodic repetition. The prefactor $\frac{1}{2}$ accounts for double counting and the integral is restricted to the supercell. Now the energy arising from the interaction of the background charge with the defect inside the reference cell is calculated out in the following way,

$$E^{intra} = \int_{\Omega} d^3r n V_{q/0}(r) = -q(\frac{1}{\Omega}\int_{\Omega} d^3r V_{q/0}(r)). \tag{3.9}$$

Here $n = \frac{-q}{\Omega}$, the compensating homogeneous background charge. Adding and rearranging (3.8) and (3.9) would allow the authors to explicitly calculate the artificial interactions from parameters like $\epsilon, q_d, \tilde{V}_{q/0}$, which can then be subtracted from the uncorrected formation energies obtained from the ab initio supercell calculations. Theoretical value of ϵ is chosen (which can be computed from various theories). For q_d , it turns out that any reasonable approximation to the defect charge distribution suffices since the sum of lattice energy and alignment correction is not sensitive to the details of q_d. And $\tilde{V}_{q/0}$ is available directly from the DFT supercell calculations. The final form of the formation energy for this paper is written down as (results of unrelaxed Ga vacancy for a set of $2 \times 2 \times 2$ supercells of the 8-atom cell are

reported here),

$$E^f(V_{Ga}^q) = E(V_{Ga}^q + bulk) - E(bulk) + E(Ga) + \mu_{Ga} - E_q^{lat} + q(E_F + \Delta_{q/b}), \tag{3.10}$$

where the last two terms the above equation are obtained by rearrangement of the sum of (3.8) and (3.9) as

$$E^{inter} + E^{intra} = E^{lat} - q\Delta_{q/0}. \tag{3.11}$$

The Fermi energy E_F is set equal to the valence-band maximum and the Ga chemical potential μ_{Ga} to that of Ga metal. The results are shown in figure 3.6. Using a point-charge model q_d the ab initio corrected formation energies

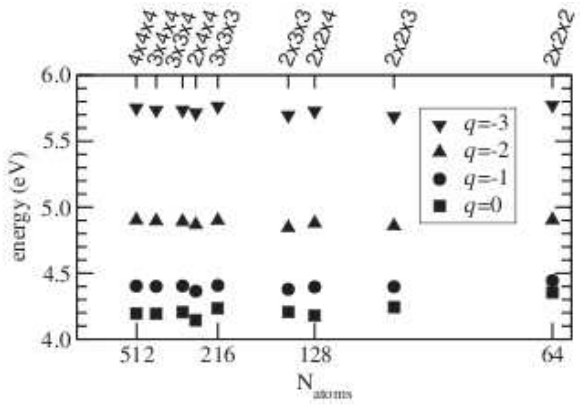

Figure 3.6: Defect formation energies of the Ga vacancy in GaAs including supercell corrections as a function of the inverse number of atoms. The Fermi energy is set equal to the valence-band maximum and the Ga chemical potential to that of Ga metal.

of all calculations above 2 X 2 X 2 agree within 0.1 eV without any empirical fit.

3.3.4 Treatment of Dabo et.al.

In the works of I. Dabo, B.Kozinsky, N.E.Singh-Miller, and N.Marzari[76] argues in favour of their analysis to compute the correct electrostatic poten-

tial for charged systems in the framework of periodic calculations. The paper even deals with extensive comparison with other methods of similar computation. In this work, they propose an alternative approach for correcting periodic image errors and show that energy convergence with respect to cell size can be obtained at moderately available computational costs. The approach advances by considering the exact electrostatic potential in open-boundary conditions or any other boundary condition as the sum of the periodic solution to the Poisson equation computed using FFT techniques (which are inexpensive in reality) and a real space correction that can be obtained on coarse grained meshes with multigrid techniques within a chosen degree of accuracy. Hence basically the idea revolves around the trick of generating a corrective potential on the basis of the boundary conditions. The corrective potential is a mutual contribution from (in fact the difference between) the potential arising from the Open Boundary Conditions (OBC) in absence of an external electric field and the potential (satisfying the PBC) due to the periodic translation of the same charge distribution. The corrective potential satisfies much simpler, smoother differential equation (essentially the Poisson's equation).

$$\nabla^2 v^{corr}(r) = -4\pi(\rho), \tag{3.12}$$

where v^{corr} is the corrective potential and ρ is an isolated charge distribution satisfying the Poisson equation. It may be said here that a careful and logical manipulation of the electron density ρ gives the corrective potential v^{corr}. The adjoining figure 3.7 gives an idea of the potentials for carbon monoxide absorbed in on a neutral platinum slab and carbon monoxide adsorbed on a charged platinum slab. The corrective potential seems to vary more smoothly than the potentials following OBC or PBC. This scheme is also tested with a point charge in a periodically repeated cubic cell and it is found that the corrective potential needs to be expanded in a power series exploiting the symmetry of the cubic cell for the convenience of computation. In Figure 3.8 we see the corrective potential in the presence of a point charge $q = +e$ in a periodically repeated cell of length L. The parabolic expansion (valid up to third order) confirms that the point charge correction

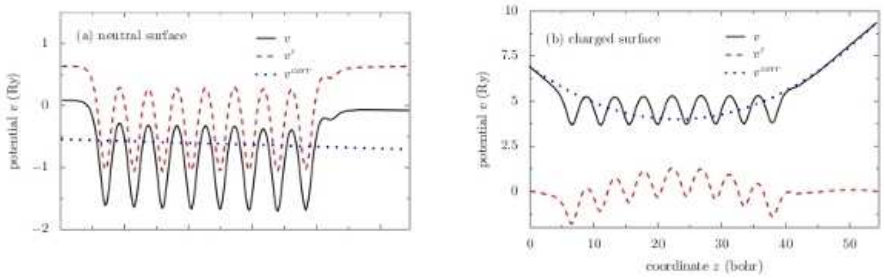

Figure 3.7: Open-boundary electrostatic potential v, periodic potential v' and electrostatic-potential correction v^{corr} averaged in the xy plane parallel to the surface for (a) carbon monoxide adsorbed on a neutral platinum slab and (b) carbon monoxide adsorbed on a charged platinum slab.

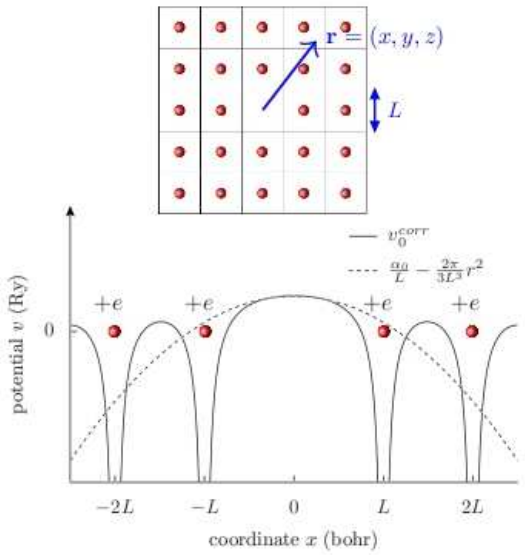

Figure 3.8: Corrective potential v^{corr} for a cubic lattice of point charges and its parabolic approximation in the vicinity of the origin.

or in reality the corrective potential is almost quadratic around the origin of the system. Strikingly mathematical analyses yield that it is even quadratic up to the third order for non-cubic lattices. Final form of the electrostatic

correction v^{corr} for an arbitrary distribution ρ would look like,

$$v^{corr}(r) = \int v_0^{corr}(r - r')\rho(r')dr', \tag{3.13}$$

where the corrective potential generated by the uniform jellium and the surrounding point charges is denoted by v_0^{corr}. The authors have compared this scheme with some of the existing schemes and found that the corrective potential gives out the Madelung constant and even a term similar to the Makov Payne formulation, but differing slightly in magnitude though. Three different cases are compared in this approach. One with a Parabolic Point-Counter charge (PCC) potential. This one claims that this scheme can correct periodic image errors up to quadrupole moment order. To obtain higher-order PCC corrections, one would need to determine more terms in the expansion of the point-charge correction beyond the parabolic contributions. Another popular choice is to implement the Gaussian Counter charge (GCC) formalism where the corrective potential is Gaussian. In this approach the corrective potential is claimed to easy in computation. The GCC method is somewhat similar to methods applied by Blochl[80] and LMCC method of Schultz. At this point the authors felt the need for another approach which is centered on the idea of the direct difference between the open boundary potential and the periodic counterpart. This exact corrective potential is coined as the Density Counter charge (DCC) potential by the authors. The DCC potential is obtained by evaluating the Coulomb integral defining v at each grid point in the unit cell. The PCC, GCC, and DCC potentials for a charged pyridazine cation in a cubic cell of length $L = 15$ bohr are plotted in figure 3.9. The PCC and GCC corrections are computed up to the dipole order. First, it should be noted that the maximal energy of the PCC potential is slightly above its GCC counterpart, reflecting the fact that the Madelung energy of an array of point charges immersed in a jellium is higher than that of a jellium-neutralized array of Gaussian charges. In addition, the maximal DCC energy is found to be above the Madelung energy, proving that the dipole PCC and GCC corrections tend to underestimate the energy of the system. Moreover, the parabolic PCC potential is not as steep

as its GCC counterpart, suggesting that the energy underestimation will be more significant for the GCC correction. Because of the cubic symmetry of the cell, the PCC and GCC potentials display the same curvature in each direction of space. In contrast, the curvature of the DCC potential is not uniform due to the nonspherical nature of the molecular charge density. This shape dependence suggests that the accuracy of the GCC correction could be improved by optimizing the geometry of the Gaussian countercharges.

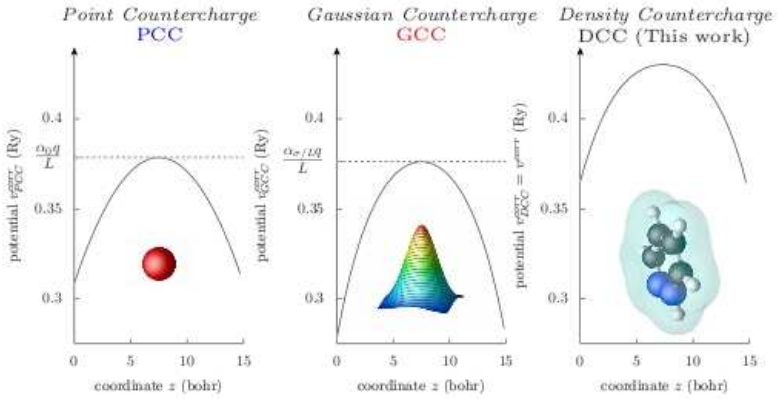

Figure 3.9: PCC, GCC, and DCC corrective potentials for a pyridazine cation $C_4H_5N_2^+$ in a cubic cell of length $L = 15$ bohr. The corrective potentials are plotted along the z axis perpendicular to the plane of the molecule. The PCC and GCC corrections are calculated up to dipole order.

$$\Delta E_{corr} = \frac{1}{2} \int v(r)\rho(r)dr. \tag{3.14}$$

Equation (3.12) gives the final form of the corrected energy pertaining to the corrected potential.

In Figure 3.10 the total energies of the Pyridazine cation have been plotted with cell size in the different corrective schemes. From the figure 3.10 it is evident that with the DCC scheme, the energy converges even more rapidly, reflecting the exponential disappearance of energy errors arising from the charge density spilling across periodic cells. Further treatments to other systems in one and two dimensional periodicity are still being worked upon. This

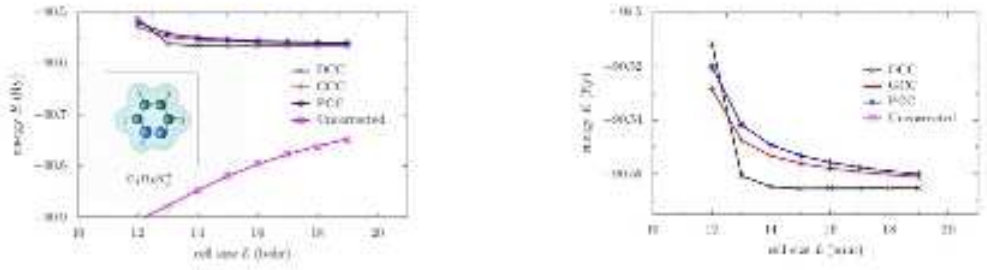

Figure 3.10: Total energy as a function of cell size for a pyridazine cation without correction and corrected using the PCC, GCC, and DCC schemes. The PCC and GCC corrections are calculated up to quadrupole order. The inset shows a pyridazine cation in a cell of size $L = 15$ bohr.

scheme in general has been reported to have improved upon the drawbacks of the Makov Payne or Schultz type formalism.

3.4 Conclusion

All the above mentioned formalims argue in favour of the periodic calculations for the charged systems. The idea is to correct for the erronious description of the electrostatics because of the periodicity of the supercell approach. We wonder if this is the only way to compute the physical quantities of interest for systems with charged defects. Each process comes with certain advantages over the other one, yet the fact remains as truth that electrostatics of the charged system is not correctly portrayed in the PBC schemes. The convergence issues are also of prime importance. All the above mentioned methodologies exploit the DFT methods to calculate the total energies and potentials required for the respective studies. The places where we wish to probe in more is the search for a Free Boundary Condition (FBC) scheme (under the DFT framework) with the exact electrostatics of the system. We wish to check the validity of the pseudopotential approach as well with a comparative idea of all the exchange correlation functionals and the

corresponding pseudopotentials for our case study. Before taking the ride through the new method of treating charged deefects I would talk through a chapter where a norm-conserving family of pseudopotentials is tested for its accuracy. To make it even more accurate non linear core correction has been added and further tested. The next chapter would deal with such a topic.

Chapitre 4

Dans ce chapitre est abordé l'utilisation de la correction non-linéaire de cœur avec des pseudo-potentiels HGH afin d'améliorer la précision des calculs effectués avec pseudo-potentiels à norme conservée, justifiant ainsi l'utilisation d'un formalisme plus simple comparé à la méthode des projecteurs augmentés (PAW). La correction non-linéaire de cœur est une façon de corriger la linéarisation apportée par l'utilisation de pseudo-potentiels. Ce chapitre montrera la validité d'une telle approche ainsi que les résultats obtenues sur les énergies d'atomisation.

Chapter 4

Hartwigsen-Goedeker-Hutter(HGH) pseudopotentials with Non Linear Core Correction (NLCC)

4.1 Introduction

As been discussed in the previous chapters, the fact DFT has proved itself to be an extremely efficient approach towards the description of ground state properties of metals, semiconductors and insulators motivates us to use it for our first stretch of calculations. In the formalism of DFT, we have seen the importance of a approximation –the exchange correlation functional. Within a given range of error bar for this approximation it is already established that DFT is the most widely used method for the electronic structure calculation in the fields of solid state physics and quatum chemistry, as reports have have been abundant in the community that, in the framework of DFT hundreds of atoms can be dealt with immense accuracy and efficiency. Another important aspect of the calculations that one may do with DFT is the use of pseudopotentials. The pseudopotentials are used to simplify the lives of researchers as they simply the calculations with less computation cost and they

also gives us a way to avoid the Dirac equation. Other wise we would have to use the Dirac equation to take take into account the relativistic effects of the all electron picture. It is known from theoretical quantum mechanics that the wavefunction ocillates near the core for any species because of the core electrons strong interaction with nucleus. This makes the all electron potential very complex to deal with in computational techniques. The pseudopotential is an effective (unreal of course) potential constructed to replace the atomic all-electron potential (Full-potential) such that core states are eliminated and the valence electrons are described by nodeless pseudo-wavefunctions. In this approach only the chemically active valence electrons are dealt with explicitly, while the core electrons are 'frozen', being considered together with the nuclei as rigid and non-polarizable. Norm-conserving pseudopotentials are derived from an atomic reference state, requiring that the pseudo and all-electron valence eigenstates have the same energies and amplitude (and thus density) outside a chosen core cutoff radius r_c. Pseudopotentials with larger cutoff radius are said to be softer, that is more rapidly convergent, but at the same time less transferable, that is less accurate to reproduce realistic features in different environments. Norm-conserving pseudopotentials emphasizes on the condition that, outside the cutoff radius, the norm of each pseudo-wavefunction be exactly same to its corresponding all-electron wavefunction. We have used Hartwigsen-Goedeker-Hutter HGH pseudopotential for this part of our calculations. The main idea is to use the pseudopotentials for accurate calculations. One can argue of course the validity of such a job. The emphasis is on the complexity-less approach of the norm-conserving pseudopotentials to produce as accurate results as that of the Projector Augmented Wave[80] (PAW) approach or that of the all-electron calculations. The success of our approach would ensure a method other than the PAW method for accurate calculations of various physical quantities. Here in this work another important concept is discussed, the *Non Linear Core Correction* (NLCC). This is an attempt to correct the otherwise implied linearization of the pseudopotential. So in a nutshell this chapter will deal with the validity of the results of calculations done with the Hartwigsen-Goedeker-Hutter(HGH) pseudopotentials with NLCC . Another important

point to be mentioned here is the fact that this pseudopotentials are implemented with the PBE exchange-correlation functionals on the wavelet basis sets. Along with the exchange-correlation functional, the representation of the Kohn-Sham wave functions is a prime concern for the DFT calculations. Usage of system independent basis sets such as plane waves[80]-[82], wavelets[43], or real space grids[83][59] a very high level of accuracy can be achieved. Basis sets of these kinds can be expanded systematically to achieve convergence according to our level of confidence. Among the systematic basis sets wavelets are reported to have all the properties that are needed for an accurate description of the system at hand. Systematic basis sets like these even allows us to implement correctly and more conveniently the hybrid functionals. As reported earlier[43], such a method is implemented in a DFT code, viz. BigDFT. As mentioned earlier it can be further clarified that the goal of this work is to show the results of the implementation of PBE functionals on wavelet basis. For the test the G2-1[84] set of molecules are taken and the atomization energies of these 55 molecules are calculated within the framework of PBE functionals implemented in BigDFT. The results of this work is duly compared with the known experimental values and also with values reported from the calculation from VASP and Gaussian03 DFT codes[85].

4.2 Theory

4.2.1 Non Linear Core Correction

The need for NLCC

In their report[87] Louie and his colleagues have put forward a method to extend the pseudopotential study primarily for the magnetic systems. The aim is to deal with problems concerning properties of magnetic materials, spin-density waves, magnetic effects on surfaces, localized impurity states in defects, etc., without much computational trouble. The method also takes care in keeping the level of accuracy as it has been in the nonmagnetic cases. Previous to their works, to take into account the magnetic effects into pseu-

dopotential calculations, in their article, Zunger[88] proposed constructing separate ionic potentials for the spin-up and spin-down electrons. Essentially they devised a spin-dependent pseudopotential approach. And in here the ionic pseudopotential in the solid depends on the spin density of the valence electrons. This spin density is obtained by interpolation between the ionic potential for the paramagnetic atom and that of the fully spinpolarized atom.

The work of Louie and his collaborators differs from the work of Zunger with a view that it is unnecessary and often undesirable to employ these spin-dependent ionic pseudopotentials. As it is well known from the literature mentioned in the previous chapters the exchange and correlation energy is usually approximated by some local (nonlinear) function of the charge density, and the kinetic energy is found from the gradient of the now obtainable singleparticle wave functions. As we have also seen that the charge density, in the pseudopotential formalism, is divided into core and valence contributions, and the energy of the core is assumed to be constant. Since the energy of the core is not varying it is hence subtracted out from the total density. Also it is to be kept in mind that quite often the core contribution is absolutely neglected, and the total energy is given by the DFT energy functional with the total charge density replaced by a (pseudo) valence charge density. The electrostatic potential due to the interaction of the ions with the core electrons is replaced by the pseudopotential. It is now pretty clear that with this trick all the interaction between the core and valence electrons is thus transferred to the pseudopotential. From the above arguments we can understand that neglecting the core electrons poses a problem. This mode of treatment linearizes the interaction which in reality is an approximation to the kinetic energy and as well to the explicitly nonlinear exchange and correlation energy. More explicitely, it is assumed in this fashion.

$$E_{XC}(\rho_c + \rho_v) = E_{XC}(\rho_c) + E_{XC}(\rho_v), \tag{4.1}$$

where $E_{XC}(\rho_c + \rho_v)$ is the total exchange correlation energy (non linear in reality). The form shows how it is linearized. At this point it is also im-

portant to look for the cases where this approximation might have worked very nicely. There can be cases where the core and the valence charge densities are well separated in space. For example we can consider the cases of various nonmagnetic molecules. Quite naturally there will be no serious errors introduced here. Most of the results reported till date hold good only because of this apparent spatial separation of the core and valence charge densities. But of cource where there is significant overlap between the two densities, the linearization, in particular of the exchange and correlation, will lead to the problem of transferability of the pseudopotential. The fact that the transferability is reduced, in turn, would incorporate systematic errors in the calculated total energy. To deal with the problem one must understand the basis nature and the origin of it. In the spin-density formalism the exchange and correlation energy depends on the local spin density as well as on the charge density. Now this additional spin dependence introduces the additional nonlinearity which is the main point of discussion in this module. Moreover it is the errors introduced by the linearization described above that have caused the discrepancies between the experimental and theoretical calculations and hence it is now necessary to use spin-dependent ionic pseudopotentials. The scheme that is to be used now will formally be addressed as Non Linear Core Correction (NLCC). NLCC treats these nonlinear terms explicitly, and the need for separate spin-up and spin-down ionic pseudopotentials is thus eliminated. What is better, the approach leads to significant improvement in the transferability of the potentials. It is henceforth understandable that this will yield more accurate results both for magnetic and non-magnetic systems.

Overview of the theory

Louie et. al., in their report[87] have given an example with the normconserving pseudopotential scheme of Hamann, Schliiter, and Chiang[89](HSC). To start with let me elaborate on the constraints with which the screened atomic pseudopotentials V_{ion}^{l} are constructed. It is to be kept in mind here that these pseudopotentials are angular-momentum-dependent. The con-

straints are -

- The valence eigenvalues from the all-electron calculation and those from the pseudopotential calculation agree for any configurational prototype.
- The all-electron wave functions and the pseudo-wave functions agree beyond a chosen core radius, r_c.

The two effective properties that are equally desirable and essential come out from these basic constraints.

- The electrostatic potential produced outside r_c, is identical for the all-electron and the pseudocharge distribution.
- The scattering properties of the all-electron atoms are reproduced with minimum error as the electronic eigenvalues move away from the prototype atomic levels.

These two properties are claimed to be the reason for ensuring a reasonable transferabihty of the pseudopotentials. The final bare-ion pseudopotentials, V_{ion}^{l} are extracted from the neutral potentials by subtracting from each neutral V^{l} the Coulomb and exchange and correlation potentials due to the pseudovalence charge density, $\rho^{v}(r)$. As for example, for a given angular momentum component l and spin component σ, the ionic potential is given by

$$V_{ion}^{l\sigma}(r) = V^{l\sigma}(r) - V_{ee}[\rho^{v}(r)] - V_{xc}[\rho^{v}(r), \xi^{v}(r)], \tag{4.2}$$

where

$$\xi^{v}(r) = \frac{\rho_{+}^{v}(r) - \rho_{-}^{v}(r)}{\rho^{v}(r)} \tag{4.3}$$

is the spin polarization of the valence charge with the $+$ and $-$ signs denoting the spin-up and spin-down electrons respectively. Ionic potentials generated this way for the nonmagnetic case, i.e. for cases where $\xi = O$, have been shown to be highly accurate in many applications[90]. In the above procedure the basic assumptions are the frozen-core approximation and a decoupling of the core charge in the determination of the exchange and correlation potential seen by the valence electrons. At this point let us not forget an important

observation about the frozen-core assumption. It, however, implies a single ionic pseudopotential which is independent of the spin polarization of the valence states. Hence evidently it is the second approximation that gives rise to the spin-dependent ionic potentials in previous work. In the HSC approach the ionic pseudopotentials are dependent on the valence configuration, since V_{xc} is a nonlinear function of the charge density and the valence charge does not cancel in their formalism. It is explicitly written as,

$$V_{xc}^{\sigma}(\rho^{v}+\rho^{c},\xi) = [V_{xc}^{\sigma}(\rho^{v}+\rho^{c},\xi) - V_{xc}^{\sigma}(\rho^{v},\xi^{v})] + V_{xc}^{\sigma}(\rho^{v},\xi^{v}), \tag{4.4}$$

where

$$\xi(r) = \frac{\rho_{+}^{v}(r)-\rho_{-}^{v}(r)}{\rho^{v}(r)+\rho^{c}(r)} \tag{4.5}$$

It is actually clear that in the construction of the ionic potential, the terms in brackets are included in the ionic potential as part of the core properties which causes the problem in the transferability of the potential. This feature is highly undesirable since it reduces the transferability of the potential. In particular, for magnetic applications, the spin-density distribution of the electrons can be extremely different both in magnitude and in profile as one goes from the atomic case to the various condensed matter systems. Hence it is improbable that any interpolation formula between spin-up and spin-down potentials generated from atoms will work to a high level of accuracy and satisfaction. To remove the dependence of the ionic pseudopotential on the valence charge a simple and straightforward trick can be applied. The form of the $V_{ion}^{l\sigma}$ can be written as -

$$V_{ion}^{l\sigma}(r) = V^{l\sigma}(r) - V_{ee}[\rho^{v}(r)] - V_{xc}[(\rho^{v}r+\rho^{c}r),\xi^{v}(r)]. \tag{4.6}$$

The total exchange and correlation potential, including the nonlinear core valence term, is now subtracted out of the neutral potential. A smart and effective implementation of this theory have been reported to have given ionic potential highly transferable and essentially independent of the spin polarization and the prototype atomic configuration. The following figure with the results illustrate the acceptability of the above mentioned theoretical

method. In this regard the basic idea of implementation can be discussed.

			All electron	No core	Full core	Partial core
		$3s^1+$	−12.76	−12.82	−12.76	−12.76
	Term	$3p^3\div$	−5.79	−5.81	−5.80	5.80
	values	$3s^0-$	−7.55	−5.63	−7.56	−7.55
		$3p^0$	1.21	-0.43	−1.21	−1.20
Si						
	Total	ΔE	−3.58	−4.05	−3.61	−3.62
	energy	error		13.1%	0.7%	1.0%
		$4d^5+$	−5.24	−5.51	−5.24	−5.25
	Term	$5s^1+$	−4.79	−4.71	−4.81	−4.80
	values	$4d^3-$	−2.01		−2.00	−1.89
		$5s^0-$	−2.08	−1.02	−2.06	−2.05
Mo						
	Total	ΔE	−4.35	−8.46	−4.38	−4.52
	energy	error		94.6%	0.8%	3.9%

Figure 4.1: Atomic term values and total energy differences between paramagnetic and fully spin-polarized atoms. Paramagnetic configurations are $3s^1 3p^3$ for Si and $4d^5 5s^1$ for Mo. All energies are in eV. ΔE is the total energy difference between the paramagnetic and the spin-polarized configuration. Superscripts indicate the electron occupation and the + signs denote the spin configuration for each orbital.

In the employment of the new potential, the core charge should be added to the valence charge whenever the exchange and correlation potential or energy is calculated. This core charge remains the same in all applications, as we are considering things within the frozen core approximation. Hence, in addition to the usual s, p,and d potentials, we need to retain the core charge density which is computed once and for all in the same atomic calculations as the pseudopotentials. It is certain that in an atomic calculation there is no difficulty in representing the core charge. In a bulk calculation, however, there are two practical considerations that must be taken care of. In any pseudopotential calculation there are small, but unavoidable errors in the calculated valence charge density. Usually this leads to a negligible error in the total energy, but when the core charge is added, any inaccuracy in the valence charge density inside the core region is multiplied by the core charge and the error in the total energy will increase proportionally. To be sure of the accuracy of the calculation, it is therefore absolutely necessary to treat the effect of the core charge as a perturbation, and a change in the total energy

as a result of this correction should not be large. The above mentioned issues can be handled by observing that the core charge has significant effect only where the core and the valence charge densities are of similar magnitude. One can therefore replace the full core charge density with a partial core charge density which is equal to the true charge density outside some radius r_c and arbitrary inside. Louie[87] and his colleagues show that r_c may be chosen as the radius where the core charge density is from 1 to 2 times larger than the valence charge density.

4.3 Tests for the pseudopotentials

The implementation of the PBE pseudopotential on the wavelet basis is tested on two different levels. With a particular family of PBE pseudopotential, essentially the Hartwigsen, Goedecker, Hutter (HGH) normconserving pseudopotentials, the first test were done. This family of pseudopotentials are known to have the same limitations as that of the HSC pseudopotentials, i.e. the core electron density is completely neglected for a prototype configuration. The results will show the performance of such pseudopotentials. It can be mentioned here for the sake of information that the results were not satisfactory and hence an improvement was sought for. The second level of this test was to account for the limitations that we found to be inherent in the method from the first test. The NLCC method was found theoretically suitable for the cause and the next set of tests were done with this new family of pseudopotentials corrected with the contribution from the core densities. In the following sections the details of the calculations are explained with results and analysis. The G2-1 test set has been taken and the atomization energies for each of the molecules are calculated. The atomization energy of a molecule E_0(M) is defined as the diffrence between the energy of the molecule ϵ_0(M) and the sum of the energies of the constituent atoms ϵ_0(X),

$$E_0(M) = \sum_{species} n\epsilon_0(X) - \epsilon_0(M). \tag{4.7}$$

For all the atoms spin polarized calculations were done. It was taken strictly into consideration that atoms were calculated in a symmetry broken ground state. This state was found to be lower in energy than the spherically high-symmetry solution. In the code care was taken as to satisfy the Hund's rule of electronic configuration for each constituent atom of each molecule. In the following section let us take a look at a brief overview of Hund's rule.

4.3.1 Hund's rule

The rules formulated by Hund help to determine the total spin S, the total spatial angular momentum L, and the total angular momentum $J = \mathbf{L} + \mathbf{S}$ of the ground state of an atom.

- If for a single atom there can be many electron states, the ground state will be determined by the one having the largest total spin S.
- Among the states with the largest total spin, the ground state is the one with the highest angular momentum quantum number L.
- For a shell less than being half-filled that ground state is the one with the lowest value of $J = \mathbf{L} + \mathbf{S}$.
- For a shell more than being half-filled that ground state is the one with the highest value of $J = \mathbf{L} + \mathbf{S}$.

These are the rules which are applied to the atoms for the calculations undertaken in this work. But to apply these rules to the molecules care must be taken so as to get the correct symmetry broken ground state. Hunds first rules are reported to be good enough for most molecules. Most molecules of interest have closed shell ground states, but there are a few exceptions. In those cases Hund's rule predicts that triplet lies below the singlet. In all the calculations done in this work the Hund's rules are applied with rigor and care.

4.3.2 Calculational parameters

The main motivation for these calculations is to use the wavelet basis set and to see the validity of the corresponding implementation of the NLCC within the PBE pseudopotentials. In order to be highly accurate with atomization energies for these calculations the parameters viz. *hgrid* and *crmult* for each atom are tested for different values. Genovese et. al.[43] have mentioned the theoretical convergence of the physical quantities calculated with respect to these parameters. *hgrid* is the grid spacing and *crmult* is a parameter which determines the extent of resolution zone that contains the exponentially decaying tails of the wave functions. Care has been taken to find the correct combination of *hgrid* and *crmult* for each atom in the list of the G2-1 test set of molecules. The *hgrid* and *crmult* are chosen in such a fashion that the error in the total energy incurred in the calculation must not exceed 10^{-5} Hartrees, which is close to an error of .25 meV. Now from figure 4.2 it is evident that for the atom hydrogen *hgrid* value of 0.30 and a *crmult* value of 6 would give us results which are satisfactorily within our accuracy need. Table 1 lists the values of the two parameters used for the elements in the set.

Once the basic parameters to work with are acheived the main calculation for all the atoms for the atomization energies are launched. As mentioned earlier all the energies of the atoms are calculated in their spin polarized state.

4.3.3 Atomization energy of molecules using PBE

The first test is performed with the PBE functionals in comparison with the results of the plane wave methods as reported in the works of Paier[85] et. al. From the figure 4.3 there are few interesting things that can be understood. In a general statement one may consider the PBE functionals as implemented on the wavelet basis set tends to underestimate the atomization energy values as calculated from the PAW and G03 codes. Of course there are atoms which have given excellent results in comparison to the all electron calculations, but this is not the kind of test that will testify for the accuracy

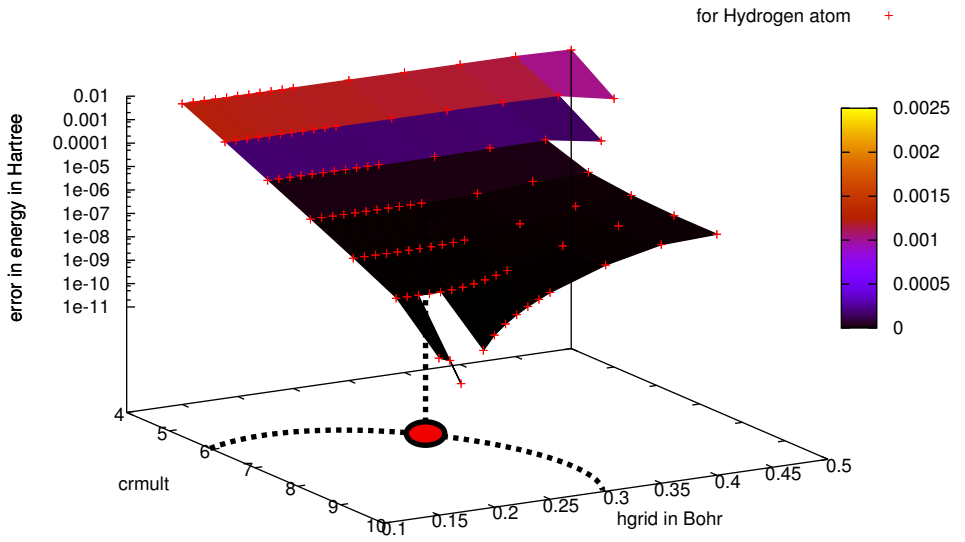

Figure 4.2: The error in total energy calculation of an H atom as a function of the *hgrid* and *crmult*. The drawn dotted contour corresponds to the ΔE value of 10^{-7} Hartree.

of the impletation of PBE on the wavelet basis set. The main motive of this work is to validate the implementation of the NLCC and its transferability. The reasons for some atoms to be giving particularly good results can be attributed to mainly two facts. One may believe as a primary reason that the approximation to the densities, without taking into account the core charges, were good enough for those prototypes. Again for molecules where there are two or more atoms, respective errors in the calculation of the total energies of each constituent atom cancelled the overall error. But obviously in general the PBE functional as implemented on the wavelet basis set tends to underestimate the atomization energy value. A careful observation of the graph would help us to understand better the sources of errors. The

Table 4.1: The elements and the corresponding hgrids and crmults.

Elements	hgrid	crmult
H	0.350	6
Li	0.300	6
Be	0.250	6
C	0.250	6
N	0.250	6
O	0.200	6
F	0.150	7
Na	0.200	8
Si	0.350	6
P	0.350	7
S	0.300	7
Cl	0.250	7

molecules like O_2, CO_2, N_2H_4, N_2, H_2O_2 have suffered the highest deviations from the all electron calculations. The presence of oxygen in many of those molecules hints towards the electronegativity of the atoms as well. Where as the role of hydrogen may be excluded as it has only one electron and hence there arises no question of the core charge. The nitrogen atom on the other hand poses some significant problems. The reason to this may be because of the strength of bonding of the nitrogen valence electrons. To associate one nitrogen atom to any other atoms to form a molecure the core charge density of the nitrogen might be perturbed and an inadequate representation of that in the pseudopotential might result in the type of errors that are exhibited in the figure. The following table shows the values as calculated with BigDFT in comparison with reported values of VASP and G03 along with the experimental values.

The average deviation of our results with this PBE pseudopotentials from that of the G03 calculations is 5.197 kcal/mol and from that of Vasp is 5.015 kcal/mol. It is expected to improve upon the implementation of the non linear core correction as with that formalism we hope to get closer to the results obtained by all electron methods.

Table 4.2: Electronic atomization energies for the molecules in the G2-1 test set using the PBE functional. Energies are in kcal/mol.

Moleulcues	AE_{PBE}	AE_{expt}	$\Delta Expt - BigDFT\%$	AE_{Vasp}	AE_{G03}	$\Delta_{Vasp-BigDFT}$	$\Delta_{G03-BigDFT}$
LiH	53.491	58.000	7.774	53.500	53.500	0.009	0.009
BeH	55.660	48.000	15.958	55.500	55.600	-0.160	-0.060
CH	82.819	84.000	1.406	84.700	84.800	1.881	1.981
OH	105.566	107.000	1.340	109.700	110.100	4.134	4.534
O2	130.381	118.000	10.492	143.300	144.000	12.919	13.619
F2	44.641	38.000	17.476	52.600	53.000	7.959	8.359
Li2	19.935	26.000	23.327	19.900	20.100	-0.035	0.165
CO	254.750	261.000	2.395	268.600	269.100	13.850	14.350
LiF	134.071	139.000	3.546	138.400	139.000	4.329	4.929
SiO	190.156	191.000	0.442	195.600	196.600	5.444	6.444
HF	136.815	142.000	3.651	141.500	142.200	4.685	5.385
CN	185.236	179.000	3.484	197.500	197.700	12.264	12.464
N2	226.867	227.000	0.059	243.700	243.900	16.833	17.033
Cl2	64.757	57.000	13.609	65.800	65.800	1.043	1.043
ClO	75.938	62.000	22.481	81.600	81.500	5.662	5.562
HCl	105.664	107.000	1.249	106.300	106.500	0.636	0.836
ClF	67.571	62.000	8.985	72.300	72.500	4.729	4.929
Na2	17.497	19.000	7.911	17.700	18.100	0.203	0.603
NO	157.290	153.000	2.804	172.000	172.500	14.710	15.210
Si2	78.775	74.000	6.453	81.300	81.400	2.525	2.625
NH	86.005	82.000	4.884	88.600	88.600	2.595	2.595
P2	121.487	116.000	4.730	121.500	121.700	0.013	0.213
S2	114.660	98.000	17.000	115.400	115.200	0.740	0.540
SO	135.196	122.000	10.816	141.500	141.300	6.304	6.104
CS	173.745	172.000	1.015	179.500	179.500	5.755	5.755
CH3	306.418	306.000	0.137	309.700	310.100	3.282	3.682
NH2	182.999	182.000	0.549	188.700	188.900	5.701	5.901
H2O	225.689	233.000	3.138	233.700	234.500	8.011	8.811
CO2	392.546	392.000	0.139	415.400	416.500	22.854	23.954
SO2	269.089	253.000	6.359	281.100	280.700	12.011	11.611
SH2	180.978	182.000	0.562	182.000	182.200	1.022	1.222
H2O2	264.498	268.000	1.307	281.600	282.600	17.102	18.102
HCN	311.872	313.000	0.360	326.300	326.500	14.428	14.628
HCO	280.544	279.000	0.553	294.900	295.500	14.356	14.956
HOCl	167.033	165.000	1.232	175.200	175.700	8.167	8.667
NH3	293.184	297.000	1.285	301.700	302.300	8.516	9.116
PH2	155.144	153.000	1.401	154.500	154.600	-0.644	-0.544
PH3	239.176	241.000	0.757	239.000	239.300	-0.176	0.124
NaCl	93.077	99.000	5.983	93.600	94.500	0.523	1.423
CH4	413.802	420.000	1.476	419.600	420.200	5.798	6.398
SiH2(1A1)	147.577	154.000	4.171	147.900	148.000	0.323	0.423
SiH3	222.992	226.000	1.331	222.200	222.600	-0.792	-0.392
SiH4	313.536	324.000	3.230	313.300	313.700	-0.236	0.164
C2H2	403.066	404.000	0.231	414.500	415.100	11.434	12.034
C2H4	559.583	562.000	0.430	571.000	571.900	11.417	12.317
C2H6	704.483	711.000	0.917	716.000	717.100	11.517	12.617
H2CO	371.528	376.000	1.189	385.000	386.300	13.472	14.772
N2H4	431.551	437.000	1.247	452.700	453.700	21.149	22.149
CH2(1A1)	174.512	182.000	4.114	178.800	179.100	4.288	4.588
CH2(3B1)	193.571	189.000	2.419	194.400	194.600	0.829	1.029
CH3OH	505.051	513.000	1.550	519.300	520.400	14.249	15.349
CH3Cl	392.693	395.000	0.584	399.400	400.200	6.707	7.507
CH3SH	470.621	473.000	0.503	477.800	478.600	7.179	7.979
Si2H6	519.258	533.000	2.578	519.500	520.400	0.242	1.142
SiH2(3B1)	125.044	131.000	4.547	131.300	131.800	6.256	6.756

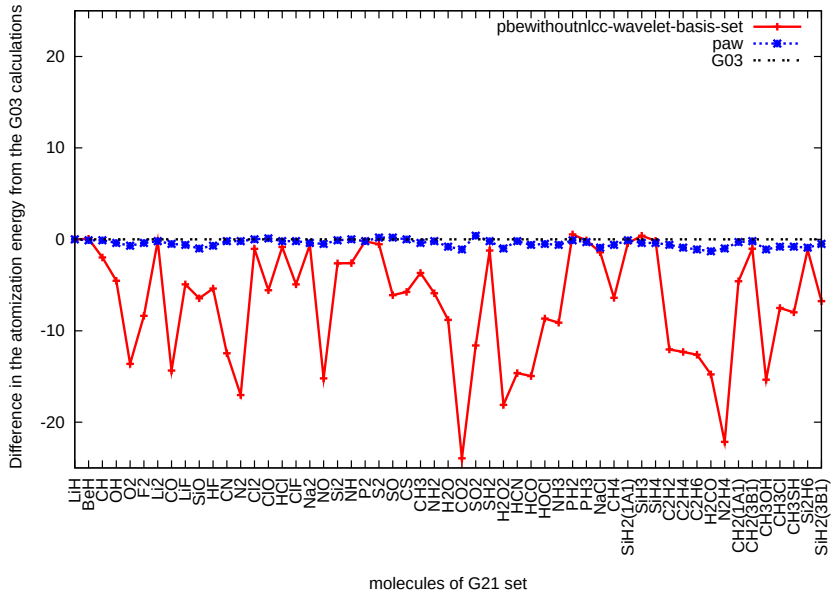

Figure 4.3: Electronic atomization energies for the molecules in the G2-1 test set using the PBE functional. Energies are plotted in kcal/mol. The all electron values from the Gaussian calculations are taken as the standard.

Geometries of the molecules

To complete the study with the PBE functionals the geometry of the molecules were also investigated. A set of sixteen di-atomic molecules have been taken. The molecules are made to go geometrical relaxation and then the bond lengths are noted down. The following plot shows the variation of the bond lengths with respect to the all electron calculations. The break criterion for the geometry optimization in BigDFT was set to $10^{-5} Hartree/Bohr$ which is equivalent to $0.0005 eV/\mathring{A}$.

The table 4.3 and the figure 4.4 are an illustration of the fact that how well the bondlength results have matched with the PAW and Gaussian calculations. The bond lengths are already very good without the NLCC calculations. One can although see a general trend. The bond length values from all the three different theoretical calculations tend to overestimate the

Table 4.3: Tabular representation of theoretical and experimental bond lengths of 16 diatomics chosen from the reduced G2 data set. Bondlengths are in angstroms.

Molecules	Expt.	PAW	G03	BigDFT	abs($\Delta BigDFT - G03$)
	in Å	in Å	in Å	in Å	in Å$\times 10^3$
BeH	1.343	1.354	1.353	1.354	1
CH	1.120	1.136	1.136	1.136	0
Cl2	1.988	1.999	2.004	1.994	10
ClF	1.628	1.648	1.650	1.645	5
ClO	1.570	1.576	1.577	1.575	2
CN	1.172	1.173	1.174	1.173	1
CO	1.128	1.136	1.135	1.135	0
F2	1.412	1.414	1.413	1.416	3
FH	0.917	0.932	0.930	0.932	2
HCl	1.275	1.287	1.288	1.286	2
Li2	2.673	2.728	2.728	2.728	0
LiF	1.564	1.583	1.575	1.575	0
LiH	1.595	1.604	1.604	1.604	0
N2	1.098	1.103	1.102	1.102	0
O2	1.208	1.218	1.218	1.220	2
Na2	3.079	3.087	3.076	3.070	6

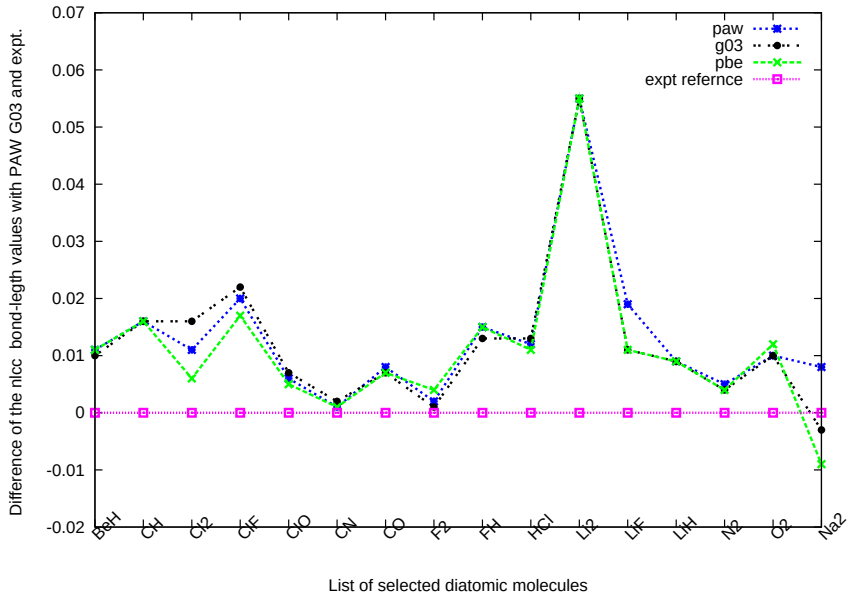

Figure 4.4: Graphical representation of theoretical and experimental bond lengths of 16 diatomics chosen from the reduced G2 data set. Bondlength differences are in angstroems.

experimental bond lengths. For most of the elements we find that the bond lengths are very good accordance with the G03 calculations. As we can see the problems for Paw with some of the molecules like LiF do not arise in our case. The reason for the agreement for the bond lengths even with inaccurate atomization energies can be explained as the following. Clearly for the energies we see a problem with the reference energies of single atoms. They are shifted in general from the *accurate* values. But since the bond length calculations depend on the force calculations, which is essentially the derivative of the energy surface. It appears that although the energy surface is shifted by a value yet the shape of the surface is calculated with relatively more accuracy and hence the force calculations are more accurate. Care was taken by Paier[85] et. al. to minimise the dicrepancies. For example in particular, the box size was increased, dipole correction was applied, and

the energy cutoff was increased. Yet the reason for this inaccuracy remains open. It is also to be kept in mind here that for Li all electrons were treated as valence electrons. There is another problem to be looked after both for the PAW calculations as well as the wavelet calculations. The problem is with the Na_2 molecule. The Na_2 molecule demand a tight convergence criterion for the geometry relaxation because of the weak interaction between the constituent Na atoms.

4.3.4 Atomization energy of molecules using PBE with NLCC

Having seen the performance of PBE as implemented on the wavelet basis (table 4.4 and figure 4.5) we are tempted to look for betterment in terms of accuarcy towards the all electron calculation. With that view as discussed in the precious sections the non linear core correction is the one interesting way that could be thought of. A new family of pseudopotential is available now under the PBE formalism with NLCC implemented in it. There are parameters that can be played around with for respective elements to get the most accurate and desirable results. Of course for atoms like hydrogen and lithium these corrections are meaningless. Yet as it will be evident from the following table and figures that considerable amount of improvement is obtained with this implementation.

A single glance would show that the implementation of the NLCC in the pseudopotentials have inproved the results by a large margin. Here also the convergence parameters are kept the same as before for each prototype configuration.

The significant improvement in the results can also be seen in the values of mean absolute deviation of the atomization energies of BigDFT-Vasp and BigDFT-G03. The average deviation of our results with this PBE pseudopotentials from that of the G03 calculations is 1.03 kcal/mol and from that of Vasp is 1.05 kcal/mol. Hence we can say at this point that in terms of closeness to the calculations of the PAW and G03 the NLCC improves the previous calculations by a factor of 5. Indeed this improvement is very

Table 4.4: Electronic atomization energies for the molecules in the G2-1 test set using the PBE functional with NLCC correction. Energies are in kcal/mol.

Moleulcues	AE_{PBE}	AE_{NLCC}	AE_{expt}	$\Delta Expt - BigDFT\%$	AE_{Vasp}	AE_{G03}	$\Delta_{Vasp-BigDFT}$	$\Delta_{G03-BigDFT}$
LiH	53.491	53.489	58.000	7.778	53.500	53.500	0.011	0.011
BeH	55.660	55.657	48.000	15.952	55.500	55.600	-0.157	-0.057
CH	82.819	84.257	84.000	0.306	84.700	84.800	0.443	0.543
OH	105.566	109.842	107.000	2.656	109.700	110.100	-0.142	0.258
O2	130.381	144.184	118.000	22.190	143.300	144.000	-0.884	-0.184
F2	44.641	54.495	38.000	43.409	52.600	53.000	-1.895	-1.495
Li2	19.935	19.935	26.000	23.328	19.900	20.100	-0.035	0.165
CO	254.750	270.133	261.000	3.499	268.600	269.100	-1.533	-1.033
LiF	134.071	140.275	139.000	0.917	138.400	139.000	-1.875	-1.275
SiO	190.156	200.394	191.000	4.918	195.600	196.600	-4.794	-3.794
HF	136.815	142.809	142.000	0.570	141.500	142.200	-1.309	-0.609
CN	185.236	197.722	179.000	10.459	197.500	197.700	-0.222	-0.022
N2	226.867	243.491	227.000	7.265	243.700	243.900	0.209	0.409
Cl2	64.757	66.572	57.000	16.793	65.800	65.800	-0.772	-0.772
ClO	75.938	82.327	62.000	32.786	81.600	81.500	-0.727	-0.827
HCl	105.664	107.164	107.000	0.153	106.300	106.500	-0.864	-0.664
ClF	67.571	73.494	62.000	18.539	72.300	72.500	-1.194	-0.994
Na2	17.497	17.481	19.000	7.995	17.700	18.100	0.219	0.619
NO	157.290	171.982	153.000	12.407	172.000	172.500	0.018	0.518
Si2	78.775	79.815	74.000	7.858	81.300	81.400	1.485	1.585
NH	86.005	87.747	82.000	7.008	88.600	88.600	0.853	0.853
P2	121.487	124.118	116.000	6.999	121.500	121.700	-2.618	-2.418
S2	114.660	114.671	98.000	17.011	115.400	115.200	0.729	0.529
SO	135.196	140.503	122.000	15.166	141.500	141.300	0.997	0.797
CS	173.745	179.232	172.000	4.205	179.500	179.500	0.268	0.268
CH3	306.418	309.409	306.000	1.114	309.700	310.100	0.291	0.691
NH2	182.999	188.102	182.000	3.353	188.700	188.900	0.598	0.798
H2O	225.689	235.435	233.000	1.045	233.700	234.500	-1.735	-0.935
CO2	392.546	416.205	392.000	6.175	415.400	416.500	-0.805	0.295
SO2	269.089	275.731	253.000	8.985	281.100	280.700	5.369	4.969
SH2	180.978	181.665	182.000	0.184	182.000	182.200	0.335	0.535
H2O2	264.498	283.128	268.000	5.645	281.600	282.600	-1.528	-0.528
HCN	311.872	326.192	313.000	4.215	326.300	326.500	0.108	0.308
HCO	280.544	293.879	279.000	5.333	294.900	295.500	1.021	1.621
HOCl	167.033	176.017	165.000	6.677	175.200	175.700	-0.817	-0.317
NH3	293.184	301.434	297.000	1.493	301.700	302.300	0.266	0.866
PH2	155.144	155.808	153.000	1.836	154.500	154.600	-1.308	-1.208
PH3	239.176	241.186	241.000	0.077	239.000	239.300	-2.186	-1.886
NaCl	93.077	95.034	99.000	4.006	93.600	94.500	-1.434	-0.534
CH4	413.802	419.374	420.000	0.149	419.600	420.200	0.226	0.826
SiH2(1A1)	147.577	148.582	154.000	3.518	147.900	148.000	-0.682	-0.582
SiH3	222.992	223.630	226.000	1.048	222.200	222.600	-1.430	-1.030
SiH4	313.536	315.582	324.000	2.598	313.300	313.700	-2.282	-1.882
C2H2	403.066	414.388	404.000	2.571	414.500	415.100	0.112	0.712
C2H4	559.583	570.842	562.000	1.573	571.000	571.900	0.158	1.058
C2H6	704.483	715.702	711.000	0.661	716.000	717.100	0.298	1.398
H2CO	371.528	387.062	376.000	2.942	385.000	386.300	-2.062	-0.762
N2H4	431.551	448.464	437.000	2.623	452.700	453.700	4.236	5.236
CH2(1A1)	174.512	178.250	182.000	2.060	178.800	179.100	0.550	0.850
CH2(3B1)	193.571	194.145	189.000	2.722	194.400	194.600	0.255	0.455
CH3OH	505.051	519.241	513.000	1.217	519.300	520.400	0.059	1.159
CH3Cl	392.693	399.551	395.000	1.152	399.400	400.200	-0.151	0.649
CH3SH	470.621	476.638	473.000	0.769	477.800	478.600	1.162	1.962
Si2H6	519.258	523.246	533.000	1.830	519.500	520.400	-3.746	-2.846
SiH2(3B1)	125.044	124.388	131.000	5.047	131.300	131.800	6.912	7.412

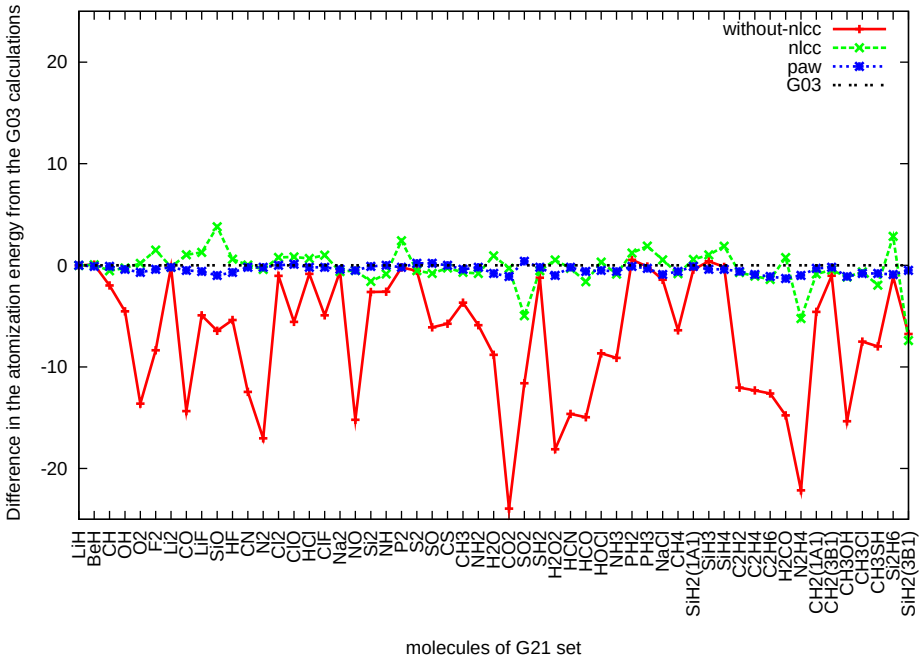

Figure 4.5: Electronic atomization energies for the molecules in the G2-1 test set using the PBE functional with NLCC. Energies are plotted in kcal/mol. The all electron values from the Gaussian calculations are taken as the standard.

significant.

Geometries of the molecules with NLCC

To complete the study with the PBE functionals with NLCC the geometry of the molecules were also investigated in the same spirit as before. the same set of sixteen diatomic molecules have been taken. The following plot in figure 4.6 shows the improvement in the variation of the bond lengths with respect to the all electron calculations. The break criterion for the geometry optimization in BigDFT was set to $10^{-5} Hartree/Bohr$ which is equivalent to $0.0005 eV/\mathring{A}$ which is same as the calculations without the NLCC.

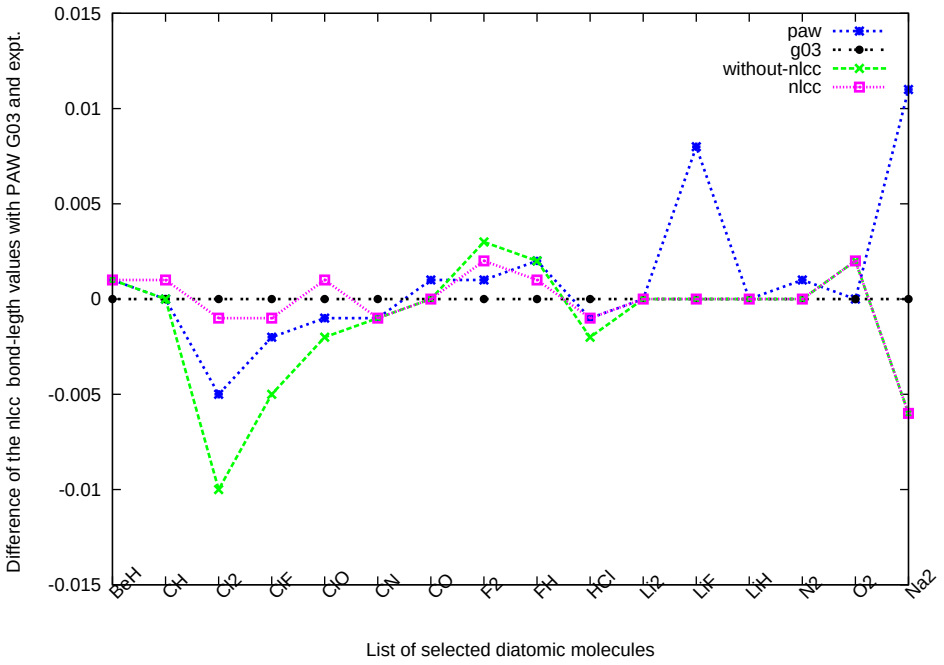

Figure 4.6: Graphical representation of theoretical and experimental bond lengths of 16 diatomics chosen from the reduced G2 data set with NLCC. Bondlength differences are in angstroms.

The bond lengths are observed to be more accurate as the figure and table above suggest. It is also noteworthy here that in comparison to PAW calculations our results have been found closer to that of the all electron gaussian calculations for most of the molecules. This indicates the extent of the success of the implementation of the NLCC in the pseudopotentials.

A closer analysis

Although as mentioned earlier the results have improved considerably with the implementation of the NLCC yet a closer look into the graphical representation (figure 4.7) would reveal some remnant discrepancies. The reason

Table 4.5: Tabular representation of theoretical and experimental bond lengths of 16 diatomics chosen from the reduced G2 data set with NLCC. Bondlengths are in angstroms.

Molecules	Expt.	PAW	G03	BigDFT(NLCC)
BeH	1.343	1.354	1.353	1.354
CH	1.120	1.136	1.136	1.137
Cl2	1.988	1.999	2.004	2.003
ClF	1.628	1.648	1.650	1.649
ClO	1.570	1.576	1.577	1.578
CN	1.172	1.173	1.174	1.173
CO	1.128	1.136	1.135	1.135
F2	1.412	1.414	1.413	1.415
FH	0.917	0.932	0.930	0.931
HCl	1.275	1.287	1.288	1.287
Li2	2.673	2.728	2.728	2.728
LiF	1.564	1.583	1.575	1.575
LiH	1.595	1.604	1.604	1.604
N2	1.098	1.103	1.102	1.102
O2	1.208	1.218	1.218	1.220
Na2	3.079	3.087	3.076	3.070

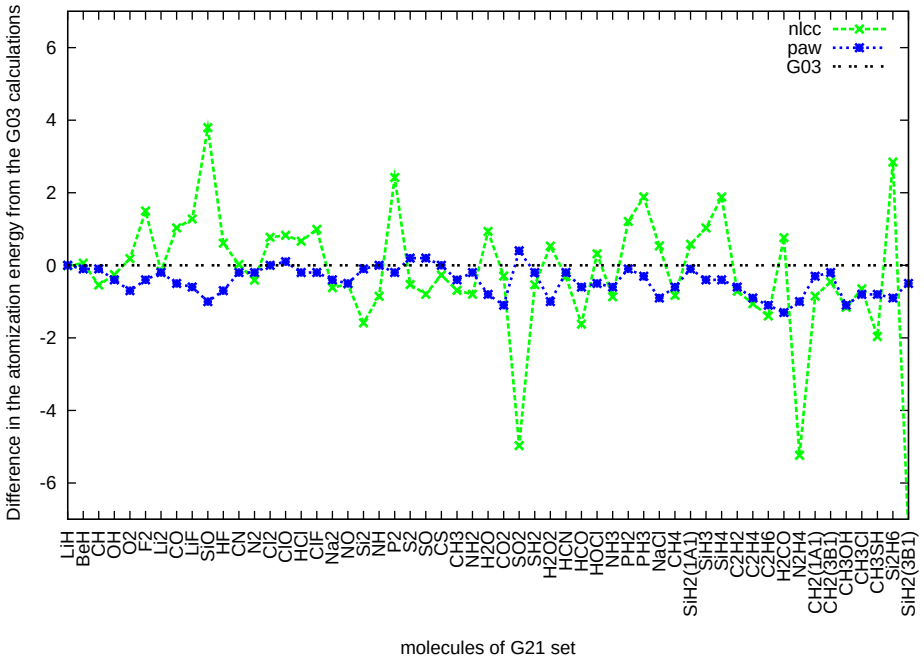

Figure 4.7: Electronic atomization energies for the molecules in the G2-1 test set using the PBE functional with only NLCC correction . Energies are in kcal/mol. This is the zoomed version of figure 4.5.

for these discrepancies are to be sought after in detail.

In figure 4.8 what we get to see is the respective contribution of each element in a particular zone of absolute deviation from the G03 values. In the figure *Di-j* is a zone of deviation in kcal/mol. Hence D0-1, D1-2, D2-4, D4-7 are the deviation ranges of 0-1 kcal/mol, 1-2 kcal/mol, 2-4 kcal/mol and 4-7 kcal/mol respectively. We can exclude hydrogen from our analysis because of two main reasons. First of all, it has only one electron and hence there is no question of fixing a special core density. Secondly it is the most frequent element in the entire list. So it is quite evident that its contribution is show in almost every range. The ranges which worry us the most are D2-4 and D4-7. Although we see some contribution of oxygen in those ranges,

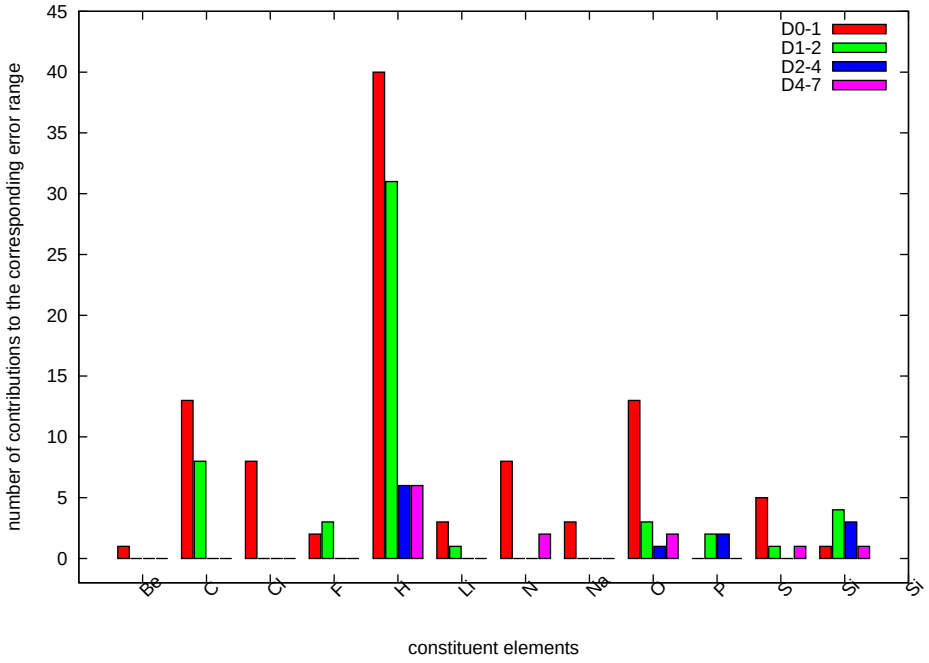

Figure 4.8: Contribution of each element in a particular zone of absolute deviation from the G03 values for the NLCC calculations.

a quick look at the table above would qualify oxygen as another of a frequent element. Its association with elements like silicon and sulphur would have forced its presence in those ranges of deviation. To this we come to the elements like silicon, sulphur, phosphorous and nitrogen. The problem with nitrogen is probably the same as discussed above. Its association with hydrogen in N_2H_4 might have perturbed the core density which is still ill represented in NLCC formalism. On the other hand the cases for silicon and sulphur are not that straightforward. Silicon is semimetallic. An intuitive approach would call for a smaller r_c. The radius r_c as described in the theory section is an important parameter in this pseudopotential approach. Another solution could be to play around with the amount of core-density to be used in the NLCC part. At the end a general algorithm is what we have tried to

find that will be applied for all the elements in the same spirit to give more accurate results. By this I mean we need to get rid of the deviation ranges D2-4 and D4-7. The fact the silicon is indeed a bit tricky to handle, let

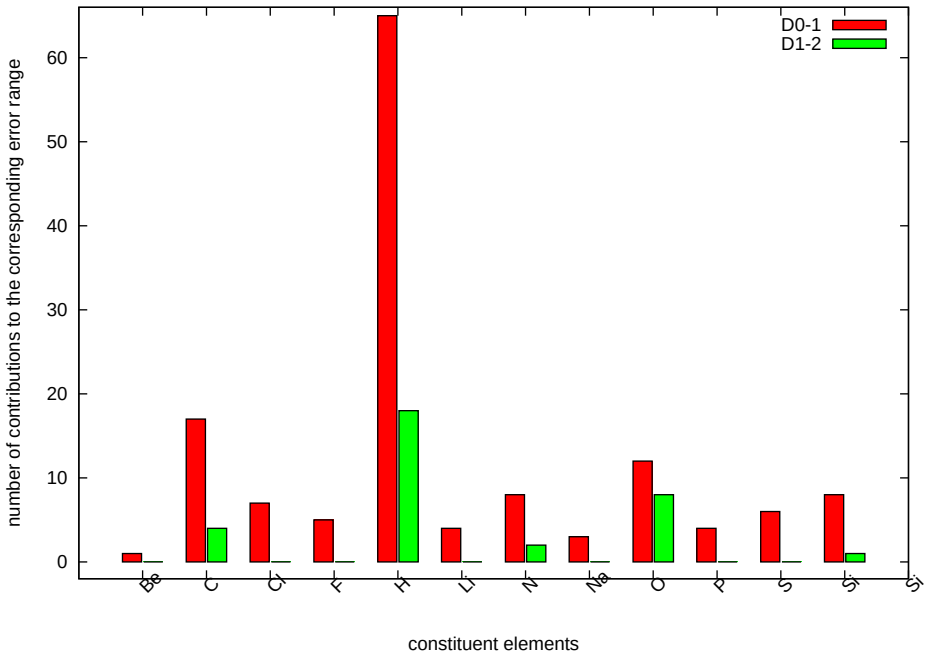

Figure 4.9: Contribution of each element in a particular zone of absolute deviation from the G03 values for the PAW calculations.

us look in figure 4.9 where I have taken the data from the work of Paier[85] and his collaborators. Here also we can see that silicon is found to be among the very few to have contributed to the relatively higher deviation zone. In this figure though we see contributions of carbon which in turn is not significant with the NLCC calculations. Hence there is an indication regarding the beahaviour of silicon in this particular picture. On the other hand in the calculations with NLCC we have to look for other discrepancies arising from sulphur and phosphorous. The problem with the phosphorous is indeed that of a smaller r_c. Calculations with smaller r_c have yielded improved results

but the physics behind this improvement is still not better understood. The question which is open at the moment is how to tackle the case of sulphur in this general approach to create the pseudopotentials with NLCC.

4.3.5 Similar effort with Linear Spin Density Approximation(LSDA)

Since the results with the calculations with the NLCC corrections to the PBE pseudopotentials were found encouraging, efforts were made to do the same under the LSDA formalism. The expected performance of those LSDA pseudopotentials were on the same lines as we experienced with the PBE + NLCC pseudopotentials. In the article by Fournier[91] et. al. the cal-

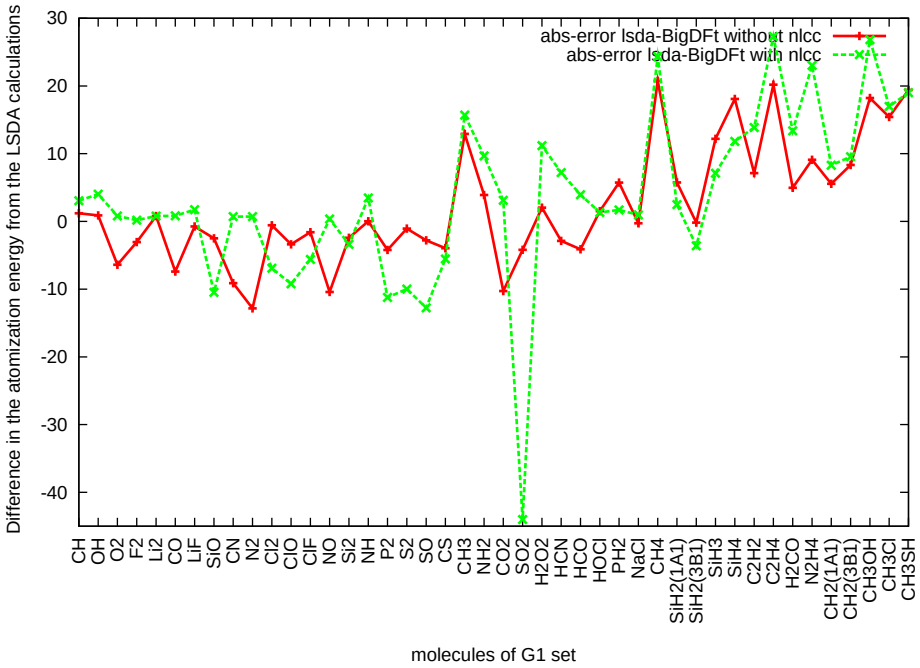

Figure 4.10: Deviation of the BigDFT values from

culations of the atomization energies are being reported. They have calcu-

lated the atomization energies by different theories like Kohn–Sham density functional theory (KS-DFT) with local spin density approximation (LSDA), two KS-DFT gradient-corrected methods, one hybrid Hartree–Fock/KS-DFT method similar to B3LYP, and the ab initio extrapolation procedures G1 and G2. They have reported that the empirical corrections improved the LSDA results greatly, while the other theories were improved slightly or not at all. We have tried to compare our results with LSDA and NLCC with the results of this report. In figure 4.10 the deviation of our calculations with their reported values are plotted for both the cases. The two cases are viz. LSDA without NLCC and LSDA with NLCC. as evident from the graph the results are not encouraging. But the reason for such discrepancy can be thought of as the error coming from the zero point energy which is neglected in the cases of LSDA calculations.

4.4 Conclusion

In this part of the research we have tried to find an effective way to implement the NLCC in the PBE and LSDA pseudopotentials on a wavelet basis. The idea was to calculate the atomization energies to a ceratin degree of accuracy and hence to use the pseudopotentials in further research. Since wavelet basis sets have shown great promist in the DFT calculations the need to implement various pseudopotentials on the wavelet basis set was felt. As of now as we have shown that the results with the NLCC implemented PBE pseudopotentials show good promise. Of course there is still room for improvement. And also the need to understand the deeper physics for few elements in the pseudopotential approach is felt. It must be highlighted that the non-conserving pseudopotentials can be as precise as PAW if NLCC is taken into acoount. We have also shown that the NLCC pseudopotential seemingly improve the overall calculations by a factor of 5, which is indeed a promising step in way of further research. Another important fact that is revealed in the above analysis is the independence of the accuracy of the geometrical structures from the jargon of NLCC in the pseudopotentials. By this we mean that even with pseudopotentials where the entire core density

is considered to be constant the geometries of the molecules are correctly predicted and understood. Having said that, we must also notice that implementation of NLCC improved the geometry part as well. The need to understand the LSDA formalism within the framework of NLCC is felt very deeply. At present the question is open as to why the discrepancy of the results would arise from the calculations of LSDA+NLCC as implemented on the wavelet basis.

In the next chapter we will go into the main part of the thesis, the treatment of the charged defects in silicon nanoclusters. Although those calculations are done without NLCC as the work was simultaneous yet for future calculations of charged defects one is tempted to use these NLCC corrected pseudopotentials. In fact the next calculations without NLCC are sure to give the geometries to a pretty high accuracy which is another reason to use such NLCC uncorrected pseudopotentials.

Chapitre 5

Ce chapitre aborde le sujet des défauts chargés dans le silicium. Jusqu'à présent, les défauts chargés ont principalement été étudiés en conditions périodiques (PBC). En effet, l'approche PBC est parfaite pour simuler un solide infini. Mais, comme je le montre dans ce chapitre, elle apporte aussi des artefacts. En particulier dans le traitement de l'électrostatique, où des traitements mathématiques important doivent être utilisés pour supprimer les interactions non désirées entre répliques. Notre approche vise à simuler correctement un défaut chargé, tout en conservant de bonne propriétés pour le matériau massif. Elle consiste à simuler le défaut dans un nano-agrégat. Le traitement de l'électrostatique est correct dans un nano-agrégat et les résultats obtenus peuvent être extrapolés au matériau massif, comme il est montré dans ce chapitre. Les perspectives de cette méthode sont aussi abordées ici.

Chapter 5

Charged Defects in Silicon Nanoclusters

5.1 Introduction

The defects as it is mentioned in the introductory chapters are studied extensively under the formalism of DFT. It may be repeated as an emphasis here as well that these calculations complement experiment in all possible ways. They not only help to interpret experimental findings and link them to an atomistic model of the relevant defects, but also provide additional data such as formation energies, geometric structures, or the character of the wavefunctions that cannot be obtained with state-of-the-art experimental methods. It is also worth mentioning again that the defect is usually modeled in a supercell, consisting of the defect surrounded by many other atoms of the host material, which is then repeated periodically throughout space. The treatment is formally known as the Periodic Boundary Condition(PBC) approach. There have been reports[92] of the effectiveness of this approach. However, it must be kept in mind that the use of supercells implies that the isolated defect is replaced by a periodic array of defects. Such a periodic array contains large imagineary defect concentrations, resulting in artificial interactions between the defects that cannot be neglected by any means. These interactions include overlap of the wavefunctions, elastic in-

teractions, and (in the case of charged defects) electrostatic interaction. A large variety of approaches to control electrostatic artifacts exists in the literature, as has been reviewed recently by Nieminen[93]. As I have mentioned in the earlier chapter (state-of-the-art chapter) supercell calculations for the charged systems must always include a compensating background charge, since the electrostatic energy of a system with a net charge in the unit cell diverges[62][66]. The most common practice is to include a homogeneous background, which is equivalent to setting the average electrostatic potential to zero. By increasing the supercell lattice constant L, the isolated defect limit can be realized in principle for $L \to \infty$. Again it is to be remembered here that the defect energy converges pretty slowly with respect to L (to be precise it is L^{-1}). The origin of this effect lies in the electrostatic interaction of the defect with its periodic images which is unphysical. There is of course an interaction of the charged defects with the compensating background. Its magnitude can be estimated from the Madelung energy of an array of point-charges with neutralizing background[62]. Makov and Payne[66] proved for isolated ions that the quadrupole moment of the charge distribution gives rise to a further term scaling like L^{-3}. For realistic defects in condensed systems, however, such corrections, scaled by the macroscopic dielectric constant ϵ to account for screening, do not always improve the convergence[94][73]. As mentioned in the chapter of the state-of-the-art there are other methods to deal with the electrostatics of these charged defects amidst the image charges and the background compensation in the PBC framework. All the calculation reported here are done with the DFT code BigDFT with the parameters converged for silicon (discussed in the previous chapter). And all the calculations are spin average. The energy convergence criterion was kept to 10^{-4} Hartree and the force convergence criterion was kept to 10^{-5} Hartree/Bohr. The total energy convergence criterion is based on the norm of the gradient of the wave-function in the convergence cycle. In the following figure 5.1 and figure 5.2 it shown in detail how the periodic extension of the supercell brings in the unphysical elastic and electrostatic interactions between the real defect and the imagineary defects. In this thesis a new approach is undertaken with a view to study the charged defects under a simple yet correct electrostatic

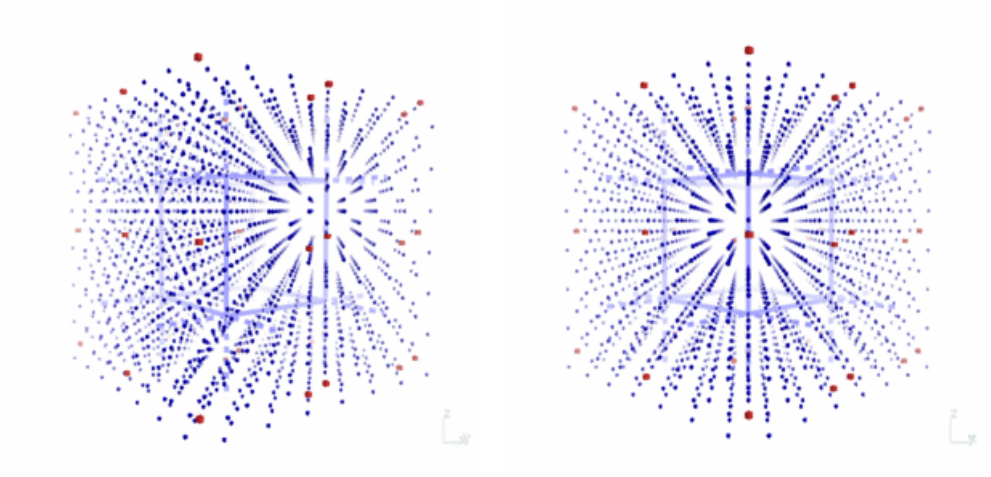

Figure 5.1: A schematic representation of the image charges around the real defect in PBC. The red dots inside the highlighted box are the real defects (charged or uncharged) and the rest are the product of the periodic extension along all directions.

model. The other method can be broadly classified as the cluster method. In the cluster approach, a reasonably large cluster of atoms truncated from the bulk with a defect at the center is used to simulate the bulk defect. For this work we have created an isolated cluster of silicon atoms saturated by hydrogen at the surface. Recent advances in electronic structure algorithms, such as real-space methods[95][96] bring a new perspective to theoretical investigations of defects in materials in this cluster approach. Over the last few years, these methods with the use of ab initio pseudopotentials have proven their efficiency and accuracy for microscopic understanding of many physical systems. In the works of Serdar Ogut and his collaborators reports have been made on atomic and electronic structures of neutral and positively charged monovacancies in bulk Si, investigated from first principles using a cluster method[97]. In their work they have done calculations in real space on bulk-terminated clusters containing up to 13 shells around the vacancy (about 200 Si atoms). Vacancy-induced atomic relaxations, Jahn-Teller distortions, vacancy wave-function characters, and relaxation and reorientation energies are calculated as a function of the cluster size and compared with available

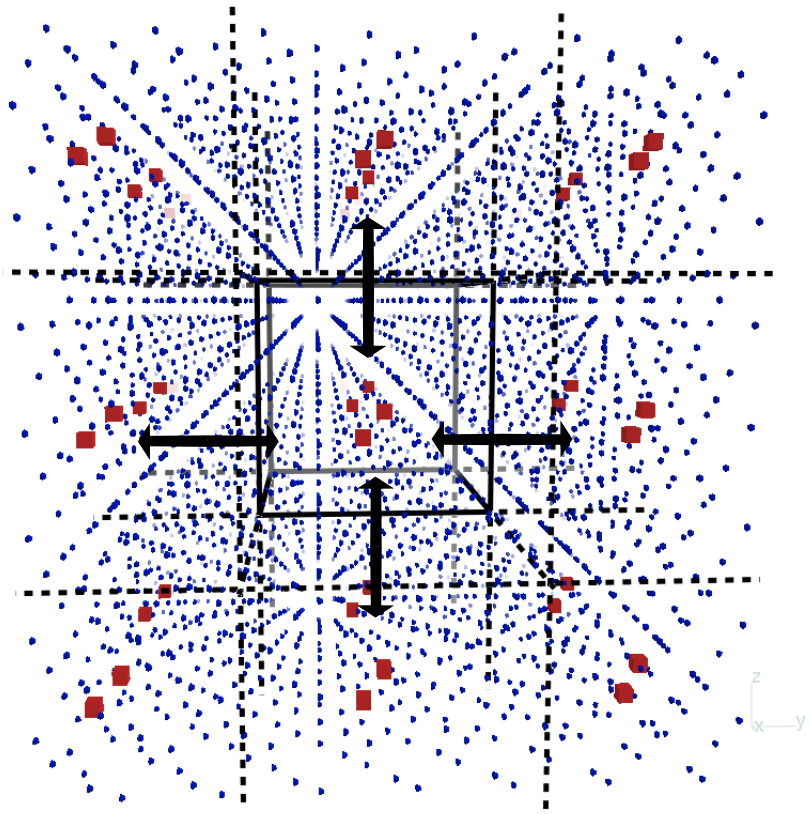

Figure 5.2: A schematic representation of the elastic and electrostatic interactions between the real defect and the image defects PBC.

experimental data. But no reports have been made since then about the applicability of this method in calculating the formation energy of vacancies along with the formulation of a realistic charged-defect electrostatics. There are two things which are very important in this approach. The first one is the surface to bulk interaction as shown in figure 5.4. Since it is an attempt to simulate bulk with a finite system we will definitely have the finite size effect which can tracked down by the proper electrostatic analysis. This surface electron density would essentially interact with the perturbed electron density around the vacancy to create a new phenomenon of trapped charges, as will be shown in the following sections. This phenomenon of trapped charge is the second aspect of this methodology. Again in our analytical model we

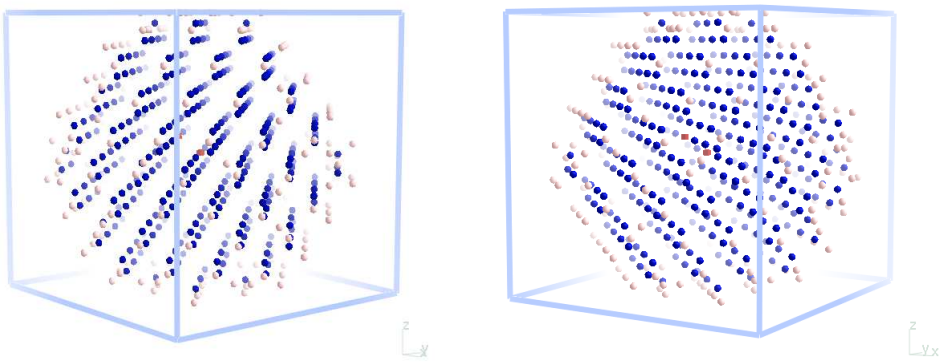

Figure 5.3: A schematic representation of the cluster method. The clusters are pacified by hydrogen atoms at the surface. The presence of only one array of red dots inside the box ensures the simplicity and realness of the defect representation.

would assume the clusters to be spherical, which in reality is true to a large extent for really large clusters. But as shown in the schematic figure the clusters are, in reality, polygons of some odd shape. Hence there is an element of shape factor in this analysis as well.

5.2 Comparison of formulae (PBC vs. FBC)

5.2.1 PBC formalism to calculate the formation energy

Since in our case we are dealing with isolated clusters, hence the boundary condition that we are using can be called Free Boundary Condition (FBC). Let us now take a look at the respective expressions, under both the frameworks of PBC and FBC, to calculate the formation energy of vacancies. In an overview study of defect analysis Van de Walle[98] et. al. have summarised a general formula to calculate the formation energy of the defects in PBC. The formation energy of a defect or impurity X in charge state q is defined

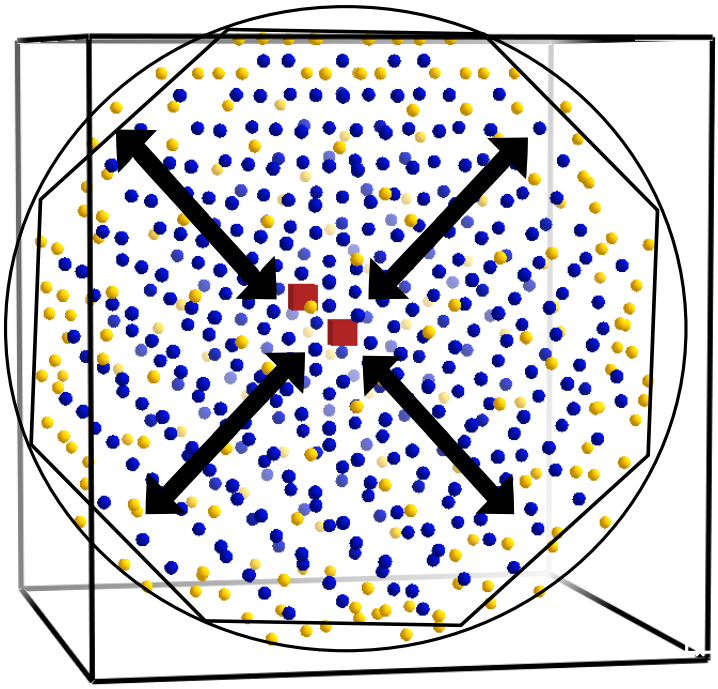

Figure 5.4: A schematic representation of the surface to bulk interaction in the isolated silicon clusters.

as

$$E^f[X^q] = E_{tot}[X^q] - E_{tot}[bulk] - \sum_i n_i\mu_i + q[E_F + E_v + \Delta V]. \qquad (5.1)$$

$E_{tot}[X]$ is the total energy derived from a supercell calculation with one impurity or defect X in the cell, and $E_{tot}[bulk]$ is the total energy for the equivalent supercell containing only the bulk species (for example Si, Ga, GaN etc.). n_i indicates the number of atoms of type i (host atoms or impurity atoms) that have been added to ($n_i > 0$) or removed from ($n_i < 0$) the supercell when the defect or impurity is created, and the μ_i are the corresponding chemical potentials of these species. For the sake of clarification here we can describe chemical potential as a physical quantity that represents the energy of the reservoirs with which atoms are being exchanged. E_F is the Fermi energy,

referenced to the valence-band maximum in the bulk. Due to the choice of this reference, the users of this method need to explicitly put in the energy of the bulk valence-band maximum, E_v , in the above mentioned expression for the formation energy of charged states. A correction term $DeltaV$ is also needed to be added to the rest of the expression, to align the reference potential in the defect supercell with that in the bulk. A problem when calculating E_v is that in a supercell approach the defect or impurity strongly affects the band structure. Therefore one cannot simply use E_v as calculated in the defect supercell. To solve this problem a two-step procedure is used: (a) The top of the valence band E_v is calculated in the bulk species by performing a band-structure calculation at the Γ point and (b) an alignment procedure is used in order to align the electrostatic potentials between the defect supercell and the bulk. The fact that E_v found for the bulk, (i.e. in a defect-free supercell) cannot be directly applied to the supercell with a defect can be attributed to the long-range nature of the Coulomb potential and the periodic boundary conditions inherent in the supercell approach. The creation of the defect has been reported to give rise to a constant shift in the potential, and this shift cannot be evaluated from supercell calculations alone since no absolute reference exists for the electrostatic potential in periodic structures. One common method is to align the electrostatic potentials by inspecting the potential in the supercell far from the impurity and aligning it with the electrostatic potential in the bulk species. This leads to a shift in the reference level ΔV, which needs to be added to E_v in order to obtain a more appropriate alignment.

5.2.2 FBC formalism to calculate the formation energy

In the scenario with FBC we try to build a formalism in similar terms. Here also we calculate the total energies of the nano clusters with and without the defects. To start with let's put the formula as the following,

$$E^f = E_{tot}[defect] - E_{tot}[bulk] + \mu_{bulk-atom} + q_{trpd}\Delta\mu + q_{sys}\mu. \qquad (5.2)$$

As we have done the calculations with vacancies in bulk silicon let me rewrite the above equation in terms of bulk silicon for the sake of clarity.

$$E^f[Si(m-vacancies)] = E_{[n-m]Si+pH} - E_{nSi+pH} + m\mu_{Si} + q_{trpd}\Delta\mu_e + q_{sys}\mu_e, \tag{5.3}$$

where $E^f[Si(m-vacancy)]$ is the formation energy of the vacancy (monovacancies or divacancies), $E_{[n-m]Si+pH}$ and E_{nSi+pH} are the total energies of the defect and the perfect system respectively. In the nano cluster there are in general n Si atoms pacivated by p H atoms at the surface. m is the number of vacancies created by removing atoms, (1 for mono vacancy and 2 for divacancy). μ_{Si} is the chemical potential of bulk silicon which can also be thought of as the energy of 1 bulk silicon atom. The most important and interesting factors are the last two factors of the formula. Although the physical importance of the quantity q_{trpd} will be explained in the following sections yet it can be helpful to put in an overview of what it is in this context. q_{trpd} is the amount of charged trapped near the defect as a consequential effect of the defect formation. It is a section of the deformed electron density near the defect and its value depends on the charge of the system. $\Delta\ mu_e$ is the difference of the Fermi energy between the defect and the perfect system due to the occurence of the defect. q_{sys} is the charge of the entire system for the charged cases. It is of no use for the uncharged cases. μ_e is the Fermi level of a particular charged system which can be considered as the reservoir from where the charge is taken. To analyse the formula further we have to analyse the electron density of the different defect systems.

5.3 Density analysis of the defect systems

5.3.1 Uncharged clusters

As it was stated earlier there will be surface effects in the approach within the FBC formalism. The surface of the nanoclusters can cause some perturbation in the electron density per unit volume near the center of the cluster. The reason behind this can be attributed to the presence of the silicon-hydrogen

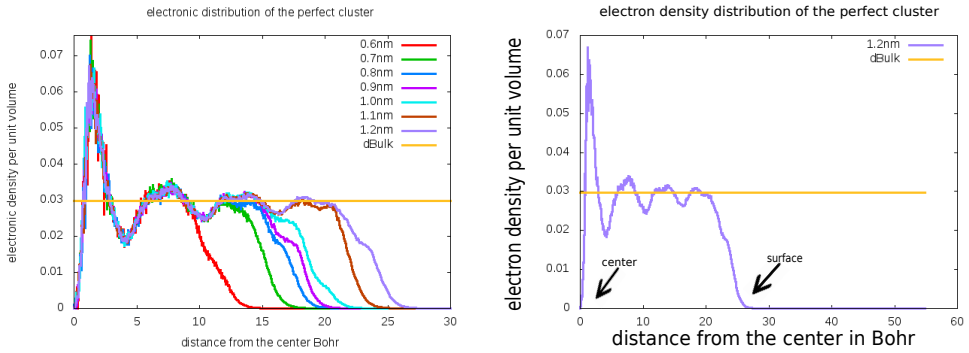

Figure 5.5: The variation of the electron density per unit volume around each shell of the nano cluster (a) for all the clusters (b) for the cluster of radius 1.2 nm

bonds at the surface which are electronically different from the bulk silicon-silicon bonds. For our analysis we have studied clusters from 0.6 nm to 1.2 nm. The surface induced phenomenon may indeed bring about a charge separation between the surface and the core center of the cluster. If we see at the figure with the variation in the electron density per unit volume around each shell of the nanocluster of a perfect cluster (without any defect) we understand that the behavior near the center is similar to that of the PBC calculations. As it is mentioned in the figure because of the surface and the surface hydrogens the electron density trails off to zero. In the figure 5.5(a) all the densities are plotted on the same plot so as to give a comparative idea of the behavior of the densities in clusters of different sizes. We see from the figure 5.6(b) that only near the vacancy (di and mono for this case) the density per unit volume of the shell tends to differ from each other. For the rest of it the curves are nicely superimposing each other. There is also a question of the convergence of the observed and calculated physical quantities with the cluster size. This question will precisely be address in the coming sections. Let us have a look at the behavior of the density for the defect states. In the figures 5.6 (a) and (b) it is shown how the electron density per unit volume near the defect is disturbed for different cluster sizes. Near the center we see because of the presence of the defects the electronic arrangement

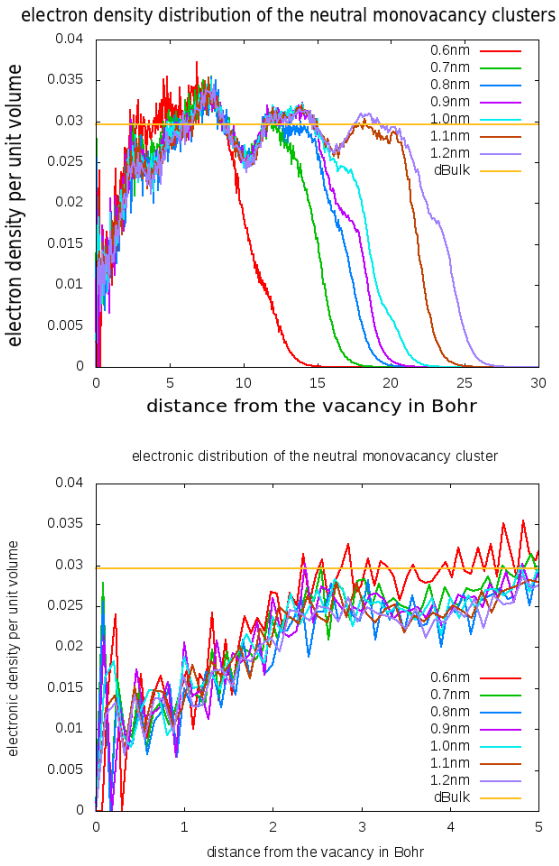

Figure 5.6: The variation of the electron density per unit volume around each shell of the nano cluster with a monovacancy (a) for all the clusters. (b) for all the clusters near the vacancy.

is different from that of the perfect clusters. A close look even at the density distribution of the divacancy clusters would confirm the perturbation of the density due to the presence of the vacancies. If we look carefully in figure 5.8 with the density plots of the largest cluster with a monovacancy and divacancy respectively, we will see a clear difference in the electron density distribution near the vacancies between the monovacancy clusters and the divacancy clusters. It forces us to think that this might be the effect of the surface and it triggers the thought of any charge separation between the surface and the center of the nano cluster.

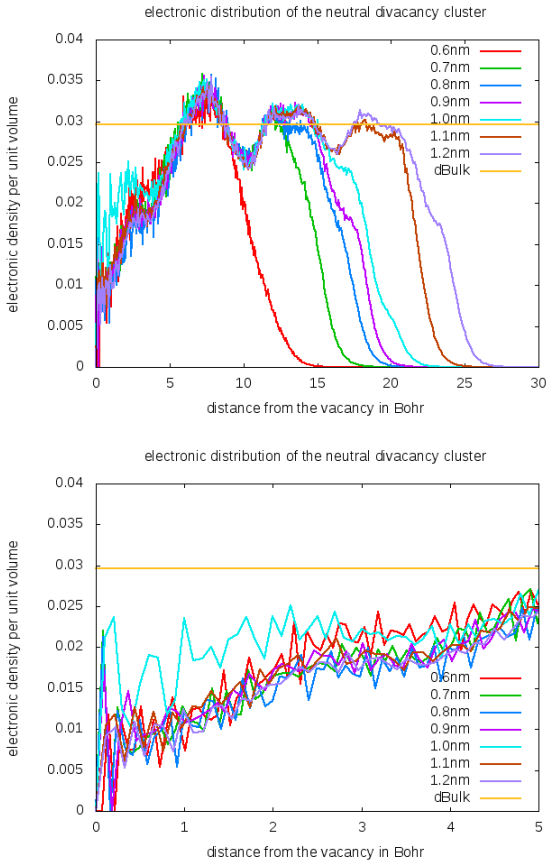

Figure 5.7: The variation of the electron density per unit volume around each shell of the nano cluster with a divacancy (a) for all the clusters. (b) for all the clusters near the vacancy.

5.3.2 Charged clusters

In this section we will have a look around the vacancy in the charged clusters. The main aim of the thesis is to create a formalism with which the charged systems can be dealt without the image charge/defect interacts of PBC formalism. Hence it is more interesting here to look into what happens to the electron density distribution in the nano clusters when the defects are charged. The overall density plots reveal a fact that near the vacancy the electronic density is disrupted due to the presence of surface. And the zoomed in figures also indicate that the charges of the system causes further

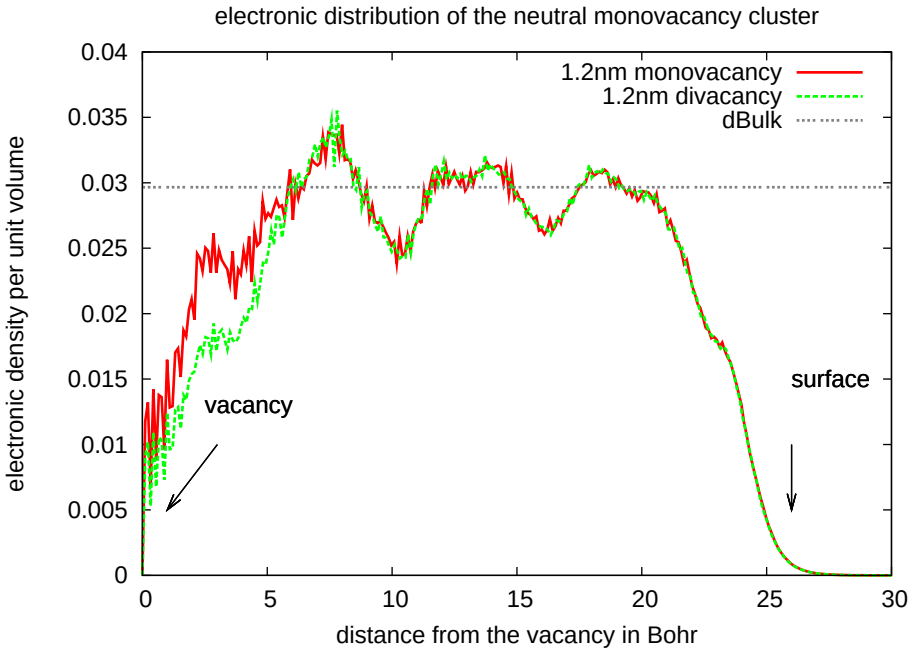

Figure 5.8: The difference in the electron density distribution near the vacancies between the monovacancy clusters and the divacancy clusters. The cluster size is 1.2nm

perturbation in the electron density near the vacancy. The question that one may think about now is what is the effect of the system charge to the electron density around the vacancy? We see from figures 5.8 , 5.9 and 5.10 of this section that only near the vacancy the density per unit volume of the shell tends to differ from each other. For the rest of it the curves are nicely superimposing each other. A further analysis with another tool would eventually reveal the finer and clearer picture.

Mulliken analysis

Mulliken population analysis[99] is one tool which helps to estimate the partial atomic charges from calculations carried out by few different methods of

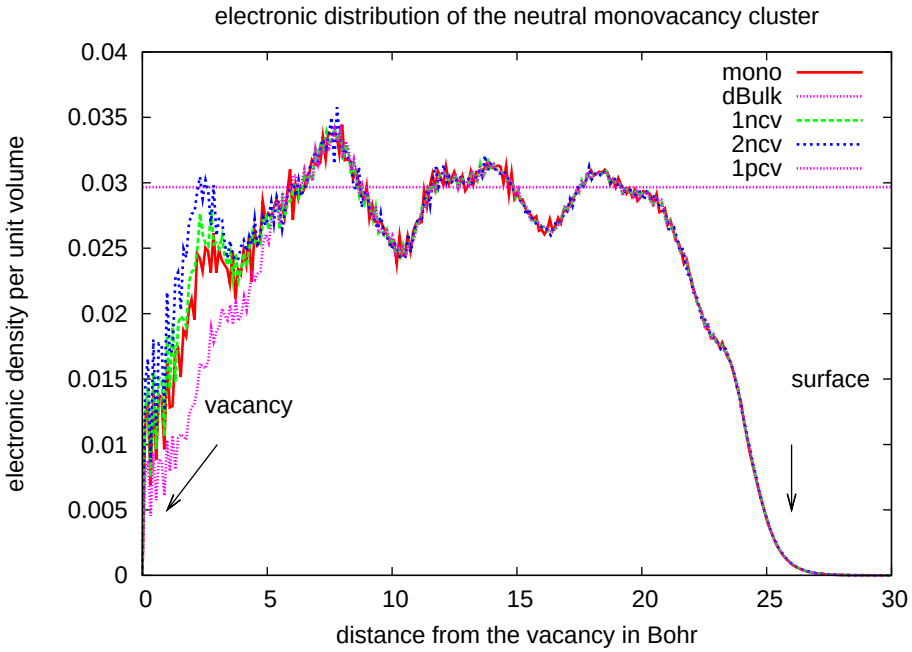

Figure 5.9: The difference in the electron density distribution near the vacancies for a monovacancy cluster with different charge states.

computational chemistry, particularly those based on the linear combination of atomic orbitals molecular orbital method. The charge or spin density distribution is studied as one of the most important properties of a molecule or a cluster. Although there is no unique definition of how many electrons are attached to an atom in a molecule or in a cluster it has nevertheless proven useful in many cases to perform such population analyses. Due to its simplicity the Mulliken population analysis has become a very familiar method to *count* electrons to be associated with an atom. As an end result of this calculation what is obtained is the *gross charge in any atomic orbital*. Which is defined in this theory as the difference between the number of electrons in an atomic orbital and the total number of electrons in the ground state of the free neutral atom. For our research this analysis is done with the

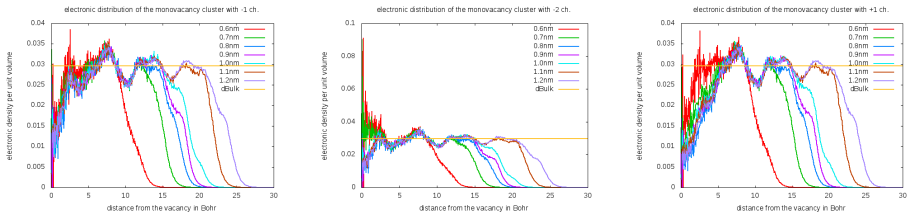

Figure 5.10: The variation of the electron density per unit volume around each shell of the nano cluster with a monovacancy (a) with 1 negative charge (b) with 2 negative charge (c) with 1 positive charge.

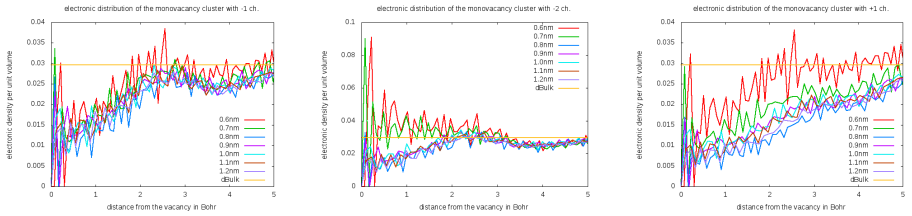

Figure 5.11: The variation of the electron density per unit volume around each shell of the nano cluster with a monovacancy (a) with 1 negative charge (b) with 2 negative charge (c) with 1 positive charge , around the vacancy.

nano clusters of all sizes for all charge states and vacancies. The following results will illustrate the difference in the population of the electrons of the atoms around the vacancy. From figure 5.12 as one can understand that the gross charge around each atom is pretty much the same for all the systems except for the zone around the vacancy. Due to the nature of the bonds deep inside the bulk we see that the number of electrons in a Si atomic orbital is slighlty greater than the total number of electrons in the ground state of the free neutral Si atom. As we go towards the surface due to the presence of the hydrogens we experience the reverse the phenomenon. Right at the surface the hydrogens tend to pull the electron density towards themselves being more electronegative than silicon. Let us see for the fact that indeed the discrepancy of the electron population is manifested near the vacancy or at the center of the cluster. In figure 5.13 (a) we show all the gross charge plots superimposed on each other, and we see that except for the zone near

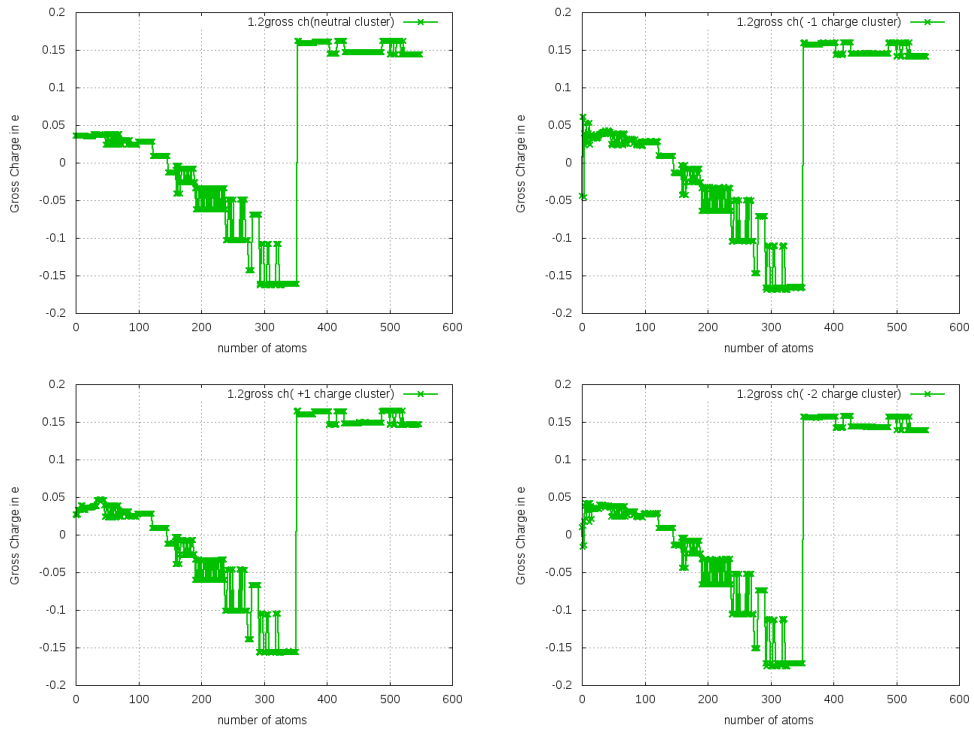

Figure 5.12: The gross charge around the atoms in a cluster of size 1.2 nm for (a) perfect cluster (b) monovacancy cluster with charge -1 (c) monovacancy cluster with charge +1 (d) monovacancy cluster with charge -2. The x-axis represents the atom ids in general. The hydrogens hence have the latter ids as the clusters are built atom centered.

the center of the cluster, in rest of the zones the plots are almost identical. At this point it is felt necessary to comment on a small difference that is observed for the case of the system with charge +1. As far as the hydrogens are concerned they are more electronegative than Silicon and hence pull the electron cloud towards themselves. But due to the presence of the positive charge in the system and, as we will show how it also affects the charge trapping near the vacancy, there is a Coulombic interaction between the positive charge of the system and the stretched electron cloud near the surface. This gives rise to a variation in the values of the grosscharges for the system with charge +1. This fact forces us to look deeper and closer in the zone of the mono vacancy (figure 5.13 (b)). Here we see that corresponding to each

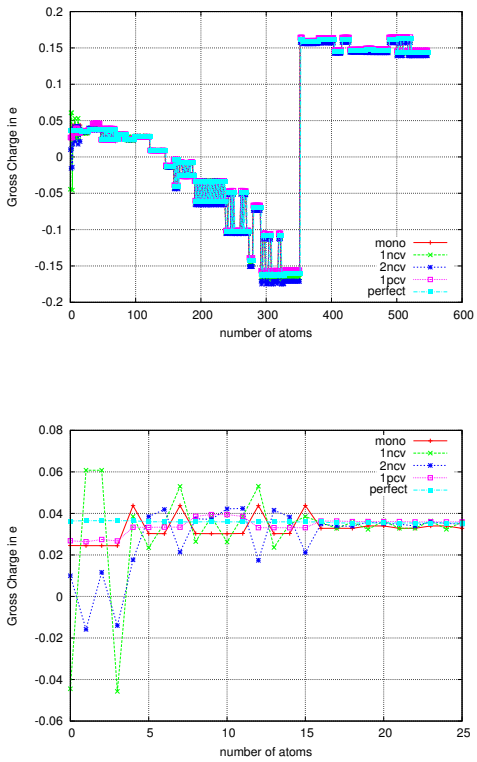

Figure 5.13: The gross charge around the atoms in a cluster of size 1.2 nm for (a) all clusters (b) all clusters around the vacancy.

charge state there is a different behavior of the grosscharge for that particular charge state. Since the 15^{th} atom or the third shell around the vacancy the gross charges tend to behave similarly. From the above figure it is not easy to quantify this effect. Now to quantify this effect we use the expression,

$$Q_{trpd} = Grosscharge_{defect} - Grosscharge_{perfect}, \tag{5.4}$$

where Q_{trpd} can be thought of a residual charge which is trapped near the vacancy, which is the difference between the grosscharge of the defect system of any charge state to that of the perfect system. Now we can try to find out whether this Q_{trpd} can be considered physical for a given analysis. Indeed if we can see that this quantity is a converged one with the size of the nano

clusters then we can understand the significance of this physical quantity in a broader physical sense. In figure 5.14 we see that with the cluster size

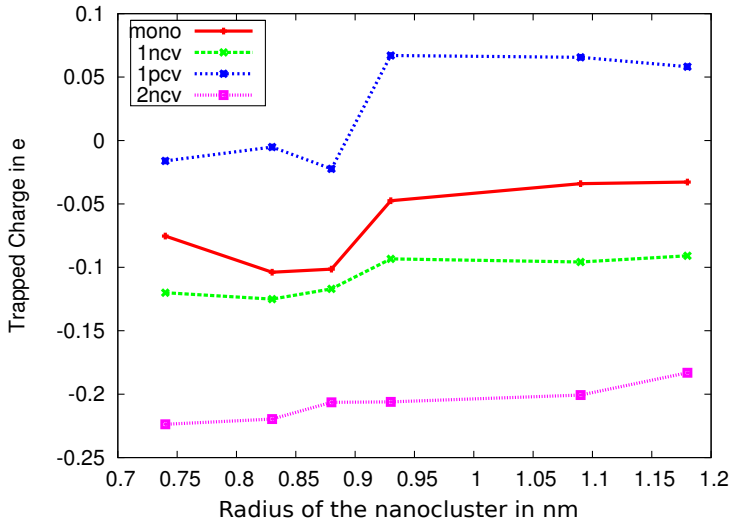

Figure 5.14: The convergenge of Q_{trpd} with cluster size.

the quantity Q_{trpd} converges to values for a cluster for each of the different charge states. We can see from the figure that the values of the Q_{trpd} have converged since the cluster size of 1.0nm, and it is only natural to consider clusters from 1.0nm for further calculation of physical quantities. A striking fact is that even if the value is very low yet the uncharged mono vacancy is a bit negatively charged. And we can see that increase in the charge of the system increases the value of Q_{trpd}. Hence Q_{trpd} is the most negative for the most negatively charged system. This of course gives an impression of the behavior of vacancies in a charged nano cluster. We can conclude from here that indeed the defect in the nano clusters has a tendency to trap charges and that quantity is dependent of the charge of the system.

Physical origin of the trapped charge

The presence of the trapped charges near the vacancy in the nano clusters is a physical phenomenon which must have a relation any change in other physical properties of the system. Results have shown as cited earlier that presence of defects changes the HOMO-LUMO gap and the band structure of any material, silicon for example in this thesis. Since we are dealing with FBC we cannot do a band structure calculation, but a diagonalisation method to calculate the HOMO-LUMO gap for the nano clusters can be used instead. In this mode of calculation we calculate the HOMO-LUMO gaps for the nano clusters of all sizes and charge states i.e. the difference between the highest occupied molecular orbital(HOMO) and the lowest unoccupied molecular orbital(LUMO). In the Free Boundary Conditions the HOMO-LUMO gap is found to be heavily overestimated for smaller clusters. But the HOMO-LUMO gap of the larger clusters are found to be converging close to the bulk value. There are questions of quantum confinement in the nano clusters of course. And the fact the HOMO-LUMO gap is heavily overesmitated in very small nano clusters owe its origin to this confinement effect. In figure 5.15 we have aligned HOMO levels so as to understand the effect of the presence of the defects. The extreme-right column shows the HOMO-LUMO gap as calculated from the 1.2 nm perfect cluster. The middle column and the extreme left column are for the neutral monovacancy and divacancy respectively. There we can see that indeed there are states introduced within the HOMO-LUMO gap of the perfect nano clusters. Which means creating one defect might mean otherwise to introduce energy states within the HOMO-LUMO gap of a perfect system. We can investigate more in the same spirit the system of the charged monovacancy. In figure 5.16 we have shown a similar figure. Here we see that taking away one electron from the system or giving one more electron to the system reduces the HOMO-LUMO gap. In other words this can be though of as an effective way to reduce the barrier of the electron flow in the bulk silicon. But there is something which is found to be striking in this analysis. It seems that an excess of negative charge in the nanoclusters increases the HOMO-LUMO gap

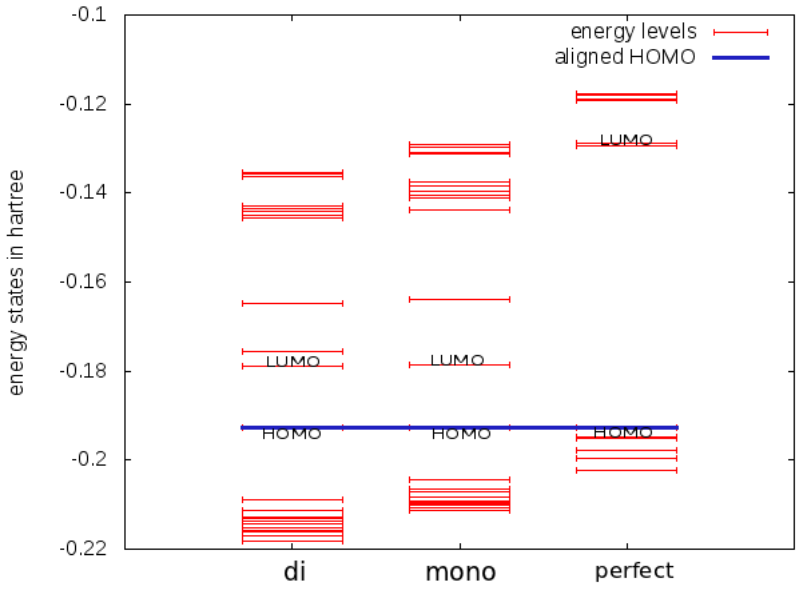

Figure 5.15: Representiing the change in the HOMO-LUMO gap due to the presence of defects (uncharged) (-1 means mono vacancy and -2 means divacancy)

.

again. In reality the HOMO-LUMO gap of a neutral monovacancy cluster is narrower than a monovacancy cluster of charge -2. We have already seen with the mulliken analysis plot that increase in the negative charge of the system will increase the negativity of the charge at the center. It may be because of this charge an excess of charge is not welcome due to the coulombic repulsion between the excess charge and the trapped charges. The argument is still an open matter for further analysis and explanation. Now coming back to the origin of the trapped charges again we must take into consideration the fact that due to the presence of the defects and the charges there is a shift in the chemical potential of the respective charge-defect systems. This shift can be quantified as

$$\Delta\mu_e = \mu_{e_{perfect}} - \mu_{e_{defect}}. \tag{5.5}$$

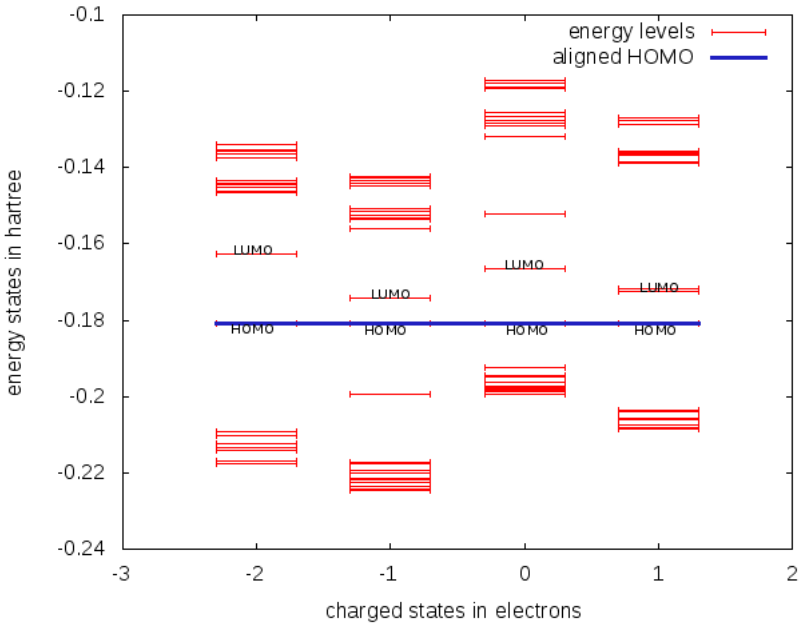

Figure 5.16: Representiing the change in the HOMO-LUMO gap due to the presence of defects (charged monovacancy with charges = -2,-1,0,1)

.

And the trapped charge Q_{trpd} is related to this shift in chemical potential by the energy required for that charge to be brought at the center around the vacancy in the cluster and we can quantify that energy as

$$E_{trapped_{charge}} = Q_{trpd}\Delta\mu_e. \tag{5.6}$$

This expression thus arrives in the formula of calculation of the formation energy. Now the following motivation would be to look for an analytical electrostatic model which must simulate this sort of a charge separation in the nanoclusters.

5.4 Comparison of results obtained

Table 5.1 shows the performance of the model we have used to calculate the formation energies. Experimental values in the spirit of the work by Watkins

Table 5.1: Table representing the comparison of the values of the formation energies of monovacancies as calculated under PBC[75] and FBC(this work) and experiment[3].

Charge	PBC	FBC	Expt.
0	3.605	3.70	3.602
-1	4.319	4.63	—
-2	4.909	4.67	—
1	3.545	3.86	—

and Corbett are still not available for the charged monovacancies and hence it is still a point of time to talk about the accuracy of the model in discussion. Yet we see our results are not far from the PBC values. Here some things are to be kept in mind. The important thing is the fact that our motive is to create a model without defect-defect interaction and devoid of any background charge concept. In the following sections we will put forward an analytical model to simulate the electrostatics of the given FBC formalism which would indeed prove that our results have a very good chance to be accurate with respect to the future experiments. The question of convergence can be raised here and we will show in due course of this thesis that the convergence issue can be tackled well with the electrostatic and elastic model of the entire formalism.

5.5 Electrostatic model

In this work we have worked out an electrostatic scheme which appears fit the atomistic model representation of the defects in bulk silicon and helps to incorporate the concept of the trapped charges into an analytical model. As the following figure will show in this approach we deal with an isolated system free from all the interactions between the image charges and the real bulk defect. Of course we have a surface to bulk interaction but as it will be shown in the following analysis that this surface to bulk interaction indeed helps to picturise the real electrostatic scenario of the cluster approach. In the following section we will try to understand how this gives rise to the

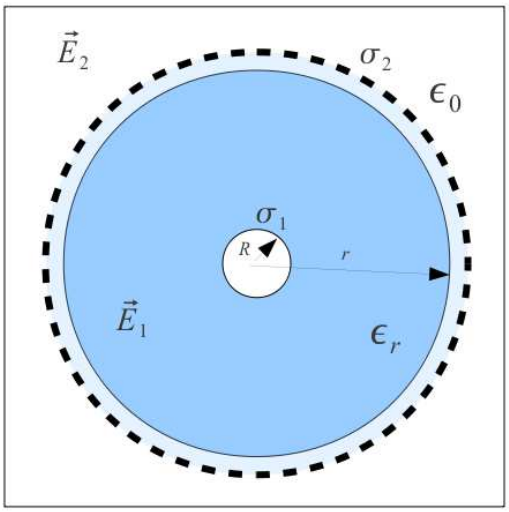

Figure 5.17: Spherical shell of radius R with a smeared surface charge and a net charge at the center with the tiny sphere.

previously shown phenomenon of trapped charges.

5.5.1 Overview

Since the surface electron density interacts with the somewhat perturbed electron density around the defect, it can be apprehended that this interaction will cause some charge separation between the surface and the center of the cluster. In this analysis we are dealing with the vacancies. Because of the absence of the atoms there are dangling bonds from the neighboring atoms of the vacancies. These electron density interacts with the surface and as a consequence of the shift in chemical porential we find the occurence of the trapped charges. The electrostatics of the entire system can be thought of a problem where it is the objective to find out the elctrostatic energy that can be stored in a cluster of 'n' Silicon atoms passivated by 'p' Hydrogen atoms at the surface. The first model that is considered here is for that of an uncharged cluster of radius 'r'. Although in reality the clusters are not strictly spherical they are assumed to be perfect spheres in the model.

5.5.2 Details

Well as shown in figure 5.17 let the cluster be a spherical shell of radius R with a net positive charge q placed at the center and a net positive chage $-q$ smeared all over the surface of the spherical shell. The spherical shell is filled with a dielectric substance with a dielectric constant ϵ_r. Among the various methods used to calculate the total electrostatic energy stored in any system, the one that is used here is with the method of finding the electrostatic field in different regions of the system. Then the electrostatic energy stored in the system will be given by:

$$W = \frac{\epsilon_0}{2} \int \epsilon_r E^2 \, d\tau \tag{5.7}$$

where the symbols have usual meaning.
Let us divide the regions in our system into two different parts, viz. for the electrostatic field inside the spherical shell, E_I, and for the electrostatic field outside the spherical shell, E_{II}. If we consider a Gaussian surface outside the spherical shell we can readily see that the total charge enclosed within the Gaussian surface is 0 and hence the field outside the spherical shell, E_{II}, is evidently 0.
Now to calculate the field inside the spherical shell we consider a sphericall Gaussian surface along the surface of the spherical shell of our model. Here the total charge enclosed is q. If we apply Gauss Law here we get:

$$\int E_I . \, da = \frac{Q_{enclosed}}{\epsilon} = \frac{q}{\epsilon_0 \epsilon_r} \tag{5.8}$$

By symmetry considerations we can see that the field inside is constant and is radially outward. Hence we can easily deduce that the field inside the shell is:

$$E_I = \frac{q}{4\pi\epsilon_0\epsilon_r r^2} \tag{5.9}$$

Now to calculate the total energy stored in the system we fall back to equation (1) and integrate over the spherical volume element $d\tau = r^2 Sin\theta d\theta d\phi dr$. Hence the final expression of the total electrostatic energy stored in the system is given by:

$$W = \frac{\epsilon_0}{2}\int \epsilon_r (\frac{q}{4\pi\epsilon_0\epsilon_r r^2})^2 r^2 Sin\theta d\theta d\phi dr \tag{5.10}$$

where the integrating limits for θ and ϕ are from 0 to π and 0 to 2π respectively and hence integrating over θ and ϕ we get 4π. And the limit of integration for r is from 0 to R. Hence from equation (4) we get:

$$W = \frac{q^2}{8\pi\epsilon_0\epsilon_r}\int_0^R \frac{1}{r^2} dr \tag{5.11}$$

5.5.3 Modification

From equation (5.11) we can see that there is a problem, for the integrated value at $r = 0$ is definitely blowing up. And it is evident from the fact that the electrostatic energy of a point charge is indeed infinite. Hence we feel the need of modifying our model a bit. Let us now assume another very tiny spherical shell around the charge q. And we restrict ourselves in knowing the electrostatic energy within the region between the two shells. Let the radius of the tiny shell be R_1. Now equation (5.11) becomes integrable again. The total energy stored within the region of our interest is now given by:

$$W = \frac{q^2}{8\pi\epsilon_0\epsilon_r}[\frac{1}{R_1} - \frac{1}{R}] \tag{5.12}$$

5.5.4 Remarks

The units of the quantities in the final expression of the total electrostatic energy are all in S.I. units. Hence the energy that will be computed from this expression will be in Joules(J). To compare with the total electronic energies of our systems we need to convert this energy in to electron-Volts (eV). The importance of this model will be explained in the following sections as we will see the correspondence of the functional similarity of derived expression to the actually calculated values. We wish to see whether this analytical model is suitable to simulate the real electrostatics of the system. In the section where we discuss the validity of this model we will show that the convergence of the formation energy of the vacancies follow the same functional trajectory as the electrostatics mentioned in this section.

5.6 Geometry of defects in nanoclusters

An important section of study regarding the defects is their geometry. A defect essentially is an inconsistency in the geometrical structure whose presence will alter the electronic structure of the material. The change in the electronic structure is often manifested in the geometrical changes that take place due to the defects. The movement of atoms around a vacancy or a foreign substitutional element can be thought of as a primary example. In a report[100] D.V. Makhov and L.J. Lewis have talked about the distortions for the divacancy in silicon. In another letter[101] S. Ogut and J. R. Chelikowsky have reported similar distorsions around the divacancies in crystalline silicon. The general understanding of these distorsions is based upon an electronic phenomenon known as the Jahn-Teller distorsion.

5.6.1 Jahn-Teller Distorsion (JT)

The formal statement of the Jahn-Teller theorem states that in a nonlinear molecule, if degenerate orbitals are asymmetrically occupied, a distortion will occur to remove the degeneracy or in other words in an electronically degenerate state, a nonlinear molecule undergoes distortion to remove the

degeneracy by lowering the symmetry and thus by lowering the energy. In context of the study of defects it is found that due to the removal of an atom to create a vacancy (or more) an untended degeneracy is enforced upon the system. To remove that, the atoms around the vacancy would move in such a fashion which would cause the total energy of the system to go down in value to attain a more stable state. Hence the real manifestation of this electronic effect of the removal of the degeneracy is found in the change in the geometry of the system in and around the defect. Since the pioneering electron paramagnetic resonance (EPR) studies of Watkins and Corbett[3], there have been controversies about the electronic and atomic structures of the divacancy in crystalline Si. These controversies have been concerned with the exact nature of the above mentioned symmetry-lowering Jahn-Teller distortions that split the degenerate deep levels. There are of course many reports which would reveal the fact that the sense and the magnitude of these distortions, as inferred from the EPR data and theoretical calculations, have been at variance. There can be two different manifestations of these JT distorsion. The *resonant bond* (RB) and the *large pairing* (LP) distorsions. In the study of D.V. Makhov and L.J. Lewis[100] a schematic diagram (figure 5.18) shown the difference between these two types. Although the results of Ogut and Chelikowsky matched the experimental analysis of Watkins and Corbett there were reports based on the results of ab initio calculations for divacancies by Saito and Oshiyama[102] proposed the inverse distortion mode, the RB mode. In the calculation as reported in works of D.V. Makhov and L.J. Lewis[100], they found that the resonant bond distortion has slightly lower energy than the pairing distortion (10 meV). And they also mentioned that the transition from one mode to the other occurs without any potential barrier and is accompanied by a rotation of the symmetry plane of the divacancy. Hence they claim that at room temperature, a divacancy should oscillate between these two distortion modes.

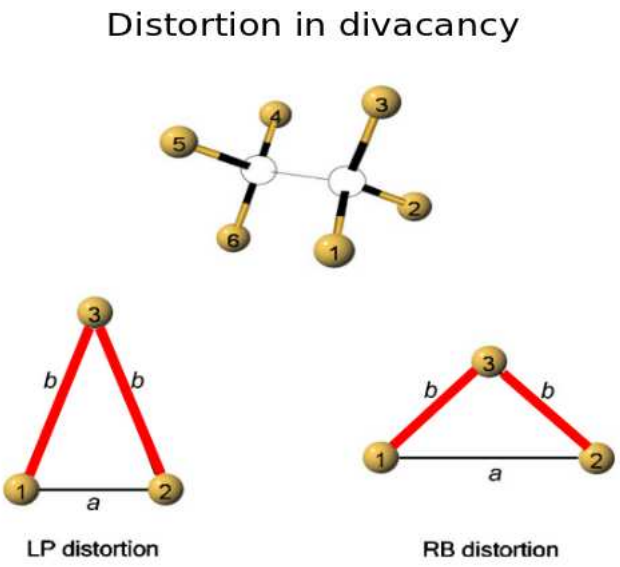

Figure 5.18: Schematic view of LP and RB divacancy distortion modes.

.

5.6.2 Jahn-Teller Distorsion in the uncharged nanoclusters

In their work[97] Ogut and his colleagues have studied the size dependence of the relaxations of the atoms around the vacancy with respect to the shells around the vacancy. Their findings were such which proved the inward movement of the neighboring atoms towards the vacancy. They even found the same for the charged cases. In the study that we undertook we also tried to find whether it is possible to observe such distortions in these silicon nanoclusters. We have tried to investigate the geometry of the vacancies in similar spirit. We did full geometry relaxation of the atoms and the cutoff for the maximum value of force in all direction on each atom was held at $10^{-5} Hartree/Bohr$ which is equivalent to $0.0005 eV/\mathring{A}$. In our analysis with the neutral divacancies we found that depending on the size of the clusters RB and LP distorsions take place around the vacancy. These distortions are therefore dependent in a particular fashion on the cluster sizes and a general statement relating the type of distorsion to that of the size of cluster can be

made. In the figure 5.19 we demonstrate the nearest neighbors of the neutral divacancy of clusters 0.9 nm and 1.2 nm. In this figure as we see the nan-

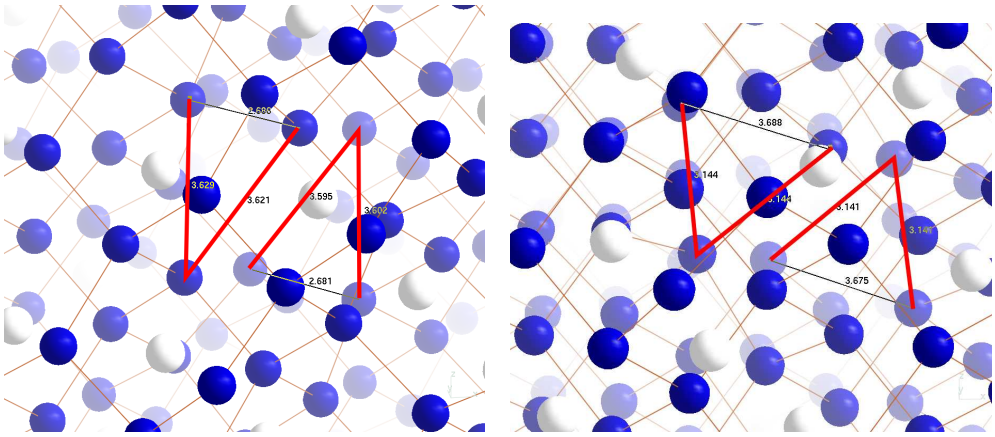

Figure 5.19: JT distorsions and the distance between the nearest neighbors of the neutral divacancy for (a) 0.9 nm cluster and (b) 1.2 nm cluster

ocluster of radius 0.9 nm exhibits the nearest meighbours of the divacancy in a LP distorsion yet the 1.2 nm cluster divacancy has undergone a RB distorsion. The clusters of sizes more 0.9 nm upto 1.2 nm have all exhibitted the same tendency. This fact can be addressed with a careful observation to the surface effect of the nanoclusters. Although the nanoclusters are considered spherical in the electrostatic model yet they are not spherical and they have the planes of the polygons on each face. The arrangement of the planes are different in clusters of different size and hence the surface effect is not *homogeneous* or *consistent* in nature for all the clusters. And we may be forced to think that this effect in the nanoclusters owe its origin to the arbitrariness of the arrangement of the surfaces. To understand the effect of the surfaces let us have a look at the monovacancies, figure 5.20. Here also we can see the JT effect around the monovacancy. If we look carefully we will notice the movement of the nearest neighbors to the vacancy in the two clusters appears different even if viewed from the same direction. By this I mean the movement of the neighbors in a preferred direction. Given the isotropy of an infinite bulk this indeed is not an issue. One can argue that in a bulk (which we are trying to simulate through our nanoclusters) these

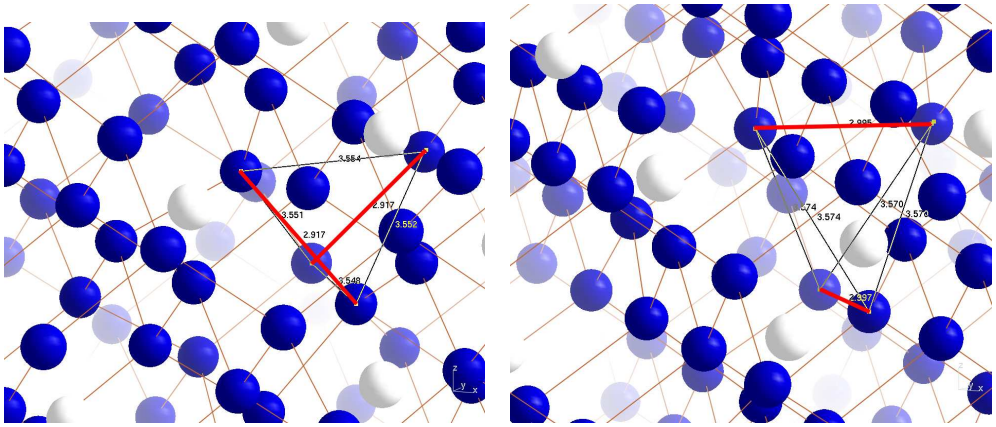

Figure 5.20: JT distorsions and the distance between the nearest neighbors of the neutral mono vacancy for (a) 1.1 nm cluster and (b) 1.2 nm cluster

two apparently different movements are equivalent. But for our system as it is finite the movement of the atoms are of course influenced by the surfaces present in a particular cluster. A schematic diagram (figure 5.21) will be helpful to understand this fact. For the sake of completeness here it must be

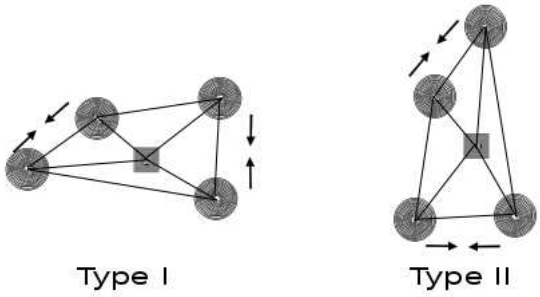

Figure 5.21: The two modes of JT distorsions as observed in the nanoclusters. When viewed from a particular direction in a finite system they appear different of course. The box inside is the vacancy and the round balls are the neighboring atoms.

mentioned that out of these two different movements both are equally likely as it does not depend on the cluster size as it was for the divacancies.

Table 5.2: Table representing the extent of the deformations in the distance between the nearest neighbors of the monovacancy in different charge states. Avg.4 is the column displaying the average distance between the 4 neighbors which are at same distance from the vacancy and Avg.2 is for the average distance between the 2 neighbors which are at the same distance from the vacancy.

Charge	Avg.4	Avg.2	% Deformation
0	3.572	2.996	-16.13
-1	3.464	3.058	-11.72
+1	3.8	3.556	-6.42
-2	3.094	3.423	+10.63

5.6.3 Jahn-Teller Distorsion in the charged nanoclusters

Let us now investigate the extent of this JT distorsion in the charged systems. As we have already seen that the presence of charge in the system affects the electron density near the vacancy it is quite natural to assume that the effect will be seen in the geometry of the system as well. In fact, as it is already mentioned before, the geometry is the manifestation of the electronic changes in the system due to the presence of the defects. Let us have a look at the comparative JT distorsions in the neutral and variously charged monovacancy clusters.

Table 5.2 along with figure 5.22 exhibits a very strange fact. Indeed from figure 5.22 we understand that the presence of charge in the system and due to the effect of the trapped charges near the vacancy the geometrical manifestation of the JT distortion is not the same in all the charged clusters. In fact we see that for all the clusters there is a tendency of 2 atoms moving such that they share a similar distance from the vacancy and their distances from the other atoms are larger of course. This is also shown in the schematic figure as mentioned before in context of the two types of distortions in the finite clusters. And we can have a measure of the deformation from the above table. The table shows that for charge states 0, -1 and +1 the distance between the atoms grouping together is respectively 16.13, 11.72 and 6.42

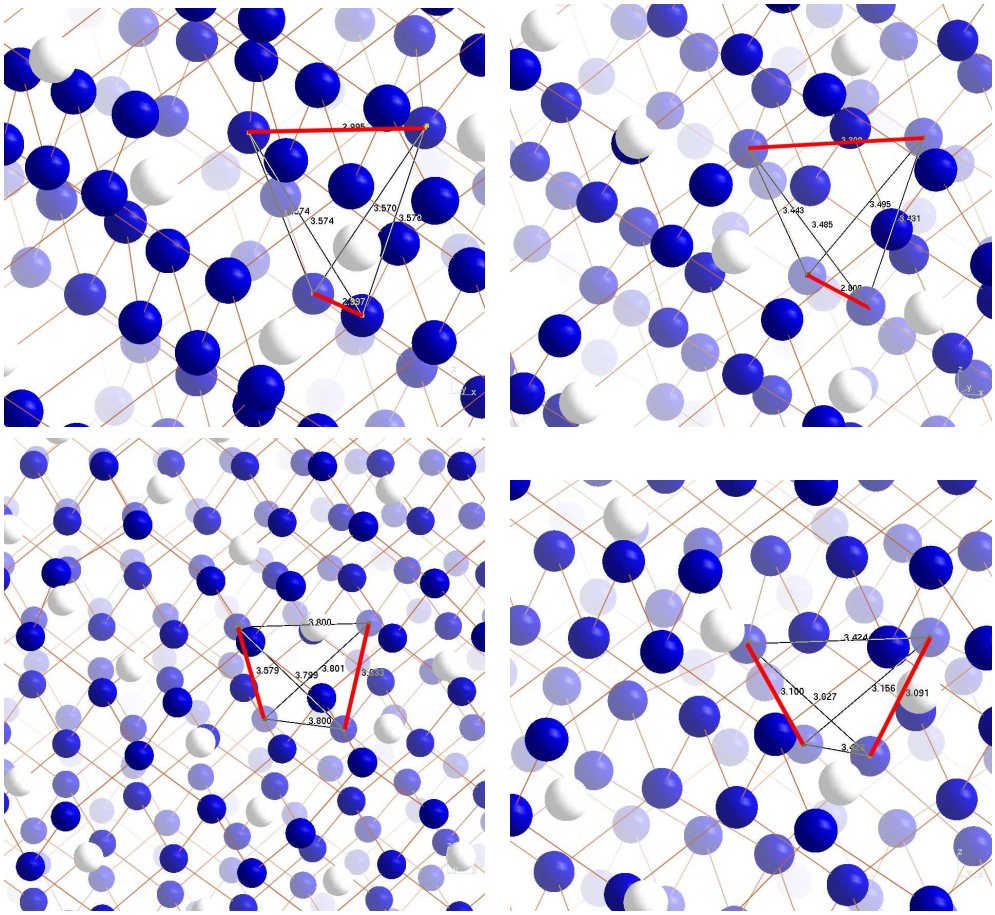

Figure 5.22: JT distorsions and the distance between the nearest neighbors of the monovacancy for 1.2 nm cluster with charges (a) 0 (b)-1 (c)1 (d)-2

percent less than the atoms being apart. Where as for the charge state -2 the distance between the atoms grouping together is 10.63 percent more than that of the other atoms which have moved apart. In this regard we may recall that even from the HOMO-LUMO gap analysis in the previous section we have known the system with -2 charge behaves differently from the others. This different mode of JT distortion must therefore be caused due to the effect of the trapped electron density near the center of the nanocluster.

5.7 A simple force model to simulate the JT distorsion

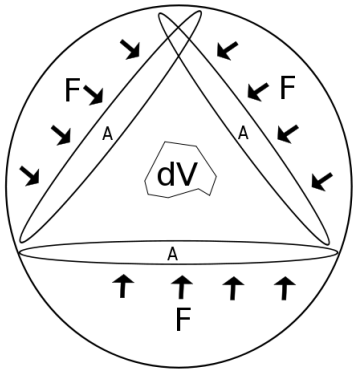

Figure 5.23: Schematic representation of a simple force model of JT distorsion
.

Owing to the fact that the atoms are moving as a manifestation of the JT distortion a simple force model can be visualized in accordance with the overall picture. In the schematic figure (figure 5.23) of the model the inward movement of the atoms towards the center of the cluster (around the vacancy) is represented. Due to the movement of the atoms the volume of the defect is changed by dV. The forces exerted on this defect volume are from all possible directions. And hence we can imagine a contour of circular areas as shown in the figure. The force per unit area for each such circular area is the pressure P exerted on the volume dV and the work done to create dV would be given as the elastic energy,

$$W_{elastic} = PdV. \tag{5.13}$$

and

$$P = \frac{Force}{Area} = \frac{C}{r^2} \tag{5.14}$$

where C is a constant and r is the radius of the nanocluster.

5.8 The combination of the electrostatic and simple force model

If we fall back on the electrostatic energy stored in the cluster to bring all the charges together the general form of the expression would look like,

$$W_{electrostatic} = A - \frac{B}{r}. \tag{5.15}$$

Hence if we combine the two models, i.e. electrostatic model and the simple force model of JT distorsion we will get the total energy required to form the vacancies in a nanocluster with the JT distorsion. Therefore we can say that the total energy required to form the vacancies in a nanocluster with the JT distorsion must have the analytical form of,

$$E_{formation} = A - \frac{B}{r} + \frac{C}{r^2.} \tag{5.16}$$

Now we can check the validity of this functional form with different values of the radii of the nanoclusters and then can simultaneouly plot the values of the calculated formation energies under the FBC formalism. This as will be explained in the through following figures will also help us to understand the convergence of the value of the formation energy in relation with the cluster size. As it is evident from the fitted curve (figure 5.24) that the value of the formation energy seems to be converging with the cluster size and hence the values quoted from the calculations of the 1.2 nm clusters can be considered to be accurate under the given formalism. This curve also indicates the physically acceptable nature of the models discussed above. The points which are away from the analytical curve are of course results of the finite size effect as one must experience in calculations like these. It also emphasies the presence of a strong surface effect when the clusters are really small. Hence it can be argued that the physical significance of the formation energy as calculated from the cluster of size 1.2 nm can be taken as standards for future bulk calculations.

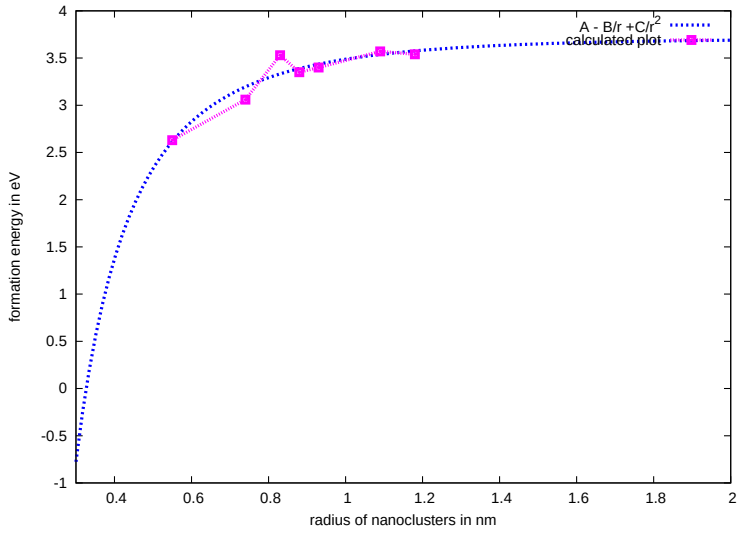

Figure 5.24: The comparison of the calculated formation energies with the analytical model and the convergence of the formation energy value with respect to the cluster size

.

5.9 Conclusions

As concluding remarks the following observations can be considered as the result and immediate finidings of the research.

- The electrostatics of the nanoclusters with defect is relatively simple and easy as compared to that of the PBC systems. The requirement of a background compensating charge is not required.

- It is also noteworthy that the defect-defect interaction along with interaction of the image charges can be avoided for the study of charge systems. Of course there is a surface to bulk effect which is an artefact of the FBC model but it is relatively simpler to deal with in the context of finding the formation energies of the defects and studying there geometries.

- The geometry of the charged defects in nanoclusters manifests most the effect of the surface. This is a bit far stretched one may presume. But indeed the surface induces the occurrence of trapped charges near the vacancy. And we have show that the geometry for each charged state is different from one another and it is obviously due to the different values of the trapped charges. Hence we see different deformations in the JT representations for different charge states. Also the forms of distortion like the RB and LP distortions are observed in this kind of an approach.

- The phenomenon of trapped charges is observed as an important feature of the FBC model which allowed us to understand the electrostatics of the nanoclusters with or without defects. We may even emphasize the ability of the vacancies to trap charges in a solid as we have found and proved in our analyses. Even for the case of PBC we have seen if we somehow manage to keep a charge in the system far enough from the vacancy (one cannot actually be very far from the vacancy in PBC because of the periodicity itself) it tends to trap that charge. Hence in general one may infer that vacancies trap charges.

5.10 Future perspectives

5.10.1 Different other defects

This analysis can be extended to the study of other defects as well. In fact even within this research we have tried to get similar results for the charged di vacancies as well. But unfortunately the required criteria for an acceptable value of forces on the atoms are not reached. The reasons may be hidden in the behavior of trapped charges for the divacancies. The electron density around the divacancy must be disturbed in a greater extent due to the surface and a spin polarized calculation of the nanoclusters would be preferred to look into the matter more deeply. All the calculations up to now are spin average calculations. But to do a spin polarized calculation on a cluster of

1.2 nm in BigDFT, the expense is huge and hence it is a bit difficult to tackle at the moment.

5.10.2 Migration energies

Another method to verify whether the results obtained by this method are believable or not is to check for other quantities which are reported in experiments. One such method is to calculate the migration energy of a vacancy. In figure 5.26 we can see a migration of vacancy pictorially. In reality we have

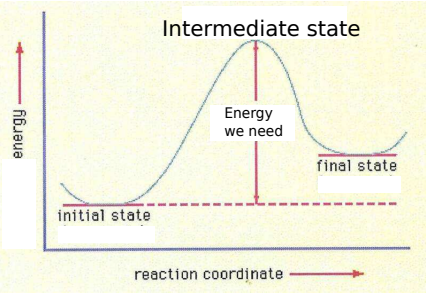

Figure 5.25: Scematic diagram to explain the concept of the migration energy .

tried already to calculate the migration energy of monovacancy within the framework of our model. We have used the DIIS[103] method to find the middle point of the journey of the vacancy from one place to the other. As per our calculations we have found out that the migration energy of the neutral monovacancy in $0.5\ eV$. As reported in the report by Watkins[63] the experimental value of the migration energy of the neutral monovacancy is $0.45\ eV$. This result encourages us to continue to do the same for other charge vacancies. Indeed along with these calculations another form of calculation is still under process. To get the contour of the entire path of migration a common procedure is to do a Nudged Elastic Band (NEB) calculation. Where all the intermediate replicas are created and total energy calculations are done on each replica. This calculation will help us to know the entire trajectory of the vacancies. But this is also to be kept in mind that these calculations are very expensive in time.

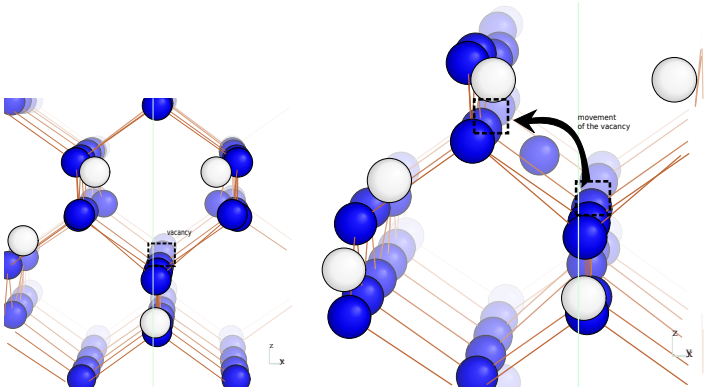

Figure 5.26: The real picture of the movement of the vacancy

5.10.3 Homothetic clusters

There is a possibility to account for the surface effect in a more analytical and quantitative manner, if we can create the clusters of different sizes with the same family of surfaces. Clusters of different sizes with same surfaces are called homothetic clusters. If we can put one cluster inside the other one they will make something like concentric clusters. We have already succeeded in making homothetic clusters of three different sizes but calculations with them took us out of the time limit of the present thesis. We believe similar calculations as done within the framework of this thesis will yield interesting quantitative facts about th surface effect in the nanoclusters.

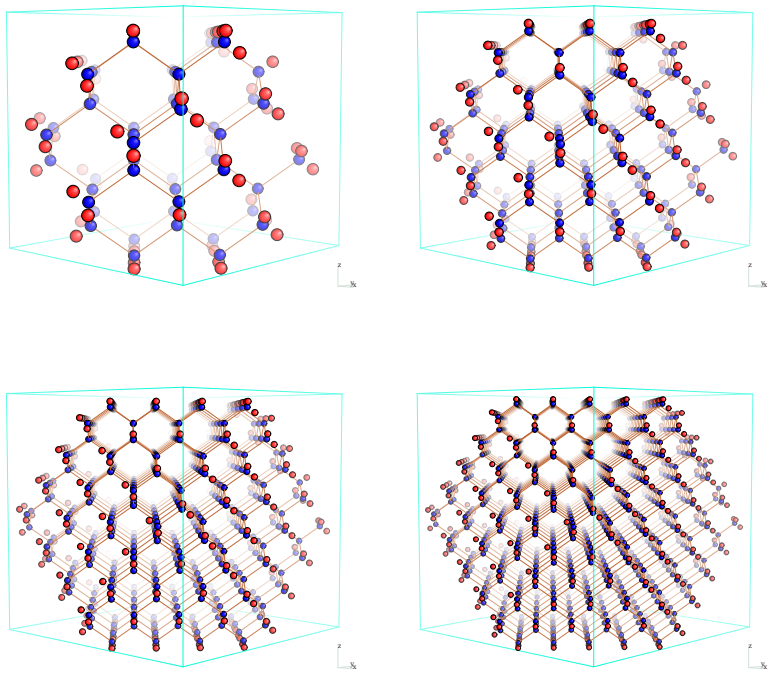

Figure 5.27: Homothetic clusters made from boxes of (a)64 (b)216 (c)512 (d)1000 silicon atoms.

Chapter 6

Final words and Perspectives

In the quest to study the charged defects of silicon we have managed to touch upon and dig into many different related topics in this branch of condensed matter physics. In terms of field study, we have gathered knowledge about almost all the techniques in the DFT framework, that scientists use to calculate various physical quantities regarding the charged defects. In that kind of a study we have summarized the advantages and disadvantages of each method. Indeed PBC methods are good to simulate a bulk, but the problem of image defect interactions is something which we cannot get rid of anyhow, barring the use of some correction factors. In the main part of this research we have tried to find an approach which would be different from the PBC formalisms. We have felt the need of not using the background compensating charge in the PBC formalism for the calculation of the charged defects. The backbone of this research is the DFT method as all the total energy calculations are done with the wavelet-based DFT code - BigDFT. Hence a brief yet detailed description of the DFT framework is included in the thesis. The important concepts about the basis sets, pseuopotentials and the exchange correlation functionals are also discussed in here. In the study with the HGH pseudopotentials, we have tried to show the reliability of those pseudos with the inclusion of the NLCC. We have shown of course that with the NLCC implemented within the HGH pseudopotentials, we can use them for very accurate calculations, as comparable to the all electron calculations.

This is a major step towards the pseudopotential calculations as it takes us towards the ultimate aim, which is to use a complexity-less scheme for accurate research. The main part of this thesis as I have already mentioned was to find a novel way to calculate the formation energy of the charged defects. We have used nanoclusters to simulate the defects and have found that the formation energy thus found are in accordance with whatever experimental values we have. We have put forward the phenomenon of the trapped charges near the vacancy in the nanoclusters which we believe affects the geometry and the energy states of the defect. Keeping that in mind we have given here an analytical electrostatic model to simulate the charge distribution in the nanoclusters. We have also done various numerical analyses to provide ample proof for the electrostatic model of the system. Although an admitted fact is that the PBC method employs less atoms than our FBC method but in our method we have dealt away with the correction factors needed otherwise for the PBC method. In future these analyses with the correct electrostatics can be used for other systems and of course for various other studies like the migration energy and diffusion of defects. We can study the effect of charge in the substitutional and interstitial defects in silicon with this cluster method. In principle the success and validity of this method would ensure further application of this to study all other point defects in this new method. It would be very useful to know about the energetics and the geometry of such defects in nanoclusters. There is of course a lot of room to study magnetic defects as well. Nanoclusters which are magnetic can also be studies within similar formalism. The effect of the trapped charges and the surfaces in the magnetic systems can be extremely interesting to look for. We can look for the various effects of the dilute doping defects and the resultant magnetism in the metal oxide systems with this method. This method will provide us with an alternative way to the model more frequently used hamiltonian methods.

In a nutshell we can say a new method to study the energetics of the defect will open up channels of research with defects in all possible environment. With the recent development to include the applicability of the Wannier functions in BigDFT, we can be hopeful of using this cluster approach to

carry out somewhat an order-N method, in terms of *localization regions*, to study some embedded systems. As for example we can talk about the molecules on surfaces which are semi-infinite systems, or even the charged defects in bulk(infinite systems). The correct electrostatics of the cluster approach makes it transferable to the embedded system calculations. Since the wavelets are localized, for each orbital a region of localization can be defined . All the operations can be carried out as applications of the Hamiltonian in the given orbital. Hence methods and theoretical tools can be developed based on order N method to perform calculation of an atomic system embedded by a tight-binding model based on Wannier functions. If the Wannier orbitals of Si bulk can be calculated beforehand, then, using tight binding methods on Wannier, one can define a hamiltonian and a self-consistent field to calculate an infinite system of Si bulk. Following steps would include the processes to deal with the defect in the embedded environment along with the relaxation of the Wannier orbitals in a cluster centered around a vacancy. It will be feasible with this mixed scheme (wavelet + tight-bindings) to describe properly charged trapped states even if dimension of the system exceed many nanometers. It is worth mentioning here that wavelets being localized themselves make it possible to do locally all operations as applications of the Hamiltonian. It terms of technical complexities wavelets are advantageous than plane waves in this particular aspect. Hence we can consider the cluster approach, as we have described in the larger part of this thesis, as the first step in the field of an order-N method to study the embedded systems. With the electrostatics and the energetics known for the cluster method the following research procedures will be immensely facilitated .

Bibliography

[1] D. A. Faux, J. R. Downes, E. P. O'Reilly, J. Appl. Phys., *82, 3754–3762 (1997).*

[2] G. A. Baraff, E. O. Kane, M. Schlüter, Phys. Rev. Lett., *43, 956–959 (1979).*

[3] G. D. Watkins, J. W. Corbett, Phys. Rev., *138, A543–A555 (1965).*

[4] G. D. Watkins, J. R. Troxell, Phys. Rev. Lett., *44, 593–596 (1980).*

[5] J. C. Bourgoin, J. W. Corbett, Rad. Effects, 36, 157–188 (1978).

[6] R. J. Needs, J. Phys. Condens. Matter *11, 10437–10450 (1999).*

[7] W.-K. Leung, R. J. Needs, G. Rajagopal, S. Itoh, S. Ihara, Phys. Rev. Lett., *83, 2351–2354 (1999).*

[8] S. J. Clark, G. J. Ackland, Phys. Rev. B, *56, 47–50 (1997).*

[9] V. V. Lukianitsa, Semiconductors, *37, 404–413 (2003).*

[10] G. M. Lopez, V. Fiorentini, Phys. Rev. B, *69, 155206–155213 (2004).*

[11] A. H. Kalma, J. C. Corelli, Phys. Rev., *173, 734–745 (1968).*

[12] L. J. Cheng, J. C. Corelli, J. W. Corbett, G. D. Watkins, Phys. Rev., *152, 761–774 (1966).*

[13] S. Goedecker, T. Deutsch, L. Billard, Phys. Rev. Lett., *88, 235501–235504 (2002).*

[14] I. Lazanu, S. Lazanu, Phys. Scr., *74, 201–207 (2006).*

[15] D.Caliste and P.Pochet, Phys. Rev. Lett. *97, 135901 (2006).*

[16] D.Caliste, K.Z.Rushchanskii, and P.Pochet , Appl. Phys. Lett. *98, 031908 (2011).*

[17] P. Hohenberg and W. Kohn, Phys. Rev. *136*. B864 (1964).

[18] W. Kohn, Reviews of Modern Physics *71* nb. 5 (1999).

[19] W. Kohn and L. J. Sham, Phys. Rev *140*, A1133 (1965).

[20] C.-O. Almbladh, U. von Barth Phys., Rev. B *31*, nb. 6 (1984).

[21] J. Chen, J. B. Krieger, Y. Li, J.G. Iafrate, Phys. Rev. A *54* nb. 5 (1996).

[22] L Fan, T.J. Ziegler J. Chem. Phys. *95*, 7401 (1991).

[23] J. P. Perdew, A. Zunger, Phys. Rev. B *23*, nb. 10 (1981).

[24] S. Kurth, J. P. Perdew, Phys. Rev. B *59* nb. 16 (1999)

[25] J. P. Perdew, K. Burke, and M. Ernzerhof, Phys. Rev. Lett. *77, 3865 (1996).*

[26] M. Ernzerhof and G. E. Scuseria, J. Chem. Phys. *110, 5029 (1999).*

[27] J. P. Perdew and Y. Wang, Phys. Rev. B *45, 13244 (1992).*

[28] J. P. Perdew, S. Kurth, A. Zupan, and P. Blaha, Phys. Rev. Lett. *82, 2544 (1999).*

[29] von Barth, U., Physica Scripta. Vol. *T109, 9–39, (2004).*

[30] Muller, J. E., Jones, R. O. and Harris, J., J. Chem. Phys. *79, 1874(1983).*

[31] Terakura, K., Oguchi, T., Williams, A. R. and Kubler, J., Phys. Rev. B *30, 4734 (1984).*

[32] Wang, C. S., Klein, B. M. and Krakauer, H., Phys. Rev. Lett. *54, 1852 (1985).*

[33] Godby, R. W. and Needs, R. J., Phys. Rev. Lett. *62, 1169 (1989).*

[34] Parr, R. G. and Yang, W., Density-Functional Theory of Atoms and Molecules,(Oxford University Press, New York 1989)

[35] von Barth, U., Chem. Scripta *26, 449 (1986).*

[36] J. Tao, J. P. Perdew, V. N. Staroverov, and G. E. Scuseria, Phys. Rev. Lett. *91, 146401 (2003).*

[37] J. P. Perdew, J. Tao, V. N. Staroverov, and G. E. Scuseria, J. Chem. Phys. *120, 6898 (2004).*

[38] J. Harris and R. O. Jones, J. Phys. F *4, 1170 (1974).*

[39] A. Gorling and M. Levy, J. Chem. Phys. *106, 2675 (1997).*

[40] A. D. Becke, J. Chem. Phys. *98, 5648 (1998).*

[41] E.R.Batista, J.Heyd, R.G.Hennig, B.P.Uberuaga, R.L.Martin, G.E.Scuseria, C.J.Umrigar and J.W.Wilkins Phys. Rev.B *74, 121102 R(2006).*

[42] J. Heyd, G. E. Scuseria, and M. Ernzerhof, J. Chem. Phys. *118, 8207 (2003)*; J. Heyd and G. E. Scuseria, ibid. *120, 7274[U+0351](2004)* ; J. Heyd and G. E. Scuseria, ibid. *121, 1187 (2004).*

[43] L. Genovese, A. Neelov, S. Goedecker, T. Deutsch, S. Ghasemi, A. Willand, D. Caliste, O. Zilberberg, M. Rayson, A. Bergman,and R. Schneider , J. Chem. Phys. *129, 014109 2008*

[44] D.R. Hamann, M. Schluter, and C. Chiang, Phys. Rev. Lett. *43, 1494 (1979).*

[45] G.B. Bachelet, D.R. Hamann, and M. Schluter, Phys. Rev. B *26, 4199 (1982).*

[46] G. Kerker, J. Phys. C *13, L189 (1980).*

[47] D. Vanderbilt, Phys. Rev. B *32, 8412 (1985).*

[48] N. Troullier and J.L. Martins, Phys. Rev. B *43, 1993 (1991).*

[49] S. Goedecker, M. Teter, and J. Hutter, Phys. Rev. B *54, 1703 (1996).*

[50] S. Goedecker , K. Maschke Phys. Rev. A *45, 88–93 (1992)* .

[51] C. Hartwigsen, S. Goedecker, and J. Hutter, Phys. Rev. B *58, 3641 (1998).*

[52] A.M. Rappe, K.M. Rabe, E. Kaxiras, and J.D. Joannopoulos, Phys. Rev. B *41, 1227(1990).*

[53] L. Kleinman and D.M. Bylander, Phys. Rev. Lett. *48, 1425 (1982).*

[54] D. Vanderbilt, Phys. Rev. B *41, 7892 (1990).*

[55] K. Laasonen, A. Pasquarello, R. Car, C. Lee, and D. Vanderbilt, Phys. Rev. B *47,10142 (1993).*

[56] G.P. Francis, and M. C. Payne, J. Phys. Condens. Matter *17, 1643, (1990).*

[57] T. L. Beck, Rev. Mod. Phys. *72, 1041 2000.*

[58] J. E. Pask, B. M. Klein, C. Y. Fong, and P. A. Sterne, Phys. Rev. B *59,12352 1999.*

[59] J. J. Mortensen, L. B. Hansen, and K. W. Jacobsen, Phys. Rev. B *71,035109 2005.*

[60] M.C.Payne, M.P.Teter,D.C.Allan,T.A.Arias,and J.D.Joannopoulos, Rev. Mod. Phys. *64, 1045(1992).*

[61] A.M.Rappe,J.D.Joannopoulos, and P.A.Bash, J. Am. Chem. Soc. *114, 6466(1992).*

[62] M.Leslie and M.J.Gillian, J. Phys. C *18, 973 (1985).*

[63] G. D. Watkins Material science in semiconductor processing 3 *227-235 (2000)*

[64] G. Feher Phys. Rev. *103 (3): 834–835, (1956)*

[65] R. O. Simmons and R. W. Balluffi Phys. Rev. *117, 52–61 (1960).*

[66] G.Makov and M.C.Payne, Phys. Rev. B. *51, 7(1995).*

[67] S.W.de Leeuw,J.W¿Perram, and E.R.Smith, Proc. R. Soc. London Ser. A*373, 27 (1980).*

[68] R.M.Martin, Phys. Rev. B *9,1998 (1974).*

[69] Peter A.Schultz, Phys. rev. Let. *84, 9 (2000).*

[70] Peter A.Schultz, Phys. rev. B *60, 1551 (1999).*

[71] M.Leslie and M.J.Gillian, J. Phys. C *18, 973 (1985).*

[72] C.Freysoldt, J.Neugebauer,C.G.Van de Walle, Phys. rev. Let. *102, 016402 (2009).*

[73] C. W. M. Castleton, A. Hoglund, and S. Mirbt, Phys. Rev.B *73, 035215 (2006).*

[74] J. Shim, E.K. Lee, Y. J. Lee, and R. M. Nieminen, Phys. Rev. B *71, 035206 (2005).*

[75] A. F. Wright and N. A. Modine, Phys. Rev. B *74, 235209 (2006).*

[76] I. Dabo, B.Kozinsky, N.E.Singh-Miller, and N.Marzari, Phys. Rev. B *77, 115139 (2008)*

[77] L. A. Curtiss, K. Raghavachari, P. C. Redfern, and J. A. Pople, J. Chem. Phys. *106, 1063 1997.*

[78] G. Sun, J. Kürti, P. Rajczy, M. Kertesz, J. Hafner, and G. Kresse, J. Mol. Struct.: THEOCHEM *624, 37 2003.*

[79] S. B. Zhang, S. H. Wei, and Z. Zunger, Phys. Rev. B *63, 075205 2001.*

[80] P. E. Blochl, Phys. Rev. B *50, 17953 1994.*

[81] G. Kresse and J. Hafner, Phys. Rev. B *47, 558 1993.*

[82] B. Hammer, L. B. Hansen, and J. K. Nørskov, Phys. Rev. B *59, 7413 1999.*

[83] E. L. Briggs, D. J. Sullivan, and J. Bernholc, Phys. Rev. B *54, 14362 1996.*

[84] L. A. Curtiss, K. Raghavachari, G. W. Trucks, and J. A. Pople, J. Chem. Phys. *94, 7221 1991.*

[85] J. Paier, R. Hirschl, M. Marsman, and G. Kresse, J. Chem. Phys. *122, 234102 2005.*

[86] S. Goedecker, M. Teter and J. Hutter, Phys. Rev. B *54, 3 1996.*

[87] S.G.Louie, S.Froyen and M.L.Cohen, Phys. Rev.B *26, 4 1982*

[88] A. Zunger, Phys. Rev. B *22, 649 1980*

[89] D. R. Hamann, M. Schluter, and C. Chiang, Phys.Rev. Lett. *43, 1494 1979*

[90] M. T. Yin and M. L. Cohen, Phys. Rev. Lett. *45, 1004 1980*

[91] R. Fournier, L. Boroukhovskaia, Theor. Chem. Acc. *112: 1–6 2004*

[92] P. Rinke, C. G. V. de Walle, and M. Scheffler, Phys. Rev. Lett. *102, 026402 (2009).*

[93] R. Nieminen, Modell. Simul. Mater. Sci. Eng. *17, 084001 (2009).*

[94] A. F. Wright and N. A. Modine, Phys. Rev. B *74, 235209 (2006).*

[95] J. R. Chelikowsky, N. Troullier, and Y. Saad, Phys. Rev. Lett. *72, 1240 1994[U+0352].*

[96] E. L. Briggs, D. J. Sullivan, and J. Bernholc, Phys. Rev. B *52, R5471 1995.*

[97] S. Ogut, H. Kim, J. R. Chelikowsky Phys. rev. B. (Rapid Comm.) *56, 18 1997.*

[98] C.G. Van de Walle, J. Neugebauer, J. Appl. Phys. *95, 8 2004.*

[99] R. S. Mulliken, J. Chem. Phys. *23, 1833 (1955).*

[100] D.V. Makhov and L.J. Lewis, Phys. Rev. B *72, 073306 2005.*

[101] S. Ogut and J. R. Chelikowsky Phys. Rev. Lett. *83, 19 (1999)*

[102] M. Saito and A. Oshiyama, Phys. Rev. Lett. *73, 866 1994.*

[103] P.Pulay, Chem. Phys. Lett. *73, 2, 393-398 (1990)*

Acknowledgments

I am extremely grateful to Nanoscience Foundation who funded this project for the first three years. All the staff members of the Foundation were very helpful with the administrative proceedings like the VISA for me and my wife, the reimbursements of the transport expenses, paper work for the tax payment etc. I would like to thank them for such a support and wish them all the best to carry on with the wonderful work of helping researchers from all around the world.

The last four months of my PhD thesis was funded by CEA and I have no words to thank for their kind consideration. I also thank all the administrative staff members to help me with all the necessary paper works needed for such an extension.

To start with I would like to thank Dr. Damien Caliste, my PhD supervisor, to have been so helpful. Through all the small and silly mistakes to the biggest blunders he kept his support and helped me in all possible ways to finish my work. There are so many important things that I learnt from him. From computer techniques to concepts of physics discussions with him always ended in my gaining some new knowledge. It was nice to know with him the different aspects of research. I can't thank him enough for his help in difficult times of the research work or even the administrative hustles. I thank him for his patience to deal with my innumerable mistakes in the research work. It was very nice to know him and his family and I would be ever thankful for his all round support.

I would take this opportunity to thank Dr. Thierry Deutsch, my director to thesis, for letting me have the opportunity to work on this interesting topic. I got to learn a lot about various aspects of physics and computer science because of many important discussions with him. I am also thankful for his kind consideration in letting me have an extension of my PhD contract, which otherwise is very difficult to have as I gather. There had been

strained patches in between but I would take the positive out of it to thank you for letting me know the hardships of research and I guess I have learnt many important things to do a good research. Thanks a lot for being there.

I would like to thank Mr. Alex Willand and Dr. Stefan Goedecker for collaborating on a project with me. Discussion through email with them had been of great help in the research.

In my laboratory there are so many people to whom I was thankful for various reasons. A special thanks to Dr. Luigi Genovese for some delightful discussions regarding the collaborative work we did. It was great to learn so many different aspects of physics and computer science from you. I would like to thank Dr. Pascal Pochet, Dr. Yann-Michel Niquet, Dr. Frédéric Lancon and Dr. Brice Videau, discussions with whom helped me to learn a lot about different things in physics and computer science. They had been very understanding and patient to all my questions irrespective of their being related to science or something else.

I had wonderful friends in the lab in the past three and half years. Each of them helped me in all possible ways and words fail me when I wish to thank them for being there with me. I would like to thank Thomas Jourdan, at whose party for the first time I got to know my friends very well. I am thankful to Emanuel Arras, who helped me with my initial proceedings in research with all sorts of things in physics and computers. I am equally thankful to Martin Presson and Margaret Gabriel Presson for their wonderful companionship. A very special thanks to Ivetta Slipukhina for being there as a constant support encouraging to be positive in times when I was down. I would like to thank Dulce Camacho for being such a wonderful friend, sharing innumerable coffees and chats of all kinds. She has also been a great source of inspiration. I would also thank Hector Mera for his tremendous support for me and my work and for the wonderful times that we got to spend together. His insight to science and inspiration to think differently have helped me a lot in my journey. To my friend Cornelia Metzig I would be extremely grateful

as well for she helped me in many ways. Discussion with her about physics, science in general, society, philosophy and many other things made my stay in the lab very enjoyable. I would also thank Eduardo Machado Charry for helping me with many small but important things regarding my thesis. His presence always lights up the place. I would also like to thank Irinia Georgina Groza for being a lovely inspiring and encouraging friend. My gratitude goes for Bhaaraathi Natarajan, discussions with whom is something which I had always enjoyed.

During my stay in France, there is a family to whom I will never be able to say how grateful I am to have known them - Genvieve Stella Moriceau and Hubert Moriceau. They have love us like their own and have helped us in every possible way to make our lives safe, healthy and enjoyable. They had been the greatest strength and I would cherish every moment of those I spent with them. With them I got to know so much about the culture in France and rest of Europe. They had been the haven where I would run every time I am in some trouble and of course they would help me with whatever they could. It's been an honor to have known them so closely.

In these three and half years I became friends with so many people. Of them all the one who became almost a part of me was Akash Chakraborty. Now, to look back in the times that we spent together, I feel it was a part of myself that was moving around with me. We drank and ate all that we could, went to places together, watched and discussed about innumerable movies, talked about all that we could find under the sun and most of all had the best possible time between us. In days of hard work and distress his support was like the protective imperceptible ether. Can I thank him at all for being a part of my senses?

Friends like Soumen Mondal, Anita Sarkar, Dibyendu Hazra, Subhadeep Dutta, Kalpana Mondal became more than family. Innumerable discussions regarding various subjects that spanned our work, culture, personal life etc. made our days in Grenoble so beautiful. A very special thanks to Soumen

Mondal for helping in with his ambidextrous power of mending household things, giving opinions in research and entrepreneurship way of life. I would also like to extend my gratitude to friends like Ayan Kumar and Kuheli Bandopadhyay, Chandan Bera, Sutirtha and Dipanwita Mukherjee, Arijit and Satarupa Roy, Abhijit Ghosh, Anupam Kundu, Sreeram Venkatpathy, Shilpi Sreeram and Pragyan, Roopak Sinha, Arpita Sinha, Dhrovi and Diu for being there and making the days in Grenoble happy and enjoyable for us. I would like to thank Biplab Mondal for lending me his camera for most of my stay here in Grenoble. It has been really like a family I wish it stays like that forever. Ananda Sankar Basu and Priyadarshini Chatterjee deserve a special bunch of thanks for being almost always the driving force of this extended family of ours. It's been a privilege to know you all.

This thesis is probably an important milestone in this journey and I guess it had started under the guidance of the teachers who I think I can never properly thank. Dr. Ananda Dasgupta is one of those teachers to whom I feel I could go at any point of time to ask any question regarding physics. It is actually a great feeling of confidence to have when day in day out someone is struggling to reach an intellectual height. I would never be able to thank him enough. Prof. Albert Gomes had been an infinite source of inspiration with his intense dedication for students and science. I would like to express my gratitude for his being there with me all those times when I needed inspiration to remain dedicated, focused and honest. I would like to thank Dr. Dipankar Sengupta, Dr. Indranath Chaudhury, Dr. Tapati Dutta, Dr. Shibaji Banerjee and Dr. Suman Bandopadhyay who had taught me so many things in science and have always inspired. I am extremely thankful to Prof. D.G. Kanhere who taught me so many different important things in physics and computer science. This PhD wouldn't have been possible if it wasn't him who inspired me to come here and work. He has been a great source of inspiration to all the students as he has been for me. I would also thank Dr. Anjali Kshirsagar, with whom I managed to learn various aspect of computational physics and physics in general. I would also like to thank Mr. Pinaki Mitra and Mr. Nimai Bhattacharya who always have preached

to me the reason to use life for the quest of higher knowledge of all kinds. I am grateful to Mrs. Jayati Acharya whose good wishes and relentless encouragement along with her sublime music lessons helped me a lot to grow as a human being and sustain under tremendous pressure.

Honestly it was my mother Mrs. Chhabi Deb who dreamt her son becoming a scientist one day. The constant motivating factor above all was my mother's dream about this day. I cannot thank her enough for having had that dream and pushing me hard enough so that I could reach where I am now. My father Mr. Amit Krishna Deb, with his utmost honesty and sincerity to life has forced me to follow the path of honesty and integrity even when I could have drifted. It's their sincere love and care for me which made me worthy of whatever I have achieved till date. I am glad that I have a brother like Mr. Ayan Krishna Deb, who loved me like his own self and even in the most difficult of our days his love was as true as the sun. I would like to thank Mr. Asesh Krishna Deb, my eldest cousin whose constant support always provided me with tremendous confidence. I would also like to thank my all other family members and all other friends whose love and affection had been a constant source of inspiration.

I would like to take this opportunity to express my gratitude for the late Mr. Samir Mukherjee who taught me through the first days of science and mathematics. I would like to thank my oldest school friends Joy Banerjee and Angshuman Samadder who had been with me though thick and thin and who have inspired me through examples all these days.

Among the friends whose constant help saw me through the initial days of the journey with physics, I would like to thank Arya Dhar, Amit Kumar Pal, Sayan Chakraborty, Beas Roy, and Sumitra Raymoulik. They taught me all that was in syllabus, made notes for me to pass, even introduced me to various new subjects. It is great to know them so closely. I would like to thank my friends Aditya Rotti, Jaydeep Belapure, Sumati Patil, Deepashri Saraf, Narendranath Patra, Sayan Mondal, Anirban Pal and Saurav

Roy because they always believed I could reach this far. I would take this opportunity to thank our *Ajji* Mrs. Subha Joshi who have always loved me so much and have inspired me immensely to thrive harder for my goal in life.

I would also thank my friend Maitra, whose constant adulation and indulgence made me believe that I can be a creative individual as well. Her support, encouragement and friendship is something which one can always take pride in. Her honesty and integrity to life itself have been a great source of inspiration to me and my family.

In the end, I would like to thank the person, thanking whom seems absolutely insignificant, for it is Mrs. Maitreyee Mookherjee, who essentially lived a life completely for my cause and sake. That she gave up her own career to be with me through the times I needed her more than ever, that she had faith in me when even I had lost faith in life, that she loved me even when I failed her, are reasons enough for not thanking her. One cannot thank someone who has done so much. Her dedication and love for me has been my energy so far. I couldn't have made it anywhere without her constant support, encouragement and love. I could have written pages for her but it would mean the same - that I wish she stays there with me forever.